To the Graduate Council:

I am submitting herewith a dissertation written by James Lane Edwin Burn entitled "Synthesis and Chemical Properties of Some Pyrazolato- and 2-Hydroxypyridinato-Bridged Dirhodium Complexes". I have examined the final copy of this dissertation for form and content and recommend that it be accepted in partial fulfillment of the requirements for the degree of Doctor of Philosophy, with a major in Chemistry.

Clifton Woods

Clifton Woods, III, Major Professor

We have read this dissertation
and recommend its acceptance:

James R. Chambers

Joseph R. Peterson

Edward S. Clark

Accepted for the Council:

Carolyn Winkel

Associate Vice Chancellor
and Dean of The Graduate School

SYNTHESIS AND CHEMICAL PROPERTIES OF SOME PYRAZOLATO- AND 2-HYDROXYPYRIDINATO-BRIDGED DIRHODIUM COMPLEXES

A Dissertation

Presented for the

Doctor of Philosophy

Degree

The University of Tennessee, Knoxville

James Lane Edwin Burn

May 1993

DEDICATION

This Dissertation is dedicated to my father,

the late James Lane Edwin Burn, Sr.

who's love of chemistry inspired me to follow this path.

ACKNOWLEDGEMENTS

I wish to thank the Department of Chemistry, The University of Tennessee, Knoxville for financial aid in the form of graduate teaching and graduate teaching/research assistantships. I also wish to thank the State of Tennessee for their support through the Center of Excellence-Science Alliance Program.

A sincere debt of gratitude is owed to Dr. Clifton Woods, III, my research advisor, for his patience, tolerance, and guidance during my educational experience at UT. His support through my darkest time kept me striving to attain the professionalism that he embodies.

A similar debt is owed to Dr. Gilbert M. Brown of the Oak Ridge National Laboratory for his scholarly assistance and the use of his laboratory and instrumentation. I would like to thank Dr. D. Paul Rillema of The University of North Carolina, Charlotte, for the acquisition of ESR spectra and his academic input, and Dr. Kelsey D. Cook for his assistance with mass spectral interpretation. I would like to thank those professors that I assisted in undergraduate instruction for their inspiration and insight into education, especially Drs. Bull, Chambers, Grimm, Kovac, Peterson, and Woods.

I thank the National Science Foundation, the United States Department of Energy, and Research Corporation for support of the work include herein, and

Bechtel National, Inc. for support in the form of employment these past two years.

I would like to thank the following fellow students for their assistance: Johnny, Louis, Paul, Jeff, Bill, Beth, Karl, Darryl, Jonathan, and Roy. I would also like to thank Linda Parsons for her editorial and technical writing guidance.

Finally, special thanks to my family for their love, patience, and support: to my Aunt Virginia and Uncle O. L. for lodging; to my wife, Kathleen, for her wisdom and for adding direction to my life; and especially to my mother, Marthanne Smith Burn, for her understanding.

ABSTRACT

Spectroscopic behaviors of dpam-containing (dpam=bis(diphenylarsino)-methane) dirhodium-μ-pyrazolato A-frame complexes have been compared to those of the (diphenylarsino)(diphenylphosphino)methane (dapm) and bis(diphenylphosphino)methane (dppm) analogs through ligand substitution and electrochemical oxidation. Thermochromism of isocyanide-containing dirhodium(I,II) compounds has been examined. To clarify the role of electronegativity of pyrazolate substituents in inducing thermochromism, dapm and dppm dirhodium A-frame species containing trifluoromethylpyrazolate ligands have been examined. Increases in electronegativity of pyrazole substituents have been shown to cause decreases in the thermochromic isomerization temperature.

Examination of dirhodium-μ-hydroxypyridinato A-frame complexes has been undertaken to evaluate spectroscopic and structural effects of bifunctional asymmetric bridgehead ligands with π systems that might induce thermochromism similar to that of the pyrazolate complexes. Neither one-electron oxidized dirhodium-μ-hydroxypyridinato species nor those containing dpam or isocyanide could be isolated. Spectroscopic properties of the complexes synthesized were similar to those of dirhodium-μ-pyrazolato analogs. Fluxional behavior of μ-hydroxypyridinate ligands was characterized using ^{31}P

NMR. This fluxional behavior depends on the bis-transoid bridges and on the 6-substitution of the hydroxypyridinate ligand. Crystal structures of two dirhodium-μ-hydroxypyridinato compounds have shown that hydroxypyridinate coordination is bidentate in the solid state. The crystal structure of an unexpected trirhodium species, $[Rh_3(\mu\text{-dppm})_2(\mu\text{-CO})_3(CO)_3][PF_6]$, has been determined.

Fast atom bombardment (FAB) and collision-induced dissociation (CID) mass spectrometries were used to study certain dirhodium-μ-pyrazolato A-frame complexes. Both the atom beam and *m*-nitrobenzyl alcohol have been shown to promote redox reactions of certain of the complexes examined by FAB. Analysis of FAB spectra were complicated by species formed by beam- and matrix-induced damage. CID tandem mass spectrometry allowed more accurate structural interpretation. Dirhodium fragmentation can be understood by correlation with reactivities of similar complexes.

Kinetics of the disproportionation of the dirhodium (I,II) bis(isocyanide) complexes with halide in methylene chloride were examined. Complex reaction kinetics were not successfully modelled. A study of initial rates indicated the reaction to be first order in dirhodium(I,II) species and to depend on chloride in a variable but explicable fashion.

TABLE OF CONTENTS

LIST OF TABLES

LIST OF FIGURES

CHAPTER 1

INTRODUCTION

A. Purpose of Research

The study of binuclear metal complexes, such as those containing rhodium, offers interest to chemists who wish to examine the behavior of complexes with two metal centers as a complement to classical Wernerian (monomeric) coordination chemistry. Also of interest is the fact that certain rhodium and dirhodium complexes demonstrate biological activity,[1] such as antitumor behavior, while others exhibit catalytic activity,[2] in such reactions as the hydroformylation reaction. In some cases a dinuclear catalyst has been found to act at least four times as rapidly as its mononuclear counterpart[2a]:

$$R\text{-}CH{=}CH_2 \xrightarrow[H_2/CO]{catalyst} R\text{-}CH_2\text{-}CH_2\text{-}CHO\ [+\ R\text{-}\underset{\displaystyle CH_3}{\underset{|}{CH}}\text{-}CHO]$$

Although the specific dirhodium complexes to be discussed here have not been examined for catalytic or biological activity, the study of these complexes can contribute to the general understanding of and future applications for rhodium compounds. Specifically, this research was conducted to examine the

changes in spectroscopic properties and reactivities of a series of novel dirhodium(I,I) complexes by means of ligand substitution, ligand addition, and electrochemical oxidation. This series is included in a larger class of complexes whose structures, as shown below, are called A-frames.[3]

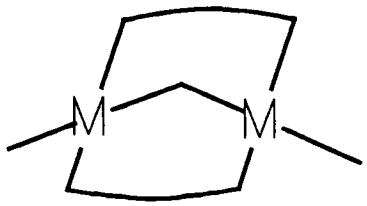

The core of this investigation involves the study of certain dirhodium complexes that contain bridgehead μ-pyrazolates. These complexes are bridged by the transoid ligands bis(diphenylarsino)methane (dpam), (diphenylarsino)(diphenylphosphino)methane (dapm), or bis(diphenylphosphino)-methane (dppm) and contain either terminal carbon monoxide (CO) or *tert*-butylisocyanide (*t*-BuNC) ligands.

The first part of the study involves two series of A-frame complexes. In the first series, transoid bis(dpam) bridged dirhodium species containing five different bridgehead μ-pyrazolates were compared with the analogous bis(dppm) complexes studied by Tortorelli[4] and the bis(dapm) complexes studied by DePriest.[5] This comparison is of interest because the bis(dpam) complexes have the largest intermetallic separation of the three types of bridged species[6] and because the arsines have been shown to be weaker donors than the corresponding phosphines.[7]

The second series studied was the pyrazolato-bridged dirhodium bis(dppm), bis(dapm), and bis(dpam) complexes containing at the bridgehead either μ-5-methyl-3-trifluoromethylpyrazolate (mtmp) or μ-3,5-bis(trifluoromethyl)-pyrazolate (btmp). The trifluoromethyl (CF_3) substitution to the pyrazolate ligands was made in order to study the effects of electronegative substituents on the pyrazolates.

The second part of the study involves similar syntheses and spectroscopic characterizations of dirhodium complexes, in which the symmetric pyrazolates have been replaced with asymmetric bridgehead ligands. This inquiry involved the use of 2-hydroxypyridinate and its 6-methyl- and 6-chloro- analogs to bridge the bis(dppm) and bis(dapm) dicarbonyl complexes.

The third area of investigation involves the use of fast atom bombardment (FAB) and collision-induced dissociation (CID) mass spectrometry (MS) to characterize selected dirhodium pyrazolates in *m*-nitrobenzyl alcohol (NBA). The utility of these techniques in characterizing these high molecular weight (i.e., $m/z > 10^3$) dirhodium complexes will be discussed.[8]

The final topic studied was the kinetics and possible mechanism of the disproportionation reaction of mixed valence rhodium dimers by using a stopped flow kinetics apparatus to mix the reactants and a diode array UV-Vis spectrophotometer to monitor the reaction. The disproportionation reaction

studied was of a green bis-isocyanide dirhodium (1.5) species in the presence of a halide ion ,X^-:

$$[Rh_2(1.5)\mu(E\hat{}E')_2\mu(Xpz)(t\text{-BuNC})_2](PF_6)_2 + X^- \rightarrow$$

$$\tfrac{1}{2}\,[Rh_2(II)\mu(E\hat{}E')_2\mu(Xpz)(t\text{-BuNC})_2X_2](PF_6) +$$

$$\tfrac{1}{2}\,[Rh_2(I,I)\mu(E\hat{}E')_2\mu(Xpz)(t\text{-BuNC})_2](PF_6),$$

where E^E' was the transoid bridging ligand dppm, dapm or dpam, Xpz was the bridgehead pyrazolate or substituted pyrazolate, and *t*-BuNC was *tert*-butylisocyanide.

B. Review of Literature

Dirhodium(I) species have been shown to be held together with many different mono- and bidentate bridging ligands. This review of relevant chemical literature will trace the development of dirhodium coordination chemistry and then focus on current reports of dirhodium(I) complexes containing bidentate bridges, especially A-frames containing dppm,[9] dapm, and dpam.

The discovery of rhodium occurred in 1803 when W. H. Wollaston isolated rose-colored rhodium salts (*rhodos*: Greek for a rose) from crude platinum extracts.[10] The initial discovery of an tertiary organophosphine was made by P. Thénard in 1847.[11] Bunsen reported tertiary organoarsine compounds beginning in 1837.[12] These classes of compounds and others, such as carbon

monoxide and the alkenes, act as π-acceptor ligands in complexes of Rh(I), d^8. The π-acceptor ligands are effective in stabilizing the low oxidation states of the metal.[13] Although extensive research into π-acid-rhodium complexes was conducted prior 1965, the major stimulus for current investigations into rhodium(I) compounds was the discovery of Wilkinson's catalyst, $Rh(I)Cl(P\phi)_3$, a selective homogeneous catalyst for alkene hydrogenation.[14] Also occurring near this time was a revolution in transition metal chemistry: the recognition of multicenter metal compounds, which was the result of the identification of "$[ReCl_4]^-$" as $[Re_3Cl_{12}]^{3-}$, a trinuclear species linked by three double bonds.[15]

The initial report identifying the bis-dppm and dpam transoid-bridged dirhodium compounds was by Mague and Mitchener and appeared in 1969.[16] These species were generally prepared from the CO reduction of $RhCl_3$ in refluxing ethanol to give $Rh(CO)_2Cl_2^-$, to which dppm or dpam was added (alternatively, the complexes can be formed from $Rh_2(\mu\text{-}Cl)_2(CO)_4$, as discussed in the experimental section). The products were assigned the structure $Rh_2(E\text{^}E')_2(CO)_2X_2$ (E^E' = dppm or dpam), which was based on a single-crystal X-ray diffraction study,[17] instead of the $[Rh(CO)Cl(dppm)_2]_n$ oligomeric species previously assigned.[18]

Although the oligomeric description of the dirhodium dppm and dpam complexes is incorrect,[19] the ability of dirhodium species to oligomerize with less bulky bidentate bridging ligands, such as 1,4-diisocyanopropane

(bridge),[20] has been established by studies of concentration-dependent 'proximity shifts' in the absorption spectra of the complexes.[21] In fact, the tendency for square planar rhodium(I) tetrakis(isocyanide) monomers to oligomerize has been shown to depend on the bulkiness of the isocyanide ligand.[22]

The first bis(μ-dapm) dirhodium species, $[RhCl(CO)(dapm)]_2$, was reported by Enlow and Woods in 1983.[23] Unlike the above dppm and dpam complexes, this complex contains a pair of asymmetric bridging ligands transoid to one another. This arrangement leads to the possibility of two isomeric forms shown below: head-to-head, HH, where each rhodium atom has an arsenic from one dpam ligand and a phosphorus atom from the other; and head-to-tail, HT, where one rhodium atom has the arsenic atom from both dpam ligands and the other rhodium atom has the phosphorus atom from both.

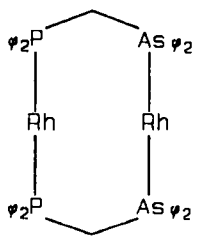

HH

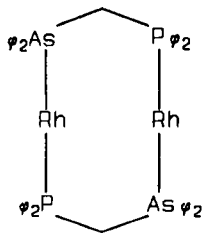

HT

In dirhodium complexes containing a pair of transoid ligands, the metal centers can also be bridged by mono- or bidentate ligands whose bonds are in the plane perpendicular to that of the transoid dppm ligands. These are called face-to-face complexes. In contrast to these early reports that described the

trans-dichlorodicarbonyl face-to-face complexes that could be thought of as two parallel Rh(I) square planes held together by the transoid bridging ligands, the two square planes of the tris-bridged complexes share the bridging apex ligand and are described by the term A-frame complexes. The examples of A-frame and face-to-face complexes are shown here[24] (A-frame to the left). It should be noted that the term dimer is no longer representative of the A-frame structure since it is no longer comprised of a pair of independent units.

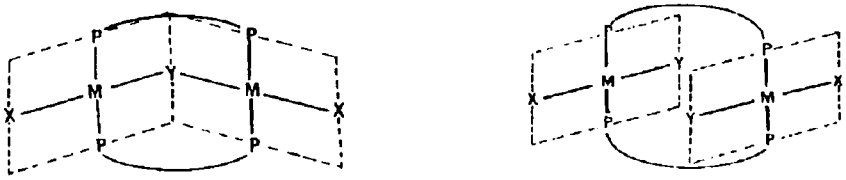

The first report of a dirhodium A-frame complex, $Rh_2(\mu\text{-}dppm_2)(\mu\text{-}S)(CO)_2$, was by Kubiak and Eisenberg,[3] who simply added solid Na_2S to a methanolic suspension of $Rh_2(\mu\text{-}dppm)_2(CO)_2Cl_2$ (this reaction is reversible upon the addition of HCl, releasing H_2S). Also proposed in that paper was the first double-A-frame structure for $Rh_2(\mu\text{-}dppm_2)(\mu\text{-}CO)_2(CO)_2I_2$, in which each rhodium atom is hexacoordinate. This dirhodium species is reported to be the product of the μ-S A-frame complex with iodomethane or iodoethane and then CO.

Having examined some of the early studies of dirhodium(I,I) complexes containing transoid dppm, dapm, or dpam ligands, more recent work involving dirhodium(I,I) species will be discussed (interim studies of transoid bridged complexes have been described by Tortorelli[4] and DePriest[5]). Neutral or

anionic bidentate ligands bridging dirhodium(I) species that are discussed in the current literature have Group 15 or 16 (Vb or VIb) atoms coordinated to the metal centers. These bridged complexes are generally stabilized by π-acids such as carbon monoxide (bridging or non-bridging), tertiary phosphines, or the chelating cycloocta-1,5-diene (COD) ligand.

In addition to transoid bis-bridged dirhodium complexes, there are many reports of dirhodium(I,I) complexes bridged by two cisoid ligands. These complexes have the two square coordination planes of the rhodium atoms in an "open book" configuration forming a 'V' and touching along the edge that contains the bridges, as shown below. Whether the cisoid or transoid configuration is favored appears to depend on the *trans*-directing ability and perhaps also on the steric bulkiness of the ligand. Both bridge orientations allow for similar metal-metal interactions.

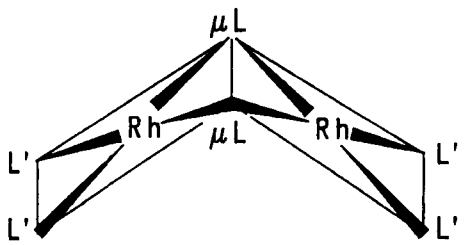

The literature reports involving the dirhodium(I) complexes with a pair of cisoid bridging ligands will be discussed and will be followed by a similar review of dirhodium(I) complexes with transoid bridges after a brief mention of an unusual but relevant dirhodium(I) species.

Interest in dirhodium(I) complexes with bidentate pyrazolate (pz) ligands led to the investigation presented in Chapter 3. Several other dirhodium(I) pyrazolate complexes, such as cisoid pz-bridged $Rh_2(\mu\text{-}pz)_2(COD)_2$ (COD = cyclooctadiene), have been reported in the literature.[25] A recent report of an unusual pz-containing dirhodium complex outlined the synthesis and crystal structure of (n-Bu_4N)[$Rh_2(CO)_4$Dcbp], whose nearly planar anion was formed by the reaction of the trianion of 3,5-pyrazoledicarboxylic acid, H_3Dcbp, with $[Rh(\mu\text{-}Cl)(COD)]_2$.[26] The crystal structure showed a very long Rh-Rh distance of 4.530 Å (Rh-Rh distance in $Rh_2(\mu\text{-}pz)_2(COD)_2$ is 3.267 Å).[27] The Dcbp pyrazolate N and carboxylate O^- bonds each occupy adjacent sites on each square planar Rh(I). The solution electrochemical data suggested that two one-electron irreversible oxidation processes occur and that electrochemical or chemical oxidation produces an insoluble product.

A type of dirhodium(I) species that contains a pair of bridging cisoid ligands is of the general form $[Rh(L)(\mu\text{-xhp})]_2$, where L is the terminal chelating ligands COD or norbornadiene, NBD, and xhp is an asymmetric bridging 6-substituted 2-hydroxypyridinate (as discussed in Chapter 4). The crystal structure of the bis(6-methyl-hp)-bridged species containing COD showed that the two μ-hp ligands are in a head-to-tail arrangement (each rhodium has a N of one hp *cis* to an O of the other), as shown below.[28] The Rh-Rh distance is 3.367 Å. In a similar report of the crystal structure of the bis(6-chloro-hp)-bridged (chp) species containing NBD terminal ligands, it was determined that the Rh-Rh

distance was 3.040 Å.[29] This decrease in the intermetallic distance is attributed to a decrease in the steric bulkiness of NBD compared to COD. The $[Rh(\mu\text{-chp})(NBD)]_2$ complex can be chemically oxidized with Ag(I) to give a $Rh_2(I,II)$ d^7-d^8 paramagnetic complex, whose Rh-Rh distance shrinks to 2.819 Å.

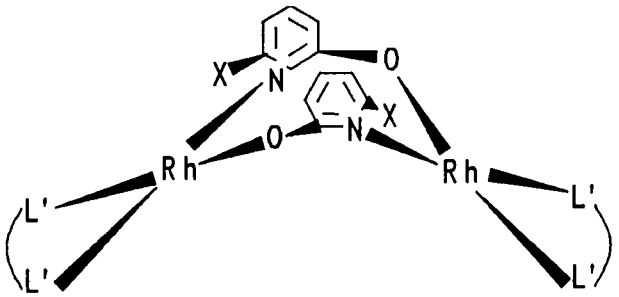

The COD or NBD ligands in this type of cisoid bis-bridged dirhodium(I) complexes are readily displaced by bubbling a solution of the complex with carbon monoxide. The complex $[Rh(\mu\text{-hp})(CO)_2]_2$ (hp = 2-hydroxypyridinate) can be prepared via this synthetic route.[30] The solution ultraviolet-visible (UV-Vis) spectra of the less sterically hindered tetracarbonyl species are not reported; therefore the presence of oligomers in solution and any associated proximity-shifted absorption bands is unknown. Oligomerization is revealed in the solid state via a single crystal X-ray diffraction (XRD) study; alternating short intramolecular and long intermolecular Rh-Rh distances occur at 2.899 and 3.410 Å, respectively.

In addition to the aforementioned procedure, the species $[Rh(\mu\text{-hp})(CO)_2]_2$ was prepared at a lower yield (45% versus 70%) by the reaction of

$[Rh(\mu\text{-}Cl)(CO)_2]_2$ with Khp in a methylene chloride and methanol ($MeCl_2$/MeOH) solution saturated with carbon monoxide.[31] When the reaction is performed under an inert atmosphere, the product is an unusual tetrarhodium complex, $[Rh_2(\mu\text{-}hp)_2(\mu\text{-}CO)(CO)_2]_2$, containing 60 valence electrons.[31] These rhodium environments are planar and form a parallelogram whose sides are 2.6197 Å and 3.0325 Å. A typical example of the lability of carbon monoxide in rhodium complexes is the interconversion in solution of the dirhodium and tetrarhodium species upon the removal or addition of CO. In fact, crystals of this Rh_4 species will form slowly from a solution of the dimer under an inert atmosphere. These crystals have been structurally characterized using XRD. The addition of two equivalents of dppm to a solution of $[Rh(\mu\text{-}hp)(CO)_2]_2$ is an alternate route to $[Rh_2(\mu\text{-}dppm)_2(\mu\text{-}hp)(CO)_2](PF_6)$,[31] a compound to be discussed in Chapter 4.

Another type of asymmetric ligand that may form similar cisoid bridges in dirhodium complexes are bidentate species containing $RNCS^-$ or $RSCS^-$ functionalities, such as 2-mercaptopyridinate (Spy). When compared with the initial A-frame μ-S complex and complexes with bridging monodentate thiolates (to be discussed below), dirhodium complexes synthesized with these ligands might be expected to actually contain monodentate bridges due to the relatively large size of the sulfur atom. This does not appear to be the case, however, as evidenced by the crystal structure of a 2-mercaptothiazolinate bis-bridged dirhodium(I) compound containing COD terminal ligands.[32] (The 2-mercaptothiazolinate ligand contains a five-membered 1,3-substituted-N,S-heterocycle.)

This complex contains the two 2-mercaptothiazolinates bridging in a head-to-tail cisoid arrangement, which keeps the Rh-Rh distance at 3.7154 Å.

Attempts to isolate a carbon monoxide analog of the dirhodium complex bridged by Spy bidentate bridges have been reported as unsuccessful.[33] However, similar asymmetric complexes containing cisoid bis(RNCS)-bridges have been characterized. Anions of thioacetanilide ($CH_3CSNHC_6H_5$) and its oxy-analog, acetanilide ($CH_3CONHC_6H_5$), have been shown to react with $[Rh(\mu\text{-}Cl)(CO)_2]_2$. The products are believed to be a mixture of HT and HH isomers. The sulfur-containing complex was less stable in any form than the corresponding acetanilidate-bridged complex. The redox properties of the dirhodium complex containing bis(acetanilido) bridges and two triphenylphosphine ($P\phi_3$) ligands are of interest because its electrochemical behavior is similar to the pyrazolate complexes to be discussed in Chapter 4. The cyclic voltammogram (CV) of the isomeric mixture of $[Rh(CO)(P\phi_3)(CH_3CONHC_6H_5)]_2$ dimers in methylene chloride/0.1 M tetra-*n*-butylammonium hexafluorophosphate ($MeCl_2$/TBAH) solutions shows reversible and irreversible one-electron oxidations at 0.04 and 1.22 volts versus the saturated calomel electrode:

$$Rh_2(I,I) \rightleftharpoons Rh_2(I,II) \rightarrow Rh_2(II,II)$$

The study of the complexes containing cisoid acetanilidate ligands was based on prior work involving complexes in which the rhodium centers were bridged by a pair of symmetric di-*p*-tolyltriazinidate (RNNNR) ligands in a cisoid

configuration.[34] The terminal *cis* ligands of the compounds studied include $P\phi_3$, triphenyl phosphine, 2,2'-bipyrdidine (bipy), and the readily displaced CO. These complexes displayed redox properties similar to the dirhodium(I,I) acetanilidate and pyrazolate species. The CVs of these species under the conditions described above display two or three one-electron processes that are generally reversible:[34c]

$$Rh_2(I,I) \rightleftharpoons Rh_2(I,II) \rightleftharpoons Rh_2(II,II) \rightleftharpoons Rh_2(II,III)$$

One-electron oxidation at the first anodic peak results in an isolable $Rh_2(I,II)(\mu\text{-RNNNR})_2$ species. The electron spin resonance (ESR) spectrum of $[Rh_2(\mu\text{-RNNNR})_2(CO)(P\phi_3)(bipy)](PF_6)$ displays one of two types of spectra depending on the solution concentration and the presence of molecular oxygen. These spectra are illustrated in Figure 1.[34c] The difference between these two spectra is attributed to the reversible formation of a superoxide species, $Rh_2(II,II)(O_2^-)$.[34c,d] In contrast, the $[Rh_2(\mu\text{-RNNNR})_2(CO)_2(bipy)](PF_6)$ complex appears to bind oxygen irreversibly,[34d] possibly due to loss of CO. The thermochromic behavior of certain paramagnetic species to be discussed in Chapter 3 has been compared to this superoxide formation, which was first identified in a tetrakis(anilopyridinate) dirhodium(II,III) species.[35]

The bidentate ligands discussed earlier that contained thio- groups differ from thiolate ligands containing a bridging sulfur atom. One recent report of a catalytically active rhodium dimer bridged by a pair of cisoid thiolate ligands

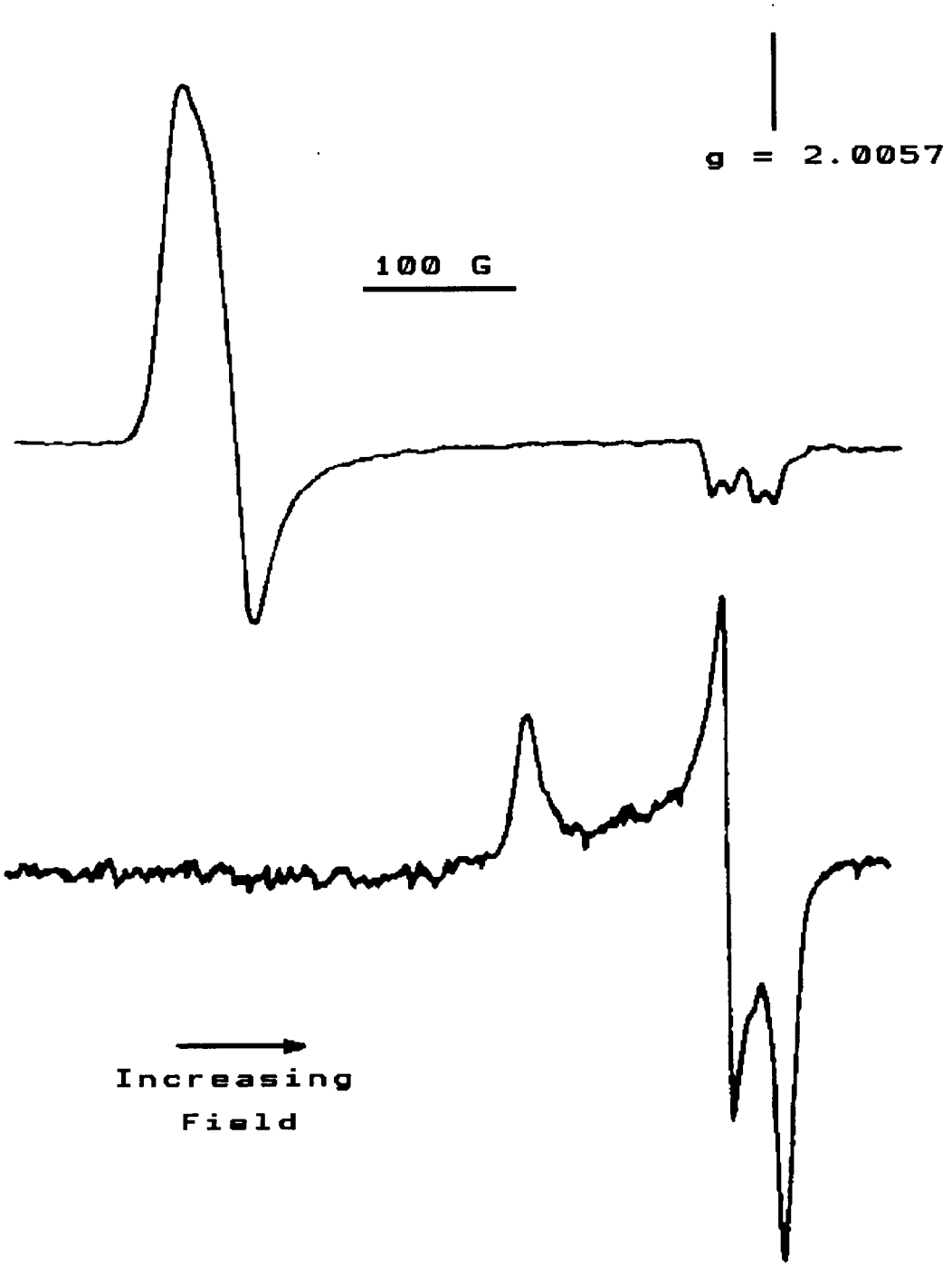

Figure 1. ESR of $Rh_2(I,II)(\mu\text{-}RNNNR)_2(CO)(P\phi_3)(bipy)^+$ at -110 °C and 1.1 x 10^{-2} M, degassed (top), and 1.5 x 10^{-4} M, oxygenated.[34c]

involved the reaction of $Rh_2(\mu\text{-}Cl)_2(CO)_4$ with one of three lead fluorothiolates, $Pb(SR)_2$ to form $Rh_2(\mu\text{-}SR)_2(CO)_4$ in yields of > 90%.[2c] A crystal structure determination found that the Rh-Rh distance is approximately 3.07 Å for the dimer containing *p*-fluorothiolate.

A similar dirhodium(I,I) tetracarbonyl complex containing one *t*-butylthiolate and one pyrazolate bridge in a cisoid configuration, $Rh_2(\mu\text{-}t\text{-}BuS)(pz)(CO)_4$, has been reported.[36] An alternate synthetic route to this species that is notable is also reported. This species can be synthesized by simply mixing an equivalent of $Rh_2(\mu\text{-}pz)_2(CO)_4$ and $Rh_2(\mu\text{-}t\text{-}BuS)_2(CO)_4$. The reaction of this species with one equivalent of dppm gives the triply-bridged species $Rh_2(\mu\text{-}dppm)(\mu\text{-}pz)(\mu\text{-}t\text{-}BuS)(CO)_2$.[37] The relative orientation of the three bridges is unknown because no structure determination has been reported. However, some sort of A-frame structure would be expected in order to maintain the square planar environment of the rhodium centers. A prediction based on the relative *trans* effects of the ligands would place the dppm ligand at the apex. The related reaction of $Rh_2(\mu\text{-}pz)_2(CO)_4$ with two equivalents of dppm gives the $[Rh_2(\mu\text{-}dppm)_2(\mu\text{-}pz)(CO)_2]^+$ complex.[38]

Having reviewed some current chemistry of dirhodium(I,I) complexes containing cisoid bis-bridges, the recent chemistry of complexes with transoid bridges will be examined below.

In addition to dppm, dapm, and dpam, other bidentate transoid π-acceptor ligands have been used to bridge the rhodium(I) centers. The ligand 2,5-diisocyano-2,5-dimethylhexane, didmh, forms a tetrakis dirhodium complex that reacts with two equivalents of dppm to form a complex with two pairs of transoid bridges.[39] Whereas the electrochemical behavior in aprotic solvents is unremarkable (no reversible couples have been observed), photochemical studies have demonstrated that this complex has the ability to undergo photoredox reactions in alkyl halide solvents:[40]

$$[Rh_2(dppm)_2(didmh)_2]^{2+} + 2CH_2Cl_2 \xrightarrow{h\nu} [Rh_2(dppm)_2(didmh)_2Cl_2]^{2+} + 2CH_2Cl\bullet$$

This is not unlike the classic photocatalytic ability of $[Rh_2(bridge)_2]^{2+}$ to produce H_2 in HCl solutions,[41] since in both instances there is strong tendency to oxidatively add Cl^-.

Another ligand that prefers the transoid configuration when bridging Rh(I) centers is 2-(diphenylphosphino)pyridine, dppp. In contrast to another asymmetric ligand, dapm, dppp forms only HT dirhodium complexes.[42] A recent report described the formation of a dirhodium (II,II) complex containing cisoid dppp ligands by the addition of two equivalents of dppp to $Rh_2(\mu\text{-}RNCNR)_2(\mu\text{-}O_2CCF_3)_2(H_2O)_2$ (RNCNR = N,N'di-*p*-tolylformamidate). This gave $Rh_2(\mu\text{-}RNCNR)_2(\mu\text{-}dppp)_2(O_2CCF_3)_2$, where the trifluoroacetate groups are monodentate axial ligands.[43] The formamidate groups are weak *trans* directors and thus lead to *cis* addition of dppp.

Literature reports of dppm bridged dirhodium species are by far the most common and generally involve A-frames. The chemical differences among analogous dppm, dapm, and dpam complexes concern the relative strengths of the P-Rh and As-Rh bonds[7] and the rhodium-rhodium distance.[6] The difference between the strengths of the P-Rh and As-Rh bonds is apparent in the synthesis of $[Rh_2(\mu\text{-}dppm_2)(RNC_4)]^{2+}$ and $[Rh_2(\mu\text{-}dpam)_2(RNC)_4]^{2+}$.[7] The complex containing dppm can be synthesized via the reaction of $[Rh(RNC)_4]^+$ with dppm;[44] whereas the dpam ligand will not displace the isocyanides. Also, the above dppm product can be made by the addition of RNC to a methanolic slurry of $[Rh(\mu\text{-}Cl)(COD)]_2$ and dppm; using dpam results in a mixture of the desired $[Rh_2(\mu\text{-}dpam)_2(RNC)_4]^{2+}$ and $[Rh(RNC)_4]^+$. Thus, it appears that the P-Rh bond is much stronger than the RNC-Rh bond, which is somewhat stronger than the As-Rh bond. These relative bond strengths will be discussed with the results of mass spectral studies in Chapter 5.

The variation in the intermetallic distance in the dppm, dapm, and dpam bis-bridged face-to-face complexes affects the overlap of orbitals that are responsible for the rhodium-rhodium interactions. The combination of the d_{z^2} and p_z orbitals causes splitting that lowers the energy gap between the highest occupied molecular orbital (HOMO) and lowest unoccupied molecular orbital (LUMO). This energy gap is responsible for the previously mentioned proximity (red) shift that is visible via UV-Vis spectroscopy. The interaction of two d^8 metal centers results in a net bond order of zero, because metal bonding and

antibonding orbitals are filled. The electronic states of face-to-face[45] and A-frame[46] dirhodium complexes have been examined in detail.

Several small molecules and anions have been used as apex ligands in recent studies involving A-frames. In addition to the pyrazole ligands used as apex bridges in the A-frame species discussed in Chapter 3, other pyrazolate-bridged complexes have been reported. The dirhodium(I,I) species with terminal CO or *t*-BuNC ligands undergo oxidative addition of the halogens Cl_2, Br_2, and I_2, or two-electron electrochemical oxidation in methylene chloride in the presence of Cl^-, Br^-, or I^- to form Rh_2(II,II) species.[6,38] These Rh_2(II,II) species have a metal-metal single bond that results from the removal of a pair of electrons from an antibonding orbital. Each Rh(II) center becomes hexacoordinate with the axial addition of the halide *trans* to the metal-metal bond. If the 4-position of the pz ligand is unsubstituted in the Rh(I) species, the addition of Br_2 or Cl_2 (but not I_2) leads to the simultaneous Br or Cl substitution at the metal and the formation of 4-bromo or 4-chloro-pyrazolate as the apex ligand in the Rh(II) complex.[6]

The reactions of RNC with $[Rh_2(\mu\text{-dppm})_2(\mu\text{-pz})(CO)_2I_2](PF_6)$ have been examined and show the expected lability of the CO ligands.[47] The terminal addition of one equivalent of RNC leads to the rearrangement of one CO from terminal to bridging and the breaking of the rhodium-rhodium bond. This asymmetric μ-CO complex can be isolated as a solid for the dppm complex but

not for the dpam complex, which loses the bridging CO upon precipitation. This instability is presumably due to the increased M-M separation. The bridging CO of either complex is readily lost by bubbling a solution with nitrogen, leaving a $Rh_2(II,II)$ complex with a metal-metal bond and terminal CO and RNC ligands. The addition of a second equivalent of RNC leads to the formation of a complex containing a bridging CO and two terminal RNC ligands. This μ-CO is also very labile. The crystal structures of $[Rh_2(\mu\text{-}dppm_2)pz_2(CO)_2I_2](PF_6)$ and $[Rh_2(\mu\text{-}dppm_2)pz_2(t\text{-}BuNC)_2I_2](PF_6)$ show Rh-Rh separations of 2.752 Å[38] and 2.829 Å,[47] respectively. The longer rhodium-rhodium distance of the bis(isocyanide) complex is likely due to the better σ donating and poorer π accepting ability of the *t*-BuNC ligands, which might result in increased electron density in the Rh antibonding orbitals.

Another interesting account of two $Rh_2(I,I)$ complexes containing pyrazolate bridges is the report of a tetrarhodium species that consists of two $Rh_2(\mu\text{-}dppm)_2(CO)_2$ backbones bridged by 3,3',5,5'-tetramethylbipyrazolate, tmbpz, ligand.[38] Conductivity studies have proved a cation/anion ratio of 1:2 in agreement with the formula $\{[Rh_2(\mu\text{-}dppm_2)(CO)_2]_2tmbpz\}(PF_6)$, but attempts at growing crystals suitable for XRD studies have been unsuccessful.[48]

Two A-frame apex ligands that are of interest because of their similarity to the xhp apex ligands to be discussed in Chapter 4 are imido and oxy ligands. The reaction of $Rh_2(\mu\text{-}dppm)_2Cl_2(CO)_2$ with two equivalents of $LiNHCH_3$ gives

the unusual amido complex, $Rh_2(\mu\text{-dppm})(\mu\text{-dppm-H})(\mu\text{-HNR})(CO)_2$, where dppm-H represents the methylene-deprotonated dppm ligand.[49] When the amido methyl group is replaced by a phenyl or *p*-tolyl group, which creates a more acidic amido group, the result is a mixture of the above μ-dppm-H complex and the bridging imido (μ-NR) A-frame complexes. The protonation of the dppm-H ligand and/or the imido ligand is reversibly accomplished by the addition of H^+ or its removal by LiNHR. Attempts to slowly grow crystals of the μ-phenylamido/imido complex in diethyl ether/toluene result in the formation of crystals of $Rh_2(\mu\text{-dppm})_2(\mu\text{-O})(CO)_2$. The oxy bridge apparently originates from trace water in the solvents. XRD of the crystal provided a structure that revealed a Rh-Rh distance of 3.082 Å and a (μ-O)-Rh distance of 2.083 Å.

In the initial report of hydroxy- and alkoxy-bridged dirhodium(I,I) dppm complexes, the (μ-OH) complex was synthesized via the protonation of the ethoxy-bridged complex using $HClO_4$ in EtOH. [13]. Alternately, the (μ-OHCl) bridged A-frame complex was prepared from $Rh_2(\mu\text{-dppm})_2Cl_2(CO)_2$ and Na_2CO_3 in aqueous ethanol. The alkoxy-bridged complexes are prepared from $Rh_2(\mu\text{-dppm})_2Cl_2(CO)_2$ and the alkoxide in the alcohol.

The (μ-OR) ligand is labile in acid solution and is readily replaced with small anionic ligands. The most interesting reactions involve the μ-OEt complex and NH_4NCS.[50] In acid solution one equivalent of NH_4NCS yields the unusual N-bound (μ-NCS) complex; without acid, one equivalent of NH_4NCS yields the

asymmetrical S-bound (μ-SCN) complex as revealed by the infrared active C≡N stretch of 2073 cm^{-1} and the AA'BB'XY pattern of the ^{31}P NMR. Additionally, the reaction of carbon monoxide with the (μ-NCS) complex gives a (μ-CN)(μ-CO) complex, while the reaction of CO with the (μ-SCN) complex leads to a complex mixture.[51] An additional equivalent of NH_4NCS to either thiocyanate bridged complex or two equivalents to the (μ-OEt) species results in the formation of $[Rh(dppm)(NCS)(CO)]_2$.

Attempts to react a (μ-OR)-bridged species in solution with CO under pressure resulted in the unexpected formation of a trinuclear rhodium species, $[Rh_3(\mu\text{-dppm})_2(\mu\text{-CO})_3(CO)_3][ClO_4]$.[52] The crystal structure of the hexafluorophosphate salt is reported in Chapter 4. The exception to this synthetic route is that when the solution of the μ-OHCl A-frame complex was exposed to CO under pressure the *trans*-$[Rh(dppm)(CO)Cl]_2$ species was formed.[51] The iridium analog undergoes a similar reaction, under milder conditions, that removes the apex μ-OHCl and oxidizes CO to CO_2. Gaseous byproducts could not be monitored during the pressurized reaction of the dirhodium complex.

Two reports of dirhodium(II,II) complexes containing a pair of cisoid dppm bridging ligands have been recently published.[53] The first report involves the reaction of a solution of $Rh_2(\mu\text{-dppm})_2(\mu\text{-CO})(CO)_2$ with one equivalent of a phenyl-substituted acetylene, $\phi C{\equiv}CR$ (R = H, ϕ), which results in the formation

of one of two products, depending on the reaction conditions. The reaction with excess $\phi C{\equiv}CH$ in toluene at room temperature gives a symmetric vinylidine A-frame species, $Rh_2(I,I)(\mu\text{-dppm})_2(\mu\text{-}C{=}CH\phi)(CO)_2$, which contains *trans*-dppm bridges and has a rhodium separation of 3.011 Å. Each Rh is in a square planar environment and receives a pair of electrons from the apex $C{=}CH\phi$ ligand. The reaction of a solution of $Rh_2(\mu\text{-dppm})_2(\mu\text{-CO})(CO)_2$ with one equivalent of $\phi C{\equiv}CR$ (R = H, ϕ) with refluxing for extended periods (R=H: 5 hours in acetone; R=ϕ: 48 hours in benzene) leads to the formation of a non-A-frame triply-bridged dirhodium complex, $Rh_2(\mu\text{-dppm})_2(\mu,\eta^2\text{-}\phi CCR)(CO)_2$, where the acetylene is bridged perpendicular to the metal-metal axis and donates two pairs of electrons to the octahedral rhodium centers. The inter-rhodium distance in the complex containing $\phi C{=}C\phi$ is 2.644 Å, which implies a single Rh(II)-Rh(II) bond. The most important feature of this structure, however, is the orientation of the dppm bridges. These ligands are cisoid, with P-Rh-P angles of approximately 118°. The cause of this rearrangement is not obvious but may be related to the steric influence of the perpendicular $\phi C{\equiv}C\phi$ ligand.

The other reports of dirhodium(II,II) complexes containing cisoid dppm complexes involve the product $Rh_2(II,II)(\mu\text{-dppm})(\mu\text{-Cl})_2Cl_2$.[53b] The first report involves the reaction of $Rh_2(II,II)(\mu\text{-}O_2CCH_3)_4$ with (a) two or (b) four equivalents of $(CH_3)_3SiCl$ (to remove acetate ligands and add chlorine to the complex) and two equivalents of dppm, resulting in (a) $Rh_2(II,II)(\mu\text{-}O_2CCH_3)_2(\mu\text{-dppm})_2Cl_2$ containing pairs of cisoid acetate and dppm bridges and terminal chloride

ligands, or (b) $Rh_2(II,II)(\mu\text{-dppm})_2(\mu\text{-Cl})_2Cl_2$ containing pairs of cisoid dppm and Cl bridges. The cisoid orientation of the bridging ligands in these complexes can be rationalized by the poor trans-directing ability of the acetate ligands in these synthetic reactions.

An alternate synthesis of $Rh_2(\mu\text{-dppm}_2)(\mu\text{-Cl})_2Cl_2$, a cisoid bis(dppm) complex, has been reported by the same author.[53c] In this synthesis, *trans*-$[Rh(dppm)(CO)Cl]_2$ is first electrochemically oxidized by two electrons in the presence of Cl^- to form $Rh(\mu\text{-dppm})_2(\mu\text{-Cl})Cl_3(CO)$. Reaction of this oxidation product with $(CH_3)_3NO$ at low temperature results in the formation of the $Rh_2(\mu\text{-dppm})_2(\mu\text{-Cl})_2Cl_2$.

Another interesting reaction of A-frame complexes involves the reported oxidative addition of tetrachloro-1,2-benzoquinone ($1,2\text{-}O_2C_6Cl_4$), to the A-frame complexes $Rh_2(\mu\text{-dppm})_2(\mu\text{-S})(CO)_2$ or $[Rh_2(\mu\text{-dppm})_2(\mu\text{-Cl})(CO)_2]^+$.[54] The A-frame product, $Rh_2(1,2\text{-}O_2C_6Cl_4)(\mu\text{-dppm})_2(\mu CO)(\mu\text{-S})(CO)$, or $Rh_2(1,2\text{-}O_2C_6Cl_4)(\mu\text{-dppm})_2(\mu CO)(\mu\text{-Cl})(CO)$ can be formulated as a $Rh_2(I,III)$ or a $Rh_2(II,II)$ complex, as is reported. The intermetallic distance was determined to be 2.964 Å, which is very long for a Rh-Rh bond. The $1,2\text{-}O_2C_6Cl_4$ bonds as a terminal chelate to one rhodium. The stretching frequency of the remaining terminal CO, which is on the other rhodium, increases by approximately 66 cm^{-1} in the chelated complex. A similar shift is reported for the stretching frequency of the terminal CO of a $Rh_2(I,I)$ species upon one- or two-electron oxidation.[38,55]

Earlier studies of a 1,2-$O_2C_6Cl_4$ dirhodium complex from the same researchers reported the formation of $Rh_2(1,2\text{-}O_2C_6Cl_4)(\mu\text{-dppm})_2(CO)$, which has a rhodium with 16 valence-electrons and a four-coordinate square planar geometry, bonded to a rhodium with 18 valence electrons and a five-coordinate square pyramidal geometry.[56] A crystal structure determination identified the Rh-Rh bond length as 2.637 Å.

This review of relevant literature illustrates the range of chemical behavior of dirhodium complexes and establishes a foundation for the discussion of the work presented in the following chapters.

CHAPTER 2

EXPERIMENTAL

A. Chemicals

1. *Gases*

a. *Argon, Ar*, MG Industries. Prepurified Ar was used as purchased.

b. *Carbon monoxide, CO*, MG Industries. Prepurified CO was used without further purification.

c. *Nitrogen, N_2*, MG Industries. Prepurified N_2 was used as purchased.

2. *Reagents*

a. *Pyrazole, Hpz*, Aldrich. Reagent grade Hpz was used as purchased.

b. *3,5-Dimethylpyrazole, H35dmpz*, Aldrich. Reagent grade H35dmpz was used as purchased.

c. *4-Bromo-3,5-dimethylpyrazole, H4b35pz*, Pfaltz and Bauer. Reagent grade H4b35pz was used as purchased.

d. *4-Methylpyrazole, H4mpz*, Aldrich. Reagent grade H4mpz was used as purchased.

e. *3,4,5-Tribromopyrazole, H345bpz.* H345bpz was prepared via the bromination (15 g, 0.09 mol) of Hpz (2 g, 0.03 mol) in 1 M aqueous potassium hydroxide solution (0.1 L) at 35° C for 1 hour. The product was precipitated by neutralization with acetic acid to pH 5-6 (pH paper) and twice purified by sublimation.[57]

f. *Hydrazine monohydrate*, Aldrich. Reagent grade hydrazine monohydrate was kept under inert atmosphere and used without further purification.

g. *1,1,1-Trifluoro-2,4-pentanedione*, Aldrich. Reagent grade 1,1,1-trifluoro-2,4-pentanedione was used as purchased.

h. *1,1,1,5,5,5-Hexafluoro-2,4-pentanedione*, Aldrich. Reagent grade 1,1,1,5,5,5-hexafluoro-2,4-pentanedione was used without further purification.

i. *5-Methyl-3-trifluoromethylpyrazole, Hmtmp.* Hmtmp was prepared by the dropwise addition of neat 1,1,1-trifluoro-2,4-pentanedione (25 g, 0.12 mol) to hydrazine monohydrate (7.2 g, 0.14 mol) in 0.2 L absolute ethanol at 5° C. The pyrazole was purified by recrystallization from toluene and then by sublimation.[58] Due to the extremely hygroscopic nature of the fluorinated methylpyrazole, a dry atmosphere was maintained throughout the synthesis, and the product was stored in a vacuum desiccator.

j. *3,5-Bis(trifluoromethyl)pyrazole, Hbtmp.* Hbtmp was prepared following the synthesis for Hmtmp, except 1,1,1,5,5,5-hexafluoro-2,4-pentanedione was used in place of 1,1,1-trifluoro-2,4-pentanedione.

k. Tert-*butylisocyanide*, t-*BuNC*, Aldrich. Reagent grade *t*-BuNC was stored under Ar and used as purchased.

l. *Ammonium hexafluorophosphate, NH_4PF_6*, Aldrich. NH_4PF_6 was dried at 100° C under vacuum and stored in a desiccator until used.

m. *Tetrabutylammonium iodide, TBAI*, Aldrich. Reagent grade TBAI was used without further purification.

n. *Tetrabutylammonium hexafluorophosphate, TBAH.* TBAH was prepared by the reaction of TBAI in minimum acetone with NH_4PF_6 in minimum acetone. TBAH was precipitated with water and recrystallized once with acetone/water and three times with hot ethanol.

o. *Silver hexafluorophosphate, $AgPF_6$*, Aldrich. Reagent grade $AgPF_6$ was stored in a desiccator in the dark and used under a dry atmosphere without further purification.

p. *Rhodium(III) chloride hydrate, $RhCl_3 \cdot xH_2O$*, was generously loaned to our research group by Johnson-Mathey. $RhCl_3 \cdot xH_2O$ was stored under vacuum and used as provided.

q. *Bis(diphenylphosphino)methane, dppm*, Strem. Reagent grade dppm was used without further purification.

r. *(Diphenylarsino)(diphenylphosphino)methane, dapm*. Dapm was made by the method described by Enlow and Woods.[23]

s. *Bis(diphenylarsino)methane, dpam*, Strem. Reagent grade dpam was used without further purification.

t. *Hydrochloric acid, HCl*, Mallinckrodt. A. C. S. grade 35% HCl was used as purchased.

u. *Perchloric acid, $HClO_4$*, Mallinckrodt. Reagent grade 70 weight% $HClO_4$ was used as purchased.

v. *Acetic acid, HOAc*, Mallinckrodt. Glacial HOAc was used as purchased.

w. *Potassium hydroxide, KOH*, Mallinckrodt. Reagent grade 85% KOH was used as purchased and weighed in a dry atmosphere.

x. *Nujol*, Plough. Nujol mineral oil was dried over sodium metal before use in making mulls for infrared spectra.

y. *Sodium*, Fisher. Reagent grade sodium metal was stored under hexanes and weighed in an inert atmosphere.

z. *Phosphorus pentoxide, P_2O_5*, Mallinckrodt. Reagent grade P_2O_5 was used as purchased.

aa. *pH paper*, Micro Essential Laboratory. A and B Phydrion Papers were used to estimate pH of aqueous solutions.

bb. *Calcium chloride*, $CaCl_2$, Mallinckrodt. Reagent grade anhydrous $CaCl_2$ was used as purchased.

cc. *Paratone N*, Exxon. Paratone N was used as provided.

3. *Solvents*

a. *Acetone*, Mallinckrodt. A. C. S. grade acetone was used as purchased.

b. *Ethanol*, Quantum Chemicals. Absolute ethanol, 200 proof, was used as purchased.

c. *Dichloromethane*, $MeCl_2$, Mallinckrodt. A. C. S. grade $MeCl_2$ was used without further purification except when used as a solvent for cyclic voltammetry. It was then dried over $CaCl_2$ and distilled from P_2O_5 immediately before use.

d. *Diethyl ether (anhydrous)*, Et_2O, Mallinckrodt. A. C. S. grade ether was used as purchased within one week after opening to reduce possible peroxide contamination.

e. *Hexanes*, Mallinckrodt. A. C. S. grade hexanes were used without further purification.

f. *Methanol*, Mallinckrodt. A. C. S. grade methanol was used as purchased.

g. *3-Nitrobenzyl Alcohol, NBA*, Aldrich. Reagent grade 3-nitrobenzyl alcohol was used as a matrix for mass spectrometry without further purification.

h. *Toluene*, Mallinckrodt. A. C. S. grade toluene was used as purchased.

i. *1,1,2,2-Tetrachloroethane*, Aldrich. Reagent grade 1,1,2,2-tetrachloroethane was used without further purification.

B. Spectroscopy

1. *Nuclear Magnetic Resonance (NMR)*

Proton-decoupled phosphorus, $^{31}P\{H\}$, NMR spectra were collected on the departmental JEOL FX90Q Fourier transform NMR spectrometer at 36.19 MHz using an external reference of 85% phosphoric acid. All samples were dissolved in degassed solvent, generally 1 mL $MeCl_2$ with enough sample to give as concentrated a solution as possible. Lock signal was provided by a sealed 5 mm tube containing d_6-acetone (Cambridge Isotopics) placed within the 10 mm tube (Wilmad) that contained the sample.

2. *Infrared Spectroscopy (IR)*

Infrared spectroscopy was performed on a Perkin-Elmer 1330 scanning infrared spectrometer, or either a Digilab FTS-20 C/V or a Biorad FTS-7 Fourier transform infrared spectrometer. Samples were prepared by grinding approximately 10 mg of solid compound into a thick mull with minimum Nujol. This mull was then spread between two sheets of polyethylene film (Gladwrap).

3. *Ultraviolet-Visible Spectroscopy (UV-Vis)*

UV-Vis spectra were obtained from either a Cary 219 spectrophotometer (Varian) or a HP8452A diode array spectrophotometer (Hewlett Packard) using quartz cells (Fisher Scientific) with a 1.0 cm path length. Certain time-dependent spectra were recorded on a Tracor-Northern TN-6500 diode array spectrophotometer. The $MeCl_2$ solvent was degassed with Ar unless otherwise noted. On all instruments the solvent was included in the blank determination.

4. *Electron Spin Resonance (ESR)*

ESR spectra were recorded on a JEOL JES-PE-1X spectrometer at the University of North Carolina at Charlotte. Solutions were made using $MeCl_2$/-toluene 4:1 by volume to freeze properly in liquid N_2.

5. *Mass Spectrometry (MS)*

Fast atom bombardment (FAB) and 8 keV collision induced dissociation (CID) mass spectra were obtained from 5-10 μL of a standard 10 mM NBA solution using the VG ZAB-EQ mass spectrometer located in the University of Tennessee Center for Mass Spectrometry.

C. Electrochemistry

1. *Electrochemical Cells*

The bottom of all cell compartments that contained the working electrode was a fine frit. An inert gas inlet was connected to the bottom of the working compartment to allow thorough purging of the $MeCl_2$/0.1 M TBAH supporting electrolyte solutions with either Ar or prepurified N_2. Another inlet above the solution protected the solution from the atmosphere. The purge gas was first bubbled through $MeCl_2$ to saturate it with $MeCl_2$ vapor and to reduce solvent loss from the working compartment. A single-compartment cell was used for cyclic voltammetry. A three-compartment "H" cell was used for bulk electrolysis. The "H" cell consisted of two outer compartments with the center compartment separating these working and counter-electrode compartments via two fine frits.

2. *Electrodes*

A three-electrode configuration was used for all electrochemical techniques. The reference electrode, a saturated calomel electrode (SCE), was separated from the working chamber by placing it in a fine-fritted filter stick that was filled with the electrolyte solution and placed within the working chamber. The working electrode for voltammetry was a 0.24 cm^2 platinum button (Beckman), and the counter was a small 2.8 cm^2 platinum grid. The working electrode for bulk electrolysis was a large 24 cm^2 platinum grid, and the counter electrode was a carbon rod.

3. *Instrumentation*

A BAS 100 Electrochemical Analyzer (Bioanalytical Systems) was used to perform bulk electrolysis and cyclic voltammetry. Cyclic voltammetry was performed using the default scan rate of 0.100 V/s unless otherwise noted, and voltammograms were plotted on the modified Houston Instruments DMP-40 plotter provided with the BAS 100.

D. Elemental Analysis

Elemental analyses were performed by Galbraith Laboratories, Inc., Knoxville, Tennessee.

E. Crystallographic Analysis

Single-crystal crystallographic analyses were performed on a Siemens R3mV diffractometer with a highly oriented graphite monochromator and a molybdenum X-ray tube. Air stable single crystals were mounted on a glass fiber with epoxy and were analyzed at ambient temperature. In order to isolate suitable single crystals from air-sensitive crystallization solutions and to then insure stability through the data collection, a few crystals in solution were pipetted into a small quantity of Paratone N, a viscous, high-molecular-weight hydrocarbon oil. A suitable crystal was then chosen with the aid of a microscope and transferred onto the end of a glass fiber mounted to a copper pin which was attached to the goniometer head. A coating of the oil on the crystal facilitated this transfer. The mounted crystal was immediately placed in a N_2 at -100° C stream by securing the goniometer on the diffractometer. In each case data were collected using the ω scan type over a 2Θ range of 4.0 to 55°. Unit cell parameters were calculated from the least-squares fit of thirty reflections

($28° \leq 2\Theta \leq 40°$). Three standard reflections (*h*00, 0*k*0, and 00*l*, when possible) were monitored throughout the data collection (every 97 reflections). Corrections for absorption were used.[59] SHELXTL PLUS structure solution software was used to solve crystal structures.[60] Patterson syntheses or direct methods were used for the initial identification of heavy atoms. All other non-hydrogen atoms were located by succeeding Fourier difference maps. Estimated standard deviations (esds) and bond lengths are given with errors in parentheses. Reported esds are taken as a minimum. The actual errors may be much as three times those reported.

F. Kinetics Studies

Kinetics studies were performed at room temperature ($23 \pm 2°$ C) using an Aminco-Morrow J4 stopped-flow apparatus modified with machined teflon to accept non-gas-tight syringes with luer tips made entirely of glass. A flow-through cell with a 1.0 cm path length was used. $MeCl_2$ was used as the solvent, and ionic strength was maintained at 0.1 M with TBAH. UV-Vis spectroscopy was used to monitor the progress of the reaction, and the resultant data were analyzed using Kinfit kinetics fitting routine (On Line Instrument Systems). Neutral density filters (0.5 and 1.0, Oriel) were used selectively to examine the influence of photon flux.

G. Spectroelectrochemical Studies

Spectroelectrochemical studies were carried out using the BAS 100 Electrochemical Analyzer, HP8452A diode array spectrophotometer, 0.1 cm path length quartz cell, and gold mesh working and counter (and SCE reference) electrodes.

H. Preparation of New (*1* - *39*) and Previously Reported (*40* - *53*) Dirhodium Complexes

1. *Dicarbonyl-μ-pyrazolato-N:N'bis[μ-methylenebis(diphenylarsine)-As:As']-dirhodium(I) hexafluorophosphate, $[Rh_2(\mu\text{-dpam})_2(CO)_2(\mu\text{-pz})](PF_6)$.*

Compound *1* was synthesized by the reaction of $[Rh_2(\mu\text{-dpam})_2(CO)_2(Cl)_2]$ (1.19 g, 1.00 mmol) with excess NH_4PF_6 (0.25 g, 1.5 mmol) in stirred acetone for one hour. Hpz (0.068 g, 1.00 mmol) was deprotonated with 0.10 M KOH in methanol (10 mL, 1.0 mmol KOH) and then added to the resulting suspension. After stirring for one hour, the red solution was evaporated to dryness under vacuum. The resulting solid was dissolved in minimum $MeCl_2$, filtered to remove KCl, and precipitated by the addition of 1:1 ether/hexanes to the cloud point.

The product was collected by suction filtration on a medium-fritted filter funnel and stored under vacuum.

IR (nujol mull): ν(CO), 1993 and 1970 cm^{-1}, ν(PF_6^-), 839 and 557 cm^{-1}. UV-Vis [λ_{max} (ε)]: 476 nm (9.6 x 10^2), 306 nm (1.5 x 10^2).

2. *Dicarbonyl-μ-3,5-dimethylpyrazolato-N:N'bis[μ-methylenebis-(diphenylarsine)-As:As']dirhodium(I) hexafluorophosphate, [Rh_2(μ-dpam)$_2$-(CO)$_2$(μ-35dmpz)](PF_6).*

Compound *2* was made with H35dmpz (0.096 g, 1.00 mmol) via the same route used for compound *1*.

IR (nujol mull): ν(CO), 1984 and 1971 cm^{-1} ν(PF_6^-), 839 and 557 cm^{-1}. UV-Vis [λ_{max} (ε)]: 471 nm (1.2 x 10^3), 307 nm (4.4 x 10^2).

3. *Dicarbonyl-μ-4-methylpyrazolato-N:N'bis[μ-methylenebis(diphenylarsine)-As:As']dirhodium(I) hexafluorophosphate, [Rh_2(μ-dpam)$_2$(CO)$_2$(μ-4mpz)](PF_6).*

Compound *3* was synthesized with H4mpz (0.082 g, 1.00 mmol) by the same method used for *1*.

IR (nujol mull): ν(CO), 1988 (sh) and 1976 cm^{-1} ν(PF_6^-), 839 and 557 cm^{-1}. UV-Vis [λ_{max} (ε)]: 476 nm (3.8 x 10^3), 304 nm (1.2 x 10^3).

4. *Dicarbonyl-μ-4-bromo-3,5-dimethylpyrazolato-N:N'bis[μ-methylenebis-(diphenylarsine)-As:As']dirhodium(I) hexafluorophosphate, [Rh_2(μ-dpam)$_2$-(CO)$_2$(μ-4b35pz)](PF_6).*

Compound *4* was synthesized with H4b35pz (0.175 g, 1.00 mmol) by the same method used for *1*.

IR (nujol mull): ν(CO), 1984 and 1968 cm^{-1} ν(PF_6^-), 839 and 557 cm^{-1}. UV-Vis [λ_{max} (ε)]: 473 nm (2.7 x 10^3), 306 nm (1.1 x 10^3).

5. *Dicarbonyl-μ-3,4,5-tribromopyrazolato-N:N'bis[μ-methylenebis(diphenyl-arsine)-As:As']dirhodium(I) hexafluorophosphate, [Rh_2(μ-dpam)$_2$(CO)$_2$(μ-345b-pz)](PF_6).*

Compound *5* was synthesized with H345bpz (0.305 g, 1.00 mmol) by the same method used for *1*.

IR (nujol mull): ν(CO), 1991 and 1979 cm^{-1}, ν(PF_6^-), 839 and 557 cm^{-1}. UV-Vis [λ_{max} (ε)]: 462 nm (1.4 x 10^3).

6. *Bis(t-butylisocyanide)-μ-pyrazolato-N:N'bis[μ-methylenebis(diphenyl-arsine)-As:As']dirhodium(I) hexafluorophosphate, [Rh_2(μ-dpam)$_2$(t-BuNC)$_2$(μ-pz)]-(PF_6).*

Compound *6* was made by the dropwise addition of *t*-BuNC (0.183 g, 2.20 mmol) to *1* (1.42 g, 1.00 mmol) in degassed acetone/$MeCl_2$/MeOH (1:1:1) under an inert atmosphere (Ar or N_2). The solution was stirred for one hour, reduced in volume under vacuum (followed by immediate degassing), and then a major impurity was removed by precipitation on the addition of ether to the cloud point. This impurity is tentatively identified as $Rh_2(\mu\text{-dppm})_2(t\text{-BuNC})_4$.[61] Compound *6* was then precipitated with additional ether. After collection on a medium-fritted filter funnel, the product was stored under vacuum.

IR (nujol mull): ν(*t*-BuNC), 2109 cm^{-1}, $\nu(PF_6^-)$, 839 and 557 cm^{-1}. UV-Vis [λ_{max} (ε)]: 497 nm (1.1 x 10^4), 315 nm (6.6 x 10^3).

7. *Bis(t-butylisocyanide)-μ-3,5-dimethylpyrazolato-N:N'bis[μ-methylene-bis(diphenylarsine)-As:As']dirhodium(I) hexafluorophosphate, [$Rh_2(\mu\text{-dpam})_2(t\text{-BuNC})_2(\mu\text{-35dmpz})](PF_6)$.*

Compound *7* was made from *2* (1.45 g, 1.00 mmol) via the synthetic route used to make *6*.

IR (nujol mull): ν(*t*-BuNC), 2102 cm^{-1}, $\nu(PF_6^-)$, 839 and 557 cm^{-1}. UV-Vis [λ_{max} (ε)]: 493 nm (7.6 x 10^3), 315 nm (9.6 x 10^3).

8. *Bis(t-butylisocyanide)-μ-4-methylpyrazolato-N:N'bis[μ-methylene-bis(diphenylarsine)-As:As']dirhodium(I) hexafluorophosphate, [Rh_2(μ-dpam)$_2$-(t-BuNC)$_2$(μ-4mpz)](PF_6).*

Compound *8* was made from *3* (1.43 g, 1.00 mmol) via the synthetic route used to make *6*.

IR (nujol mull): ν(*t*-BuNC), 2106 cm^{-1}, ν(PF_6^-), 839 and 557 cm^{-1}. UV-Vis [λ_{max} (ε)]: 496 nm (1.0 x 10^4), 316 nm (8.6 x 10^3).

9. *Bis(t-butylisocyanide)-μ-4-bromo-3,5-dimethylpyrazolato-N:N'bis-[μ-methylenebis(diphenylarsine)-As:As']dirhodium(I) hexafluorophosphate, [Rh_2(μ-dpam)$_2$(t-BuNC)$_2$(μ-4b35pz)](PF_6).*

Compound *9* was made from *4* (1.53 g, 1.00 mmol) via the synthetic route used to make *6*.

IR (nujol mull): ν(*t*-BuNC), 2104 cm^{-1}, ν(PF_6^-), 839 and 557 cm^{-1}. UV-Vis [λ_{max} (ε)]: 493 nm (1.1 x 10^4), 317 nm (1.1 x 10^4).

10. *Bis(t-butylisocyanide)-μ-3,4,5-tribromopyrazolato-N:N'bis[μ-methylene-bis(diphenylarsine)-As:As']dirhodium(I) hexafluorophosphate, [Rh_2(μ-dpam)$_2$-(t-BuNC)$_2$(μ-345bpz)](PF_6).*

Compound *10* was made from *5* (1.66 g, 1.00 mmol) via the synthetic route used to make *6*.

IR (nujol mull): ν(*t*-BuNC), 2107 cm^{-1} ν(PF_6^-), 839 and 557 cm^{-1}. UV-Vis [λ_{max} (ε)]: 480 nm (2.4 x 10^3), 308 nm (2.2 x 10^3).

11. *Bis(t-butylisocyanide)-μ-pyrazolato-N:N'bis[μ-methylenebis(diphenylarsine)-As:As']dirhodium(1.5) hexafluorophosphate, $[Rh_2(\mu\text{-dpam})_2(t\text{-BuNC})_2(\mu\text{-pz})](PF_6)_2$.*

To synthesize compound *11*, compound *6* was electrochemically oxidized by one electron in bulk (0.077 g, 0.050 mmol, 4.8 C) at +0.300 V in 0.1 M TBAH $MeCl_2$ solution. The green product was isolated from the TBAH supporting electrolyte by evaporation to dryness under reduced pressure, adding degassed MeOH, and stirring for 0.5 hour. The product that precipitated from MeOH was collected on a medium-fritted filter funnel and stored under vacuum.

IR (nujol mull): ν(*t*-BuNC), 2165 cm^{-1}, ν(PF_6^-), 839 and 557 cm^{-1}. UV-Vis [λ_{max} (ε)]: 608 nm (1.0 x 10^2), 435 nm (1.7 x 10^3). NIR [λ_{max} (ε)]: 1185 nm (2.0 x 10^2), 910 nm (5.7 x 10^2).

12. *Bis(t-butylisocyanide)-μ-3,5-dimethylpyrazolato-N:N'bis[μ-methylene-bis(diphenylarsine)-As:As']dirhodium(1.5) hexafluorophosphate, $[Rh_2(\mu\text{-dpam})_2(t\text{-BuNC})_2(\mu\text{-35dmpz})](PF_6)_2$.*

Compound *12* was prepared from *7* (0.078 g, 0.050 mmol) by one-electron oxidation at +0.275 V following the same methods used for *11*.

IR (nujol mull): ν(*t*-BuNC), 2166 and 2155 cm^{-1} ν(PF_6^-), 839 and 557 cm^{-1}. UV-Vis [λ_{max} (ε)]: 610 nm (1.8 x 10^2), 444 nm (2.5 x 10^3). NIR [λ_{max} (ε)]: 1190 nm (3.4 x 10^2), 925 nm (8.5 x 10^2). ESR: (133 K) g_{aniso} = 2.06, 2.00, 1.995.

13. *Bis(t-butylisocyanide)-μ-4-methylpyrazolato-N:N'bis[μ-methylene-bis(diphenylarsine)-As:As']dirhodium(1.5) hexafluorophosphate, $[Rh_2(\mu\text{-dpam})_2(t\text{-BuNC})_2(\mu\text{-4mpz})](PF_6)_2$.*

Compound *13* was prepared from *8* (0.077 g, 0.050 mmol) by one-electron oxidation at +0.300 V following the same methods used for *11*, except that this compound could not be isolated from the supporting electrolyte (TBAH) after oxidation of the dirhodium(I,I) complex.

UV-Vis [λ_{max}]: 610 nm, 442 nm. NIR [λ_{max}]: 1185 nm, 915 nm.

14. *Bis(t-butylisocyanide)-μ-4-bromo-3,5-dimethylpyrazolato-N:N'bis-[μ-methylenebis(diphenylarsine)-As:As']dirhodium(1.5) hexafluorophosphate, $[Rh_2(\mu\text{-dpam})_2(t\text{-BuNC})_2(\mu\text{-4b35pz})](PF_6)_2$.*

Compound *14* was prepared from *9* (0.082 g, 0.050 mmol) by one-electron oxidation at +0.350 V following the same methods used for *11*.

IR (nujol mull): ν(*t*-BuNC), 2168 and 2154 (sh) cm^{-1} ν(PF_6^-), 839 and 557 cm^{-1}. UV-Vis [λ_{max} (ε)]: 605 nm (6.1 x 10), 436 nm (9.4 x 10^2). NIR [λ_{max} (ε)]: 1150 nm (1.2 x 10^2), 915 nm (2.4 x 10^2). C-H analysis: (calculated/found) %C 43.81/42.32; %H 3.85/3.91.

15. *Bis(t-butylisocyanide)-μ-3,4,5-tribromopyrazolato-N:N'bis[μ-methylene-bis(diphenylarsine)-As:As']dirhodium(1.5) hexafluorophosphate, $[Rh_2(\mu\text{-dpam})_2(t\text{-BuNC})_2(\mu\text{-345bpz})](PF_6)_2$.*

Compound *15* was prepared from *10* (0.088 g, 0.050 mmol) by one-electron oxidation at +0.475 V following the same methods used for *11*.

IR (nujol mull): ν(*t*-BuNC), 2171 and 2160 (sh) cm^{-1} ν(PF_6^-), 839 and 557 cm^{-1}. UV-Vis [λ_{max} (ε)]: 615 nm (1.2 x 10^2), 440 nm (2.5 x 10^3). NIR [λ_{max} (ε)]: 1155 nm (3.1 x 10^2), 905 nm (6.5 x 10^2). ESR: (room temp.) g_{iso} = 2.17; (77 K) g_{aniso} = 2.06, 2.00, 1.996.

16. *Dicarbonyl-μ-5-methyl-3-trifluoromethylpyrazolato-N:N'bis[μ-methylenebis-(diphenylphosphine)-P:P']dirhodium(I) hexafluorophosphate, $[Rh_2(\mu\text{-dppm})_2(CO)_2(\mu\text{-mtmp})](PF_6)$.*

Compound *16* was synthesized by the dropwise addition of $mtmp^-$ (1.00 mmol), formed by the addition of 10 mL of 0.10 M KOH in methanol (1.0 mmol KOH) to Hmtmp (0.151 g, 1.00 mmol), to $[Rh_2(\mu\text{-dppm})_2(CO)_2(\mu\text{-Cl})](PF_6)$ (1.21 g, 1.00 mmol) in acetone. The product was isolated by the same procedure that was used for *1*.

IR (nujol mull): ν(CO), 1990.5 and 1975.1 cm^{-1}; $\nu(PF_6^-)$, 839 and 557 cm^{-1}. UV-Vis[λ_{max} (ε)]: 485 nm (9000). $^{31}P\{H\}$ NMR: δ, 17.34 ppm; J(Rh-P), 126.95 Hz.

17. *Dicarbonyl-μ-3,5-bis(trifluoromethyl)pyrazolato-N:N'bis[μ-methylene-bis(diphenylphosphine)-P:P']dirhodium(I) hexafluorophosphate, $[Rh_2(\mu\text{-dppm})_2(CO)_2(\mu\text{-btmp})](PF_6)$.*

Compound *17* was synthesized by the same method used for *16*, using Hbtmp (0.201 g, 1.00 mmol).

IR (nujol mull): ν(CO), 1996.3 and 1982.8 cm^{-1}; $\nu(PF_6^-)$, 839 and 557 cm^{-1}. $^{31}P\{H\}$ NMR: δ, 18.45 ppm; J(Rh-P), 124.511 Hz. UV-Vis [$\lambda_{max}(\varepsilon)$]:480 nm ($8 \times 10^3$).

18. *Dicarbonyl-μ-5-methyl-3-trifluoromethylpyrazolato-N:N'bis[μ-((diphenylarsino)(diphenylphosphino)methane)-As:P]dirhodium(I) hexafluorophosphate, $[Rh_2(\mu\text{-dapm})_2(CO)_2(\mu\text{-mtmp})](PF_6)$.*

Compound *18* was synthesized by the reaction of $[Rh_2(\mu\text{-dapm})_2(CO)_2(Cl)_2]$ (1.19 g, 1.00 mmol) with excess NH_4PF_6 (0.25 g, 1.5 mmol) with stirring for one hour. Mtmp$^-$, formed by the addition of 10 mL of 0.10 M KOH in methanol (1.0 mmol KOH) to Hmtmp (0.151 g, 1.00 mmol), was added to the resulting suspension, and the product was isolated by the same procedure that was used for *1*.

IR (nujol mull): ν(CO), 1992.5 and 1979.0 cm^{-1}; ν(PF_6^-), 839 and 557 cm^{-1}. $^{31}P\{H\}$ NMR: (head-to-tail), δ, 26.78 ppm, J(Rh-P), 148.93; (head-to-head) δ, 22.22 ppm; J(Rh-P), 124.51 Hz; J', 9.77 Hz. UV-Vis [$\lambda_{max}(\varepsilon)$]: 478 nm (1.7 x 10^4).

19. *Dicarbonyl-μ-3,5-bis(trifluoromethyl)pyrazolato-N:N'bis[μ-((diphenylarsino)(diphenylphosphino)methane)-As:P]dirhodium(I) hexafluorophosphate, $[Rh_2(\mu\text{-dapm})_2(CO)_2(\mu\text{-btmp})](PF_6)$.*

Compound *19* was synthesized by the same method used to prepare *18*, using btmp$^-$ (1.00 mmol).

IR (nujol mull): ν(CO), 1992.5 and 1977.0 cm^{-1}; ν(PF_6^-) 839 and 557 cm^{-1}. $^{31}P\{H\}$ NMR: (head-to-tail) δ, 26.16 ppm; J(Rh-P), 146.48 Hz; (head-to-head) δ, 20.10 ppm; J(Rh-P), 122.07 Hz. UV-Vis [$\lambda_{max}(\varepsilon)$]: 470 nm ($1.0 \times 10^4$).

20. *Dicarbonyl-μ-5-methyl-3-trifluoromethylpyrazolato-N:N'bis[μ-methylene-bis(diphenylphosphine)-P:P']dirhodium(1.5) hexafluorophosphate, $[Rh_2(\mu\text{-dppm})_2(CO)_2(\mu\text{-mtmp})](PF_6)_2$.*

Compound *20* was prepared from *16* (0.065 g, 0.050 mmol) by one-electron oxidation at +0.900 V following the same methods used for *11*.

IR (nujol mull): ν(CO), 2079.3 and 2034.9 cm^{-1}; ν(PF_6^-), 839 and 557 cm^{-1}. C-H analysis: (calculated/found) %C 46.58/45.27; %H 3.29/3.42.

21. *Dicarbonyl-μ-3,5-bis(trifluoromethyl)pyrazolato-N:N'bis[μ-methylene-bis(diphenylphosphine)-P:P']dirhodium(1.5) hexafluorophosphate, $[Rh_2(\mu\text{-dppm})_2(CO)_2(\mu\text{-btmp})](PF_6)_2$.*

Compound *21* was prepared from *17* (0.070 g, 0.050 mmol) by one-electron oxidation at +1.050 V following the same methods used for *11*.

IR (nujol mull): ν(CO), 2081.2 and 2038.8 cm^{-1}; ν(PF_6^-), 839 and 557 cm^{-1}. C-H analysis: (calculated/found) %C 44.93/43.34; %H 2.98/3.00.

22. *Dicarbonyl-μ-5-methyl-3-trifluoromethylpyrazolato-N:N'bis[μ-((diphenylarsino)(diphenylphosphino)methane)-As:P]dirhodium(1.5) hexafluorophosphate,* $[Rh_2(\mu\text{-dapm})_2(CO)_2(\mu\text{-mtmp})](PF_6)_2$.

Compound *22* was prepared from *18* (0.079 g, 0.050 mmol) by oxidation at +1.000 V following the same synthetic methods used for *11*.

IR (nujol mull): ν(CO), 2077.3 and 2034.9 cm^{-1}; ν(PF_6^-)839 and 557 cm^{-1}.

23. *Dicarbonyl-μ-3,5-bis(trifluoromethyl)pyrazolato-N:N'bis[μ-((diphenylarsino)(diphenylphosphino)methane)-As:P]dirhodium(1.5) hexafluorophosphate,* $[Rh_2(\mu\text{-dapm})_2(CO)_2(\mu\text{-btmp})](PF_6)_2$.

Compound *23* was prepared from *19* (0.082 g, 0.050 mmol) by oxidation at +1.100 V using the same procedure used for compound *11*.

IR (nujol mull): ν(CO), 2073.5 and 2034.9 cm^{-1}; ν(PF_6^-), 839 and 557 cm^{-1}.

24. *Bis(t-butylisocyanide)-μ-5-methyl-3-trifluoromethylpyrazolato-N:N'bis-[μ-methylenebis(diphenylphosphine)-P:P']dirhodium(I) hexafluorophosphate,* $[Rh_2(\mu\text{-dppm})_2(t\text{-BuNC})_2(\mu\text{-mtmp})](PF_6)$.

Compound *24* was made from *16* (1.33 g, 1.00 mmol) via the synthetic route used to make *6*.

IR (nujol mull): ν(*t*-BuNC), 2108.2 and 2071.5 (sh) cm^{-1}; ν(PF_6^-), 839 and 557 cm^{-1}. $^{31}P\{H\}$ NMR: δ, 18.32 ppm; J(Rh-P), 139.16 Hz. UV-Vis [$\lambda_{max}(\varepsilon)$]: 500 nm (1.7 x 10^4), 305 nm (1.8 x 10^4).

25. *Bis(t-butylisocyanide)-μ-3,5-bis(trifluoromethyl)pyrazolato-N:N'bis-[μ-methylenebis(diphenylphosphine)-P:P']dirhodium(I) hexafluorophosphate, [Rh_2(μ-dppm)$_2$(t-BuNC)$_2$(μ-btmp)](PF_6).*

Compound *25* was made from *17* (1.34 g, 1.00 mmol) via the synthetic route used to make *6.*

IR (nujol mull): ν(*t*-BuNC), 2110.1 and 2067.7 cm^{-1}; ν(PF_6^-), 839 and 557 cm^{-1}. $^{31}P\{H\}$ NMR: δ, 16.36 ppm; J(Rh-P), 139.16 Hz. UV-Vis [λ_{max} (ε)]: 495 nm (1.5 x 10^4), 300 nm (1.5 x 10^4).

26. *Bis(t-butylisocyanide)-μ-5-methyl-3-trifluoromethylpyrazolato-N:N'bis-[μ-((diphenylarsino)(diphenylphosphino)methane)-As:P]dirhodium(I) hexafluorophosphate, [Rh_2(μ-dapm)$_2$(t-BuNC)$_2$(μ-mtmp)](PF_6).*

Compound *26* was made from *18* (1.58 g, 1.00 mmol) via the synthetic route used to make *6.* Unlike the preparation of the dppm and dpam analogs, there appears to be little tendency to form $Rh_2(dapm)_2(t\text{-}BuNC)_4$ as an impurity in this synthesis, and thus the first crop isolated is the desired product.

IR (nujol mull): ν(*t*-BuNC), 2123.6 cm-1; ν(PF_6^-), 839 and 557 cm^{-1}. $^{31}P\{H\}$ NMR: (head-to-tail) δ, 26.39 ppm, J(Rh-P), 168.46 Hz; (head-to-head) δ,25.28 ppm; J(Rh-P), 141.61 Hz. UV-Vis [λmax(ε)]: 496 nm (1.4 x 10^4); 304 nm (1.7 x 10^4).

27. *Bis(*t*-butylisocyanide)-μ-3,5-bis(trifluoromethyl)pyrazolato-N:N'bis-[μ-((diphenylarsino)(diphenylphosphino)methane)-As:P]dirhodium(I) hexafluoro-phosphate, [Rh_2(μ-dapm)$_2$(t-BuNC)$_2$(μ-btmp)](PF_6).*

Compound *27* was synthesized from *19* (1.63 g, 1.00 mmol) via the same procedure used for *6*.

IR (nujol mull): ν(*t*-BuNC), 2114.0 cm^{-1}; ν(PF_6^-), 839 and 557 cm^{-1}. $^{31}P\{H\}$ NMR: (head-to-tail) δ, 25.82 ppm, J(Rh-P), 156.01 Hz; (head-to-head) δ, 24.138 ppm; J(Rh-P), 151.36 Hz. UV-Vis [λ_{max} (ε)]: 485 nm (1.1 x 10^4); 299 nm (1.8 x 10^4).

28. *Bis(*t*-butylisocyanide)-μ-5-methyl-3-trifluoromethylpyrazolato-N:N'bis-[μ-methylenebis(diphenylphosphine)-P:P']dirhodium(1.5) hexafluorophosphate, [Rh_2(μ-dppm)$_2$(t-BuNC)$_2$(μ-mtmp)](PF_6)$_2$.*

The green compound *28* was prepared from *24* (0.072 g, 0.050 mmol) by one-electron oxidation at +0.250 V following the same methods used for *11*.

IR (nujol mull): ν(*t*-BuNC), 2169.9 and 2158.3 (sh) cm^{-1}; ν(PF_6^-), 839 and 557 cm^{-1}. UV-Vis [$\lambda_{max}(\varepsilon)$]: 428 nm (1.8 x 10^4), 588 nm (9 x 10^2), 865 nm (6 x 10^2). ESR: (room temp.) g_1 = 2.0865; g_2 = 1.9421; (77 K): g_1 = 2.2130, g_2 = 2.1738, g_3 = 2.0696, g_4 =2.0081, g_5 =1.993.

29. *Bis(t-butylisocyanide)-μ-3,5-bis(trifluoromethyl)pyrazolato-N:N'bis-[μ-methylenebis(diphenylphosphine)-P:P']dirhodium(1.5) hexafluorophosphate, [Rh_2(μ-dppm)$_2$(t-BuNC)$_2$(μ-btmp)](PF_6)$_2$.*

Compound *29* was prepared from *25* (0.074 g, 0.050 mmol), by one-electron oxidation at +0.400 V following the same methods used for *11*.

IR (nujol mull): ν(*t*-BuNC), 2171.8 cm^{-1}; ν(PF_6^-), 839 and 557 cm^{-1}. UV-Vis [$\lambda_{max}(\varepsilon)$]: 420 nm (1.5 x 10^4), 580 nm (1.4 x 10^4), 860 nm (6.4 x 10^3). ESR: (room temp.) g_1 = 2.1533; g_2 = 2.0009: (77 K) g_1 = 2.2113, g_2 = 2.1731, g_3 = 2.0140.

30. *Bis(t-butylisocyanide)-μ-5-methyl-3-trifluoromethylpyrazolato-N:N'bis-[μ-((diphenylarsino)(diphenylphosphino)methane)-As:P]dirhodium(1.5) hexa-fluorophosphate, [Rh_2(μ-dapm)$_2$(t-BuNC)$_2$(μ-mtmp)](PF_6)$_2$.*

Compound *30* was prepared from *26* (0.079 g, 0.050 mmol) by one-electron oxidation at +0.350 V following the same methods used for *11*.

IR (nujol mull): ν(*t*-BuNC), 2169.9 and 2158.3 (sh), cm^{-1}; ν(PF_6^-), 839 and 557 cm^{-1}. UV-Vis: [$\lambda_{max}(\varepsilon)$] 425 nm (1.7 x 10^4), 580-650 nm (1.6 x 10^3), 870 nm (1.0 x 10^3). ESR: (room temp.) g_1 = 2.1366. C-H analysis: (calculated/found) %C 46.83/46.48; %H 3.99/4.06.

31. *Bis(*t*-butylisocyanide)-μ-3,5-bis(trifluoromethyl)pyrazolato-N:N'bis-[μ-((diphenylarsino)(diphenylphosphino)methane)-As:P]dirhodium(1.5) hexafluorophosphate, $[Rh_2(\mu\text{-dapm})_2(t\text{-BuNC})_2(\mu\text{-btmp})](PF_6)_2$.*

Compound *31* was prepared from *27* (0.082 g, 0.050 mmol) by one-electron oxidation at +0.450 V following the same methods used for *11*.

IR (nujol mull): ν(*t*-BuNC), 2169.9 cm^{-1}; ν(PF_6^-), 839 and 557 cm^{-1}. UV-Vis: ($\lambda_{max}(\varepsilon)$] 440 nm (1.1 x 10^4), 607 nm (1.5 x 10^3). ESR: (room temp.) g_1 = 2.1586;(77 K) g_1 = 2.0570, g_2 = 1.9994, g_3 = 1.9894. C-H analysis: (calculated/found) %C 45.34/43.06; %H 3.69/3.80.

32. *Dicarbonyl-μ-6-methyl-2-oxypyridinato-O:N-bis[μ-methylenebis(diphenylphosphine)-P:P']dirhodium(I) hexafluorophosphate, $[Rh_2(\mu\text{-dppm})_2(CO)_2(\mu\text{-mhp})](PF_6)$.*

Compound *32* was synthesized by the same method used for *16* except using mhp^-, which was formed by the addition of 10 mL of 0.10 M KOH in methanol (1.0 mmol KOH) to Hmhp (0.109 g, 1.00 mmol) .

IR (nujol mull): ν(CO), 1981 and 1968 cm^{-1}, ν(C=O) (2-pyridionate), 1600 cm^{-1} , ν(PF_6^-), 839 and 557 cm^{-1}. UV-Vis [λ_{max} (ε)]: 496 nm (7.6 x 10^3) , 302 nm (1.9 x 10^4). $^{31}P\{H\}$ NMR: δ, 22.25 ppm, J(Rh-P), 126.96 Hz.

33. *Dicarbonyl-μ-6-chloro-2-oxypyridinato-O:N-bis[μ-methylenebis(diphenylphosphine)-P:P']dirhodium(I) hexafluorophosphate, [Rh_2(μ-dppm)$_2$(CO)$_2$(μ-chp)]-(PF_6).*

Compound *33* was synthesized with Hchp (0.130 g, 1.00 mmol) by the same method used for *16.*

IR (nujol mull): ν(CO), 1986 and 1964 cm^{-1}, ν(C=O) (2-pyridionate), 1597 cm^{-1}, ν(PF_6^-), 839 and 557 cm^{-1}. UV-Vis [λ_{max} (ε)]: 494 nm (8.0 x 10^3), 292 nm (1.5 x 10^4). $^{31}P\{H\}$ NMR: δ, 22.05 ppm, J(Rh-P), 126.95 Hz.

34. *Dicarbonyl-μ-2-oxypyridinato-O:N-bis[μ-methylenebis(diphenylphosphine)-P:P']dirhodium(I) hexafluorophosphate, [Rh_2(μ-dppm)$_2$(CO)$_2$(μ-hp)](PF_6).*

Compound *34* was synthesized with Hhp (0.095 g, 1.00 mmol) under a CO atmosphere following the same method as for *16.*

IR (nujol mull): ν(CO), 1983 and 1966 cm^{-1}, ν(C=O) (2-pyridionate), 1607 cm^{-1}, ν(PF_6^-), 839 and 557 cm^{-1}. $^{31}P\{H\}$ NMR: very broad multiplet centered at δ= 23.80 ppm.

35. *Dicarbonyl-μ-6-methyl-2-oxypyridinato-O:N-bis[μ-((diphenylarsino)-(diphenylphosphino)methane)-As:P]dirhodium(I) hexafluorophosphate, $[Rh_2(\mu\text{-dapm})_2(CO)_2(\mu\text{-mhp})](PF_6)$.*

Compound *35* was synthesized in an inert atmosphere by the reaction of $[Rh_2(\mu\text{-dapm})_2(CO)_2(Cl)_2]$ (1.19 g, 1.00 mmol) with $AgPF_6$ (0.578 g, 2.00 mmol) by stirring in acetone in darkness for one hour. The solvent was removed via rotary evaporator, and 15 mL $MeCl_2$ was added. This suspension was filtered to remove AgCl, and mhp^- (1.00 mmol) was added to the resulting solution. The product was isolated by the procedures described for compound *1*.

IR (nujol mull): ν(CO), 1991 and 1969 cm^{-1}, ν(C=O) (2-pyridionate), 1604 cm^{-1}, ν(PF_6^-) 839 and 557 cm^{-1}. UV-Vis [λ_{max} (ε)]: 488 nm (1.1×10^4), 298 nm (2.1×10^4). $^{31}P\{H\}$ NMR: (-25°C) head-to-tail isomers: δ, 29.35 ppm, J(Rh-P), 148.95 Hz; δ, 26.36 ppm, J(Rh-P), 146.45 Hz; head-to-head isomers: δ, 24.71 ppm, J(Rh-P), 125.12 Hz; δ, 22.93 ppm, J(Rh-P), 127.02 Hz.

36. *Di(^{13}C)carbonyl-μ-6-methyl-2-oxypyridinato-O:N-bis[μ-((diphenylarsino)-(diphenylphosphino)methane)-As:P]dirhodium(I) hexafluorophosphate, [Rh_2(μ-dapm)$_2$(^{13}CO)$_2$(μ-mhp)](PF_6).*

Compound *36* was synthesized by the same method used for *35*, except ^{13}C enriched CO was used in the synthesis of the starting material, compound *40*.

IR (nujol mull): ν(CO), 1931 and 1913 cm^{-1}, ν(C=O), (2-pyridionate), 1598 cm^{-1}, ν(PF_6^-), 839 and 557 cm^{-1}. ^{31}P{H} NMR: (-25°C) head-to-tail isomers: δ, 28.95 ppm, J(Rh-P), 148.96 Hz, J(P-C), 14.7 Hz; δ, 27.17 ppm, J(Rh-P), 151.42 Hz, J(P-C), 14.7 Hz.

37. *Dicarbonyl-μ-6-chloro-2-oxypyridinato-O:N-bis[μ-((diphenylarsino)-(diphenylphosphino)methane)-As:P]dirhodium(I) hexafluorophosphate, [Rh_2(μ-dapm)$_2$(CO)$_2$(μ-chp)](PF_6).*

Compound *37* was synthesized with chp$^-$ (1.00 mmol) by the same method as *35*.

IR (nujol mull): ν(CO), 1983 and 1966 cm^{-1}, ν(C=O) (2-pyridionate), 1597 cm^{-1}, ν(PF_6^-), 839 and 557 cm^{-1}. UV-Vis [λ_{max} (ε)]: 490 nm (1.1 x 10^4), 294 nm (2.3 x 10^4). ^{31}P{H} NMR, head-to-tail isomer: δ, 24.04 ppm, J(Rh-P), 148.92 Hz.

38. *Dicarbonyl-μ-2-oxypyridinato-O:N-bis[μ-((diphenylarsino)(diphenylphosphino)methane)-As:P]dirhodium(I) hexafluorophosphate, $[Rh_2(\mu\text{-dapm})_2(CO)_2(\mu\text{-hp})](PF_6)$.*

Compound *38* was synthesized with hp^- (1.00 mmol) by the same method as *35*.

IR (nujol mull): ν(CO), 1978 and 1959 cm^{-1}, ν(C=O) (2-pyridionate), 1597 cm^{-1}, $\nu(PF_6^-)$, 839 and 557 cm^{-1}. $^{31}P\{H\}$ NMR, head-to-tail isomer: δ, 30.36 ppm, J(Rh-P), 148.92. Hz; head-to-head isomer: δ, 23.40 ppm, J(Rh-P), 131.83 Hz.

39. *Bis[μ-methylenebis(diphenylphosphine)-P:P']-tri-μ-carbonyl-tricarbonyl-triangulo-trirhodium(I) hexafluorophosphate, $[Rh_3(\mu\text{-dppm})_2(CO)_3(\mu\text{-CO})_3](PF_6)$.*

Compound *39* was formed during an attempt to grow crystals of *34* in $MeCl_2$/hexanes saturated with CO. The perchlorate analog of this trirhodium species was first reported by Deraniyagala and Grundy.[52]

40. *Di-μ-chlorobis(dicarbonylrhodium(I)), $Rh_2(\mu\text{-Cl})_2(CO)_4$.*

$Rh_2(\mu\text{-Cl})_2(CO)_4$ was prepared by passing CO saturated with ethanol over $RhCl_3 \cdot xH_2O$ that had been placed in a fritted chamber that had been heated to 100° C and was allowed to remain at this temperature for three hours.

The resulting rose-red solid was purified by sublimation at 75° C onto a cold finger chilled by ice/water. The product was stored in a desiccator.

41. *Dicarbonyl-μ-chlorobis[μ-methylenebis(diphenylphosphine)-P:P']-dirhodium(I) hexafluorophosphate,* $[Rh_2(\mu\text{-dppm})_2(CO)_2(\mu\text{-Cl})](PF_6)$.

This material, which was the precursor for dimers that contain μ-dppm transoid bridging ligands, was made via the synthesis of Mague and Sanger,[62] except that dry NH_4PF_6 was used in place of sodium tetraphenylborate.

42. *Dicarbonyldichlorobis[μ-methylenebis(diphenylarsine)-P:P']dirhodium(I),* $[Rh_2(\mu\text{-dpam})_2(CO)_2(Cl)_2]$.

This material, which was used to prepare dimers that contain μ-dpam ligands, was made by the dropwise addition of 2 equivalents of dpam to one equivalent of Rh_2-$(\mu\text{-Cl})_2(CO)_4$, both in minimum toluene. The product precipitated from the stirred solution and was recrystallized from acetone/ether.

43. *Dicarbonyldichlorobis[μ-((diphenylarsino)(diphenylphosphino)methane)-As:P]dirhodium(I),* $[Rh_2(\mu\text{-dapm})_2(CO)_2(Cl)_2]$.

This material was used to prepare dimers that contain μ-dapm transoid bridges. The synthesis was identical to that used for *42*, except that dapm was used in place of dpam.[5]

44. *Dicarbonyl-μ-4-bromo-3,5-dimethylpyrazolato-N:N'bis[μ-methylenebis-(diphenylphosphine)-P:P']dirhodium(I) hexafluorophosphate, $[Rh_2(\mu\text{-dppm})_2(CO)_2(\mu\text{-4b35pz})](PF_6)$.*

This dimer was synthesized via the method described by Tortorelli.[4]

45. *Bis(t-butylisocyanide)-μ-4-bromo-3,5-dimethylpyrazolato-N:N'bis-[μ-methylenebis(diphenylphosphine)-P:P']dirhodium(I) hexafluorophosphate, $[Rh_2(\mu\text{-dppm})_2(t\text{-BuNC})_2(\mu\text{-4b35pz})](PF_6)$.*

This dimer was synthesized via the method described by Tortorelli.[4]

46. *Dicarbonyl-μ-4-bromo-3,5-dimethylpyrazolato-N:N'bis[μ-methylenebis-(diphenylphosphine)-P:P']dirhodium(I,II) hexafluorophosphate, $[Rh_2(\mu\text{-dppm})_2(CO)_2(\mu\text{-4b35pz})](PF_6)_2$.*

This dimer was synthesized via the method described by Tortorelli.[4]

47. *Bis(t-butylisocyanide)-μ-4-bromo-3,5-dimethylpyrazolato-N:N'bis-[μ-methylenebis(diphenylphosphine)-P:P']-dirhodium(I,II) hexafluorophosphate, $[Rh_2(\mu\text{-dppm})_2(t\text{-BuNC})_2(\mu\text{-4b35pz})](PF_6)_2$.*

This dimer was synthesized via the method described by Tortorelli.[4]

C-H analysis: (calculated/found) %C 48.65/48.20; %H 4.27/4.22.

48. *Bis(t-butylisocyanide)-μ-3,5-dimethylpyrazolato-N:N'bis[μ-methylene-bis(diphenylphosphine)-P:P']dirhodium(I,II) hexafluorophosphate, $[Rh_2(\mu\text{-dppm})_2(t\text{-BuNC})_2(\mu\text{-35dmpz})](PF_6)_2$.*

This dimer was synthesized via the method described by Tortorelli.[4]

49. *Dicarbonyl-μ-4-bromo-3,5-dimethylpyrazolato-N:N'bis[μ-((diphenylarsino)(diphenylphosphino)methane)As:P]dirhodium(I) hexafluorophosphate, $[Rh_2(\mu\text{-dapm})_2(CO)_2(\mu\text{-4b35pz})](PF_6)$.*

This dimer was synthesized via the method described by DePriest.[5]

50. *Bis(t-butylisocyanide)-μ-4-bromo-3,5-dimethylpyrazolato-N:N'bis-[μ-((diphenylarsino)(diphenylphosphino)methane)-As:P]dirhodium(I) hexafluorophosphate, $[Rh_2(\mu\text{-dapm})_2(t\text{-BuNC})_2(\mu\text{-4b35pz})](PF_6)$.*

This dimer was synthesized via the method described by DePriest.[5]

51. *Dicarbonyl-μ-4-bromo-3,5-dimethylpyrazolato-N:N'bis[μ-((diphenylarsino)(diphenylphosphino)methane)-As:P]dirhodium(I,II) hexafluorophosphate,* $[Rh_2(\mu\text{-dapm})_2(CO)_2(\mu\text{-4b35pz})]\ (PF_6)_2$.

This dimer was synthesized via the method described by DePriest.[5]

C-H analysis: (calculated/found) %C 46.12/45.12; %H 4.05/4.09.

52. *Bis(t-butylisocyanide)-μ-4-bromo-3,5-dimethylpyrazolato-N:N'bis-[μ-((diphenylarsino)(diphenylphosphino)methane)-As:P]dirhodium(I,II) hexafluorophosphate,* $[Rh_2(\mu\text{-dapm})_2(t\text{-BuNC})_2(\mu\text{-4b35pz})](PF_6)_2$.

This dimer was synthesized via the method described by DePriest.[5]

53. *Bis(t-butylisocyanide)-μ-3,5-dimethylpyrazolato-N:N'bis[μ-((diphenylarsino)(diphenylphosphino)methane)-As:P]dirhodium(I,II) hexafluorophosphate,* $[Rh_2(\mu\text{-dapm})_2(t\text{-BuNC})_2(\mu\text{-35dmpz})](PF_6)_2$.

This dimer was synthesized via the method described by DePriest.[5]

CHAPTER 3

EXAMINATION OF PYRAZOLATO-BRIDGED DIRHODIUM COMPLEXES

This study of dirhodium-μ-pyrazolato A-frame complexes, as illustrated below in Figure 2, was carried out in order to assess the relative effects of ligand modifications and one-electron oxidation on the chemical properties of these types of compounds. The first aspect of the study of these complexes involved the synthesis and characterization of a series of bis-bridged dirhodium compounds containing transoid bis(diphenylarsino)methane (dpam). The second aspect of the study involved an inquiry into the thermochromic behavior that was noted in the one-electron oxidized complexes. Section A focuses on complexes containing dpam bridges and one of four of its pyrazolate or methylated and/or brominated pyrazolate derivatives. Described in section B are two trifluoromethyl-substituted pyrazolato-bridged complexes that contain the transoid ligands bis(diphenylphosphino)methane (dppm) or (diphenylarsino)-

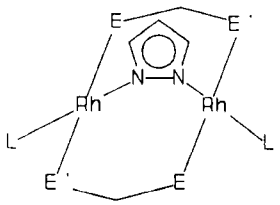

Figure 2. Structure of a Pyrazolato-bridged Dirhodium A-frame Complex (E^E' is the transoid bridge and L is the terminal ligand).

(diphenylphosphino)methane (dapm). The complexes contain carbon monoxide (CO) or *tert*-butylisocyanide (*t*-BuNC) as terminal ligands.

A. Bis(diphenylarsino)methane Bridged Dirhodium Complexes

Each dpam bridged dirhodium complex that was studied contained one of the five bridgehead μ-pyrazolates illustrated below in Figure 3. Anions of pyrazole (pz), 3,5-dimethylpyrazole (35dmpz), 4-methylpyrazole (4mpz), 4-bromo-3,5-dimethylpyrazole (4b35pz), and 3,4,5-tribromopyrazole (345bpz) were used in the synthesis of the $Rh_2(I,I)$ dicarbonyl and of the $Rh_2(I,I)$ and $Rh_2(I,II)$ bis(isocyanide) complexes. The fifteen dpam-containing species studied are listed in Table I. The trends to be noted in the discussion of these compounds parallel those observed in the studies of the bis(diphenylphosphino)methane (dppm) analogs by Tortorelli[4] and of the (diphenylphosphino)(diphenylarsino)-

	X	Y
pz	H	H
35dmpz	Me	H
4mpz	H	Me
4b35pz	Me	Br

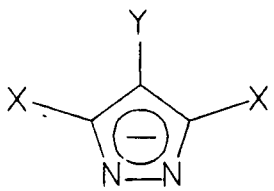

Figure 3. Pyrazolates Discussed in Section A.

Table I

Bis(dpam)dirhodium Compounds Discussed in Chapter 3, Section A.

1. $[Rh_2(\mu\text{-dpam})_2(CO)_2(\mu\text{-pz})](PF_6)$
2. $[Rh_2(\mu\text{-dpam})_2(CO)_2(\mu\text{-35dmpz})](PF_6)$
3. $[Rh_2(\mu\text{-dpam})_2(CO)_2(\mu\text{-4mpz})](PF_6)$
4. $[Rh_2(\mu\text{-dpam})_2(CO)_2(\mu\text{-4b35pz})](PF_6)$
5. $[Rh_2(\mu\text{-dpam})_2(CO)_2(\mu\text{-345bpz})](PF_6)$
6. $[Rh_2(\mu\text{-dpam})_2(t\text{-BuNC})_2(\mu\text{-pz})](PF_6)$
7. $[Rh_2(\mu\text{-dpam})_2(t\text{-BuNC})_2(\mu\text{-35dmpz})](PF_6)$
8. $[Rh_2(\mu\text{-dpam})_2(t\text{-BuNC})_2(\mu\text{-4mpz})](PF_6)$
9. $[Rh_2(\mu\text{-dpam})_2(t\text{-BuNC})_2(\mu\text{-4b35pz})](PF_6)$
10. $[Rh_2(\mu\text{-dpam})_2(t\text{-BuNC})_2(\mu\text{-345bpz})](PF_6)$
11. $[Rh_2(\mu\text{-dpam})_2(t\text{-BuNC})_2(\mu\text{-pz})](PF_6)_2$
12. $[Rh_2(\mu\text{-dpam})_2(t\text{-BuNC})_2(\mu\text{-35dmpz})](PF_6)_2$
13. $[Rh_2(\mu\text{-dpam})_2(t\text{-BuNC})_2(\mu\text{-4mpz})](PF_6)_2$
14. $[Rh_2(\mu\text{-dpam})_2(t\text{-BuNC})_2(\mu\text{-4b35pz})](PF_6)_2$
15. $[Rh_2(\mu\text{-dpam})_2(t\text{-BuNC})_2(\mu\text{-345bpz})](PF_6)_2$

methane (dapm) analogs by DePriest.[5] When compared to these previously studied complexes, the dpam-containing dirhodium complexes are of interest because the intermetallic distance is the largest of the three classes, i.e., Rh-Rh separation increases as dpam > dapm > dppm species.[6]

Four analytical tools were used to characterize the dpam-containing dirhodium complexes: infrared spectroscopy (IR) to monitor the environment of the terminal ligands, cyclic voltammetry to study electrochemical behavior, electron spin resonance spectroscopy (ESR) to examine the magnetic behavior of $Rh_2(I,II)$ d^7-d^8 isocyanide-containing species, and ultraviolet-visible spectroscopy (UV-Vis) to observe electronic behavior. One drawback unique to the study of the dpam complexes, compared to the dppm and dapm complexes, is the inability to obtain useful NMR information because arsenic, unlike phosphorus, is non-magnetic.

The compounds were synthesized via the reaction of hydrated $RhCl_3$ with carbon monoxide to form $Rh_2(\mu\text{-}Cl)_2(CO)_4$, which was then used to make $Rh_2(\mu\text{-dpam})_2(CO)_2Cl_2$, the starting material for the pyrazolate A-frame complexes. The μ-pyrazolato-bridged dicarbonyl complexes were synthesized from the reaction of $Rh_2(\mu\text{-dpam})_2(CO)_2Cl_2$ with the potassium salt of the appropriate pyrazolate and a twofold excess of NH_4PF_6.

The corresponding isocyanide complexes were synthesized from the carbonyl complexes. In order to displace the pair of carbon monoxide terminal

ligands (good π-acids) with a isocyanide (a better σ donor), 2.2 equivalents of the neat *tert*-butylisocyanide (10% excess) were added to a solution of the dicarbonyl species. A larger excess of the isocyanide tended to displace the bridging pyrazolate, especially if the ligand were less basic, i.e., those containing electronegative bromine atoms, 4b35pz or 345bpz. Insufficient isocyanide resulted in incomplete displacement of CO, leaving an inseparable mixture of the bis(isocyanide) and isocyanide-carbonyl compounds.

These difficulties with the isocyanide syntheses were apparent from the spectra, especially in the infrared (IR) spectrum where the unique C≡O and C≡N stretching frequencies can be monitored. IR spectroscopy provides a good means of monitoring the environment of the rhodium since stretches of the terminal ligands are infrared active and very sensitive to slight changes in the metal's electronic environment. This sensitivity results from the π-backbonding between the metal and the terminal ligands.

For the dirhodium (I) complexes containing carbon monoxide (*1-5*), a pair of characteristic C≡O stretching frequencies is centered in the range of 1993 to 1968 cm^{-1}, as listed in Table II. For the isocyanide-containing complexes, a C≡N stretch just above 2100 cm^{-1} is seen for the dirhodium (I) species (*6-10*). A blue shift (towards higher energy) of approximately 60 cm^{-1} is seen upon one-electron electrochemical oxidation, as illustrated in complexes *11-15*. This

Table II

Infrared Data for Chapter 3, Section A

	Compound[a]	$\nu_{(CO)}$	$\nu_{(NC)}$, cm^{-1}
1.	*$[Rh_2(\mu\text{-dpam})_2(CO)_2(\mu\text{-pz})](PF_6)$*	1993	
		1970	
2.	*$[Rh_2(\mu\text{-dpam})_2(CO)_2(\mu\text{-35dmpz})](PF_6)$*	1984	
		1971	
3.	*$[Rh_2(\mu\text{-dpam})_2(CO)_2(\mu\text{-4mpz})](PF_6)$*	1988(sh)	
		1976	
4.	*$[Rh_2(\mu\text{-dpam})_2(CO)_2(\mu\text{-4b35pz})](PF_6)$*	1984	
		1968	
5.	*$[Rh_2(\mu\text{-dpam})_2(CO)_2(\mu\text{-345bpz})](PF_6)$*	1991	
		1979	
6.	*$[Rh_2(\mu\text{-dpam})_2(t\text{-BuNC})_2(\mu\text{-pz})](PF_6)$*		2109
7.	*$[Rh_2(\mu\text{-dpam})_2(t\text{-BuNC})_2(\mu\text{-35dmpz})](PF_6)$*		2102
8.	*$[Rh_2(\mu\text{-dpam})_2(t\text{-BuNC})_2(\mu\text{-4mpz})](PF_6)$*		2106
9.	*$[Rh_2(\mu\text{-dpam})_2(t\text{-BuNC})_2(\mu\text{-4b35pz})](PF_6)$*		2104
10.	*$[Rh_2(\mu\text{-dpam})_2(t\text{-BuNC})_2(\mu\text{-345bpz})](PF_6)$*		2107
11.	*$[Rh_2(\mu\text{-dpam})_2(t\text{-BuNC})_2(\mu\text{-pz})](PF_6)_2$*		2165
12.	*$[Rh_2(\mu\text{-dpam})_2(t\text{-BuNC})_2(\mu\text{-35dmpz})](PF_6)_2$*		2166
			2155
14.	*$[Rh_2(\mu\text{-dpam})_2(t\text{-BuNC})_2(\mu\text{-4b35pz})](PF_6)_2$*		2154(sh)
			2168
15.	*$[Rh_2(\mu\text{-dpam})_2(t\text{-BuNC})_2(\mu\text{-345bpz})](PF_6)_2$*		2160(sh)
			2171

[a] Spectra taken as Nujol mulls sealed between polyethylene sheets.

increase in the terminal ligand stretching frequency as the metal electron density decreases is indicative of the metal-terminal ligand π-backbonding.

Cyclic voltammetry was then used to study the electrochemical behavior of the $Rh_2(I)(dpam)_2$ pyrazolates. As represented in Figure 4, cyclic voltammograms (CVs) in 0.1M tetrabutylammonium hexafluorophosphate in methylene chloride (TBAH/$MeCl_2$) displayed two redox couples. The first is a quasi-reversible single-electron couple at positive potentials ranging from roughly 0.9 to 1.0 volts (versus SCE) for the carbonyl complexes and 0.2 to 0.5 volts (versus SCE) for the isocyanide complexes. The second couple in the CV is a quasi- or irreversible single-electron couple occurring at potentials that are 0.2 to 0.5 volts more positive. This redox behavior was found to be qualitatively similar to the corresponding dppm and dapm complexes. Peak potentials for compounds *1-10* are listed in Table III.

The comparable ease of oxidation observed for the isocyanide- versus the carbonyl-containing complexes can be explained by the decrease in backbonding capacity of the isocyanide ligands. This indicates a relative stabilization of the highest occupied molecular orbital (HOMO) in the dicarbonyl compounds. One-electron oxidation of the dpam-containing complexes was more difficult than that of the corresponding dapm and dppm analogs due to the higher oxidation potentials of the dpam-containing complexes.[6] In other words, the greater the rhodium-rhodium separation, the greater the potential required

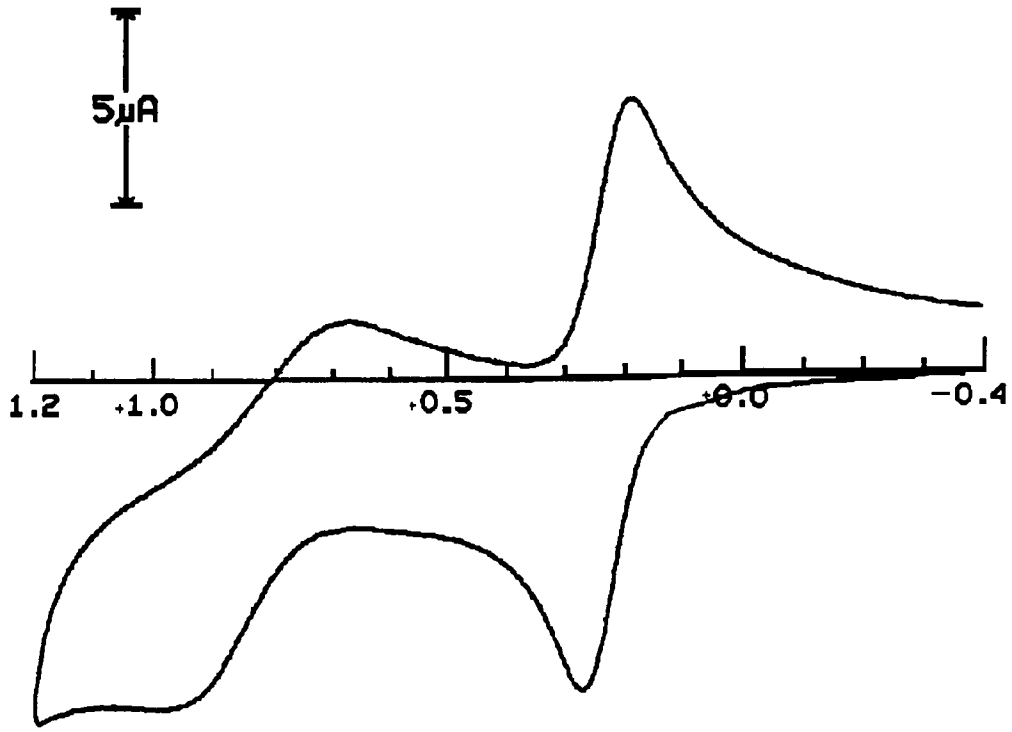

Figure 4. A Cyclic Voltammogram of *7* in 0.1 M TBAH/$MeCl_2$ (V vs. SCE).

Table III

Peak Potentials (mV vs. SCE) of Bis(dpam)dirhodium (I,I) Complexes in 0.1 M TBAH/$MeCl_2$

Compound	$E_{p1,a}$ [a]	$E_{p1,c}$	$E_{p2,a}$	$E_{p2,c}$
1.	1035	846	1172	-[b]
2.	920	836	1250	1100
3.	955	842	1150	-[b]
4.	997	900	1289	1150
5.	1130	845	1271	-[b]
6.	278	201	902	625
7.	258	183	996	680
8.	275	200	911	667
9.	314	231	902	676
10.	656	439	1034	760

[a] $E_{pn,a/c}$ = Potential of peak **n**; a, c = anodic and cathodic peaks, respectively.

[b] These cathodic peaks were not well defined.

to remove an electron. This denotes a greater stabilization of the HOMO in the dpam complexes and thus is indicative of a metal-based antibonding HOMO for all three transoid bridged dirhodium classes.

Each rhodium begins as a d^8 in $Rh_2(dpam)_2(CO)_2(Cl)_2(I,I)$ compound, which results in the metal-metal orbital interaction as $\sigma^2\pi^4\delta^2\delta^{*2}\pi^{*4}\sigma^{*2}$, with a net bond order of zero. Although the A-frame distortion of the μ-pyrazolate addition alters the δ-orbital overlap, the d^8-d^8 HOMO likely remains an antibonding orbital of largely metal character. The theoretical A-frame model of d^7 dirhodium complexes by Hoffman and Hoffman[46] contains a LUMO of b_2 symmetry. Therefore, the d^8 HOMO may be assigned as an orbital with b_2 symmetry that is primarily metal antibonding. The two anodic waves seen in the CVs may thus be attributed to the losses of antibonding electrons, resulting in Rh-Rh bond orders of one-half and one, respectively.

Selective one-electron oxidation at the first anodic wave of the isocyanide-containing species afforded the electrosynthesis of a paramagnetic green mixed-valence $Rh_2(I,II)(t\text{-BuNC})_2$ pyrazolate complex. Because the mixed-valence species was somewhat insoluble in methanol, separation of unoxidized starting material and TBAH supporting electrolyte is easily achieved.

It is interesting to note that, unlike the dppm and dapm series, the dpam-containing dirhodium (I,II) dicarbonyl complexes could not be isolated due to the spontaneous reduction back to the $Rh_2(I,I)$ in methanol. The complex

$Rh_2(I,II)(4mpz)(t\text{-}BuNC)_2$ is the only mixed-valence isocyanide species that exhibits the same behavior.

Since the $Rh_2(I,II)(t\text{-}BuNC)_2$ pyrazolate complexes are paramagnetic, ESR spectroscopy was used to probe their electronic properties. Both room-temperature solution and frozen-solution (4:1 $MeCl_2$/toluene) ESR spectra were recorded for *12* and *15*. Room-temperature ESR spectra exhibited isotropic signals at *g* values of roughly 2.17. No discernible hyperfine splitting was observed in either spectrum.

While preparing the solutions for low-temperature ESR study, reversible thermochromic behavior was observed; the solutions, which were green at room temperature, turned red-orange upon cooling to approximately -100°C and remained so down to -196°C. The green high-temperature and red-orange low-temperature forms observed will be designated as the α and β isomers, respectively. While the frozen-solution ESR spectra at -140°C of *12* and its dapm analog showed signals of both the α and β isomers, the solutions displayed the red-orange color of the β isomer. The frozen-solution ESR spectra of the β isomers of *12* and *15* at -196°C exhibited anisotropic signals, comprised of three components with *g* values of roughly 2.06, 2.00, and 1.99. These spectra are similar to the dapm analogs of *12* and *15*, and the dppm analog of *12*. In contrast, the dppm analog of *15* remained green and showed no trace of its β isomer down to -196°C.[55]

Examination of the ESR spectra of dpam-, dapm-, and dppm-containing complexes led to the discovery of two features that lead to the lowering of the α to β transition temperature: (1) the substitution of arsenic atoms with phosphorus atoms in the transoid bridge, i. e., $\alpha \rightarrow \beta$ transition temperature varies as dpam > dapm > dppm complexes, and (2) the bromination of the pyrazolate ligand. The second feature aroused speculation as to the cause of variation in transition temperature. The likely mode of the influence of the bromine substituent is either a resonance effect involving the filled *p* orbitals of the bromine atom and the aromatic π orbitals of the pyrazolate, or an inductive effect of the electronegative bromine atoms on the pyrazolate ring. This question prompted further study and will be resolved in section B.

The change in color and ESR spectra with decreasing temperature of the $Rh_2(I,II)(t\text{-BuNC})_2$ complexes is indicative of either structural or electronic isomerization. ESR results for the dppm-containing analogs[55] suggested that unpaired spin density was located on the pyrazolate ligand. This suggests that the HOMO is a ligand-based orbital in the β isomer.

For an electronic isomerization, the thermochromic and accompanying ESR spectral behavior would be indicative of a shift in relative orbital energies for a pair of orbitals that includes the metal-metal antibonding HOMO of the α isomer and a nearby ligand-based orbital. If filled in the α isomer, the ligand-based orbital would become the half-filled HOMO in the β isomer. This addition

of one electron to the metal antibonding orbital would change the net metal-metal bond order to zero and result in a $Rh_2(I,I)$ complex. If this ligand-based HOMO of the low-temperature β isomer were normally unoccupied in the α isomer, then a decrease in temperature would result in a transfer of the electron from the room-temperature HOMO and a half-filled ligand-based HOMO for the β isomer. This temperature-induced transition would thus result in a full metal-metal bond and a $Rh_2(II,II)$ complex with an odd-electron ligand.

Since dinuclear Rh(I) and Rh(II) complexes can be readily differentiated spectroscopically, evidence of electronic α-β isomerism might be detected by frozen-solution IR and/or UV-Vis spectroscopy. Attempts to conduct low-temperature UV-Vis spectroscopy of the β isomer were unsuccessful, and no significant change was observed by Tortorelli in the low-temperature infrared spectra of the β isomers.[55] Tortorelli's observation suggests that the temperature-dependent isomerization is likely structural in nature.

Another interesting note is that only solutions of the paramagnetic complexes exhibited near-infrared (NIR) transitions, as reported in Table IV with the UV-Vis data. These transitions imply that there are occupied orbitals with energies near that of the HOMO. The UV-Vis spectra of the green mixed-valence complexes are dominated by absorbances near 440 nm.

The most prominent feature in the UV-Vis spectra of the $Rh_2(I,I)(CO)_2$ pyrazolate complexes, *1-5*, is the highest wavelength band with λ_{max} of

Table IV

UV-Vis-NIR Spectroscopic Data for Chapter 3, Section A.

Compound	λ_{max} (ε)	λ_{max} (ε)
1.	476 nm (9.6×10^2)	306 nm (1.5×10^2)
2.	471 nm (1.2×10^3)	307 nm (4.4×10^2)
3.	476 nm (3.8×10^3)	304 nm (1.3×10^3)
4.	473 nm (2.7×10^3)	306 nm (1.1×10^3)
5.	462 nm (1.4×10^3)	
6.	497 nm (1.1×10^4)	315 nm (6.6×10^3)
7.	493 nm (7.6×10^3)	315 nm (9.6×10^3)
8.	496 nm (1.0×10^4)	316 nm (8.6×10^3)
9.	493 nm (1.1×10^4)	317 nm (1.1×10^4)
10.	480 nm (2.4×10^3)	308 nm (2.2×10^3)
11.	608 nm (1.0×10^2)	435 nm (1.7×10^3)
	1185 nm (2.0×10^2)	910 nm (5.7×10^2)
12.	610 nm (1.8×10^3)	444 nm (2.5×10^3)
	1190 nm (3.4×10^2)	925 nm (8.5×10^2)
13.[a]	610 nm	442 nm
	1185 nm	915 nm
14.	605 nm (6.1×10^2)	436 nm (9.4×10^2)
	1150 nm (1.2×10^2)	915 nm (2.4×10^2)
15.	615 nm (1.2×10^2)	440 nm (2.5×10^3)
	1155 nm (3.1×10^2)	905 nm (6.5×10^2)

[a] This compound could not be isolated from TBAH.

approximately 470 nm. The dirhodium (I,I) isocyanide complexes, *6-10*, have a maximum absorbance at roughly 490 nm. These absorbances are assigned to the HOMO $\rightarrow$ LUMO transitions. There is a red shift in the UV-Vis transition energy for the isocyanide complexes relative to the carbonyl complexes. As previously mentioned, the carbonyl ligands are superior to the isocyanides as π-acids and thus are better at accepting electron density from the rhodium atoms. This stronger interaction stabilizes the metal-based HOMO of the carbonyl-containing complex compared to that of the isocyanide-containing complex. The higher energy HOMO for the bis(isocyanide) complex explains the observation that the HOMO $\rightarrow$ LUMO transition occurs at longer wavelengths than in analogous dicarbonyl complexes only if a LUMO of relatively constant energy is assumed for both types of complexes. This suggests that the LUMO has little or no terminal ligand character.

B. Dirhodium Complexes Containing Apex Trifluoromethyl-pyrazolates

The second series of μ-pyrazolato-dirhodium complexes examined in this study consisted of compounds which had either μ-5-methyl-3-trifluoromethyl-pyrazolate (mtmp) or μ-3,5-bis(trifluoromethyl)pyrazolate (btmp) at the bridgehead, as shown below in Figure 5. The primary purpose of the study described in this section was to investigate how the pyrazolate bromine substituents influenced the thermochromic α-β transition temperature for the mixed-valence isocyanide-containing complexes described in section A. This mode of interaction was likely either (1) a resonance interaction of the bromine's filled *p* orbitals with the π orbitals of the aromatic pyrazolate, or (2) an inductive effect of the bromine atoms on the pyrazolate. Trifluoromethyl (CF_3-) substitution to the pyrazole was made to give complexes with an electronegative substituent on the pyrazole ring similar to that of the brominated dppm- and dapm-containing complexes discussed by Tortorelli[4] and DePriest.[5] The CF_3-groups, however, lack bromine's ability to interact with the pyrazolate π system.

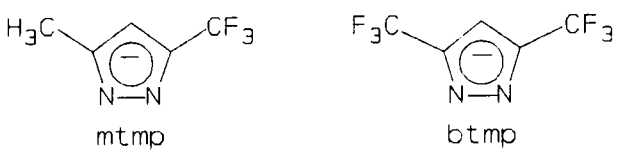

Figure 5. Apex Pyrazolate Bridges Used in Section B.

This section involves the study of dirhodium mtmp and btmp complexes containing a pair of either dppm or dapm transoid bridges and a pair of carbonyl or *tert*-butylisocyanide terminal ligands. Table V lists the sixteen complexes studied in section B. The $Rh_2(I,I)(dppm)_2$ complexes were synthesized from $[Rh_2(\mu\text{-}dppm)_2(\mu Cl)(CO)_2](PF_6)$ and the selected potassium pyrazolate. The $Rh_2(I,I)(dapm)_2$ complexes were synthesized in the same manner as the $Rh_2(I,I)(dpam)_2$ complexes discussed in section A. The μ-mtmp and μ-btmp $Rh_2(I,II)$ complexes were electrochemically synthesized and isolated as discussed in the previous section.

The spectroscopic techniques used in section A were also used to examine the CF_3-pyrazolate complexes: IR to monitor the C≡O and *t*-BuN≡C electron density, CV to study the redox behavior, ESR to examine dirhodium(I,II) d^7-d^8 species, and UV-Vis to monitor the electronic transitions. Additionally, ^{31}P NMR was used to observe the magnetic environment of the rhodium-bound phosphorus atoms of the dppm and dapm transoid bridges.

The btmp and mtmp complexes exhibit the same unique C≡O and C≡N infrared stretching frequencies noted in the previous section. Table VI lists the infrared frequencies observed for the CF_3-containing compounds. For rhodium(I,I) complexes with the carbonyl terminal ligands, a pair of characteristic C≡O stretching frequencies appear in the range of 1996 to 1975 cm^{-1}. Upon one-electron electrochemical oxidation to a $Rh_2(I,II)$ complex, each $\nu_{(C\equiv O)}$ is blue

Table V

μ-Trifluoromethyl-pyrazolate Dinuclear Rhodium Complexes Discussed in Chapter 3, Section B.

16.	$[Rh_2(\mu\text{-dppm})_2(CO)_2(\mu\text{-mtmp})](PF_6)$
17.	$[Rh_2(\mu\text{-dppm})_2(CO)_2(\mu\text{-btmp})](PF_6)$
18.	$[Rh_2(\mu\text{-dapm})_2(CO)_2(\mu\text{-mtmp})](PF_6)$
19.	$[Rh_2(\mu\text{-dapm})_2(CO)_2(\mu\text{-btmp})](PF_6)$
20.	$[Rh_2(\mu\text{-dppm})_2(CO)_2(\mu\text{-mtmp})](PF_6)_2$
21.	$[Rh_2(\mu\text{-dppm})_2(CO)_2(\mu\text{-btmp})](PF_6)_2$
22.	$[Rh_2(\mu\text{-dapm})_2(CO)_2(\mu\text{-mtmp})](PF_6)_2$
23.	$[Rh_2(\mu\text{-dapm})_2(CO)_2(\mu\text{-btmp})](PF_6)_2$
24.	$[Rh_2(\mu\text{-dppm})_2(t\text{-BuNC})_2(\mu\text{-mtmp})](PF_6)$
25.	$[Rh_2(\mu\text{-dppm})_2(t\text{-BuNC})_2(\mu\text{-btmp})](PF_6)$
26.	$[Rh_2(\mu\text{-dapm})_2(t\text{-BuNC})_2(\mu\text{-mtmp})](PF_6)$
27.	$[Rh_2(\mu\text{-dapm})_2(t\text{-BuNC})_2(\mu\text{-btmp})](PF_6)$
28.	$[Rh_2(\mu\text{-dppm})_2(t\text{-BuNC})_2(\mu\text{-mtmp})](PF_6)_2$
29.	$[Rh_2(\mu\text{-dppm})_2(t\text{-BuNC})_2(\mu\text{-btmp})](PF_6)_2$
30.	$[Rh_2(\mu\text{-dapm})_2(t\text{-BuNC})_2(\mu\text{-mtmp})](PF_6)_2$
31.	$[Rh_2(\mu\text{-dapm})_2(t\text{-BuNC})_2(\mu\text{-btmp})](PF_6)_2$

Table VI

Infrared Data for Chapter 3, Section B

	Compound[a]	$\nu_{(CO)}$	$\nu_{(NC)}$, cm^{-1}
16.	$[Rh_2(\mu\text{-dppm})_2(CO)_2(\mu\text{-mtmp})](PF_6)$	1990.5	
		1975.1	
17.	$[Rh_2(\mu\text{-dppm})_2(CO)_2(\mu\text{-btmp})](PF_6)$	1996.3	
		1982.8	
18.	$[Rh_2(\mu\text{-dapm})_2(CO)_2(\mu\text{-mtmp})](PF_6)$	1992.5	
		1979.0	
19.	$[Rh_2(\mu\text{-dapm})_2(CO)_2(\mu\text{-btmp})](PF_6)$	1992.5	
		1977.0	
20.	$[Rh_2(\mu\text{-dppm})_2(CO)_2(\mu\text{-mtmp})](PF_6)_2$	2079.3	
		2034.9	
21.	$[Rh_2(\mu\text{-dppm})_2(CO)_2(\mu\text{-btmp})](PF_6)_2$	2081.2	
		2038.8	
22.	$[Rh_2(\mu\text{-dapm})_2(CO)_2(\mu\text{-mtmp})](PF_6)_2$	2077.3	
		2034.9	
23.	$[Rh_2(\mu\text{-dapm})_2(CO)_2(\mu\text{-btmp})](PF_6)_2$	2073.5	
		2034.9	
24.	$[Rh_2(\mu\text{-dppm})_2(t\text{-BuNC})_2(\mu\text{-mtmp})](PF_6)$		2108.2
			2071.5
25.	$[Rh_2(\mu\text{-dppm})_2(t\text{-BuNC})_2(\mu\text{-btmp})](PF_6)$		2110.1
			2067.7
26.	$[Rh_2(\mu\text{-dapm})_2(t\text{-BuNC})_2(\mu\text{-mtmp})](PF_6)$		2123.6
27.	$[Rh_2(\mu\text{-dapm})_2(t\text{-BuNC})_2(\mu\text{-btmp})](PF_6)$		2114.0
28.	$[Rh_2(\mu\text{-dppm})_2(t\text{-BuNC})_2(\mu\text{-mtmp})](PF_6)_2$		2169.9
			2158.3
29.	$[Rh_2(\mu\text{-dppm})_2(t\text{-BuNC})_2(\mu\text{-btmp})](PF_6)_2$		2171.8
30.	$[Rh_2(\mu\text{-dapm})_2(t\text{-BuNC})_2(\mu\text{-mtmp})](PF_6)_2$		2169.9
			2158.3
31.	$[Rh_2(\mu\text{-dapm})_2(t\text{-BuNC})_2(\mu\text{-btmp})](PF_6)_2$		2169.9

[a] Spectra taken as Nujol mulls sealed between polyethylene sheets.

shifted by approximately 80 cm^{-1}. For complexes containing terminal isocyanide ligands, a C≡N stretch at approximately 2110 to 2068 cm^{-1} was seen for the dirhodium (I,I) species, with a blue shift of 60 to 90 cm^{-1} upon one-electron electrochemical oxidation. As mentioned in section A., the stretching frequencies increase with oxidation due to the decrease in rhodium electron density that is available for backbonding. This results in an increase in bond order of the terminal ligand.

The Rh_2(I,I) trifluoromethyl pyrazolate complexes have electrochemical behavior analogous to that of the pyrazolate complexes studied previously. Two redox couples are observed in the CVs taken in 0.1 M TBAH/$MeCl_2$ when cycled from -1.4 to +1.6 volts vs SCE. Peak potentials are given in Table VII. The first couple is a quasi-reversible single-electron transfer at positive potentials ranging from roughly 0.2 to 0.4 volts for the carbonyl-containing complexes and roughly 0.9 to 1.0 volts for the isocyanide-containing complexes. The second single-electron couple is quasi- or irreversible and occurs near 1.3 volts for complexes with either pair of terminal ligands.

The difference in potentials of the first couple for the carbonyl- and isocyanide-containing complexes can be understood by examining the terminal ligand-metal interaction. Like the dpam-containing complexes of the previous section, the HOMOs of these μ-pyrazolato-dicarbonyl complexes are stabilized through Rh-C≡O π-backbonding. Backbonding is reduced when the C≡O

Table VII

Peak Potentials (mV vs. SCE) of μ-mtmp and μ-btmp Dirhodium (I,I) Complexes in 0.1 M TBAH/$MeCl_2$

Compound	$E_{p1,a}$ [a]	$E_{p1,c}$	$E_{p2,a}$	$E_{p2,c}$
16.	895	732	-[b]	-[c]
17.	1031	885	-[b]	-[c]
18.	991	844	1418	ca. 1150
19.	1062	917	1460	ca. 1250
24.	234	91	1369	ca. 1100
25.	377	254	1415	1000
26.	327	204	1322	ca. 1200
27.	405	265	1367	ca. 1250

[a] $E_{pn,a/c}$ = Potential of peak **n**; a, c = anodic and cathodic peaks, respectively.

[b] These second cathodic peaks occurred near the solvent limit ca. 1600 mV.

[c] The second couple of these complexes featured broad, low-current cathodic waves near 780 and 950 mV, respectively.

ligands are replaced by *t*-BuN≡C ligands, which are poorer π-acceptors than are the CO ligands. This terminal ligand substitution leaves more electron density on the metal centers of the isocyanide-containing complexes and thus destabilizes the rhodium-based HOMO. The ease of oxidation of the isocyanide-containing complexes confirms a higher energy HOMO.

A comparison of the potentials of the $Rh_2(I,I) \rightarrow Rh_2(I,II)$ redox couple for the dppm-, dapm-, and dpam-containing complexes revealed another trend. When a phosphorus atom of the dppm ligand is replaced with a larger arsenic atom of the dapm transoid bridge, the separation between the metal centers increases.[6] As the rhodium-rhodium distance increases for a set of analogous complexes with identical pyrazolate and terminal ligands, the one-electron oxidation becomes more difficult ($E_{p1,a}$ dpam> $E_{p1,a}$ dapm> $E_{p1,a}$ dppm). This observation, as noted in the previous section, is evidence that the HOMO of these complexes is a Rh-Rh metal antibonding orbital, which is stabilized by increasing the intermetallic distance.

Like the isocyanide-containing dirhodium(I,I) complexes in section A., selective one-electron oxidation of the first anodic process seen in the CV produced the green paramagnetic $Rh_2(I,II)(t\text{-BuNC})_2$ pyrazolate complexes. Unlike the dpam-containing dirhodium(I,I) dicarbonyls in section A., one-electron oxidation of the dapm- and dppm-containing dirhodium(I,I) dicarbonyls produced isolable brown $Rh_2(I,II)(CO)_2$ pyrazolates. Both species have a Rh-Rh bond

order of one-half. Again, because each desired dirhodium(I,II) product was unusually insoluble in methanol, all complexes were isolated.

Electron spin resonance spectroscopy was used to examine the electronic properties of the thermochromic isocyanide-containing paramagnetic complexes. Room-temperature solution ESR spectra of the four CF_3-containing μ-pyrazolato-dirhodium(I,II) complexes, *28-31*, exhibited an isotropic signal at *g* values of roughly 2.15 (2.09 for *28*). No hyperfine splitting was observed in the room-temperature spectra. The frozen-solution spectra displayed three-component anisotropic signals with *g* values of roughly 2.22, 2.19, and 2.03 for the α isomer, and at roughly 2.06, 2.00, and 1.99 for the β isomer. Complexes containing transoid dppm ligands, *28* and *29*, displayed signals of the high-temperature α isomer at -196°C. The spectrum of *28*, which contained the less electronegative mtmp, also displayed a low-temperature β signal, which was first noticeable at -130°C. Although dapm-containing complexes *30* and *31* showed only β forms at -196°C, they behaved like *15* and exhibited both α and β isomers at an intermediate temperature of -130°C. The ESR spectrum of *30* contained the stronger β signal, and that of *31*, which contains the more electronegative btmp, exhibited the stronger α signal. The distribution of α and β isomers at 22°C, -130°C, and -196°C, as monitored by ESR spectroscopy, are summarized for *28-31* in Table VIII. The ESR spectra of *28* (α and β), *29* (α), and *31* (β) are illustrated in Figure 6.

Table VIII

Presence of α and β Isomers, via ESR, in the Isocyanide-containing dirhodium(I,II) Complexes Discussed in Chapter 3, Section B.

	Isomer present at		
Compound	22°C	-130°C	-196°C
28.	α	α + (β)	α + β
29.	α	α	α
30.	α	(α) + β	β
31.	α	α + (β)	β

[a] Parentheses indicate the lower ESR intensity.

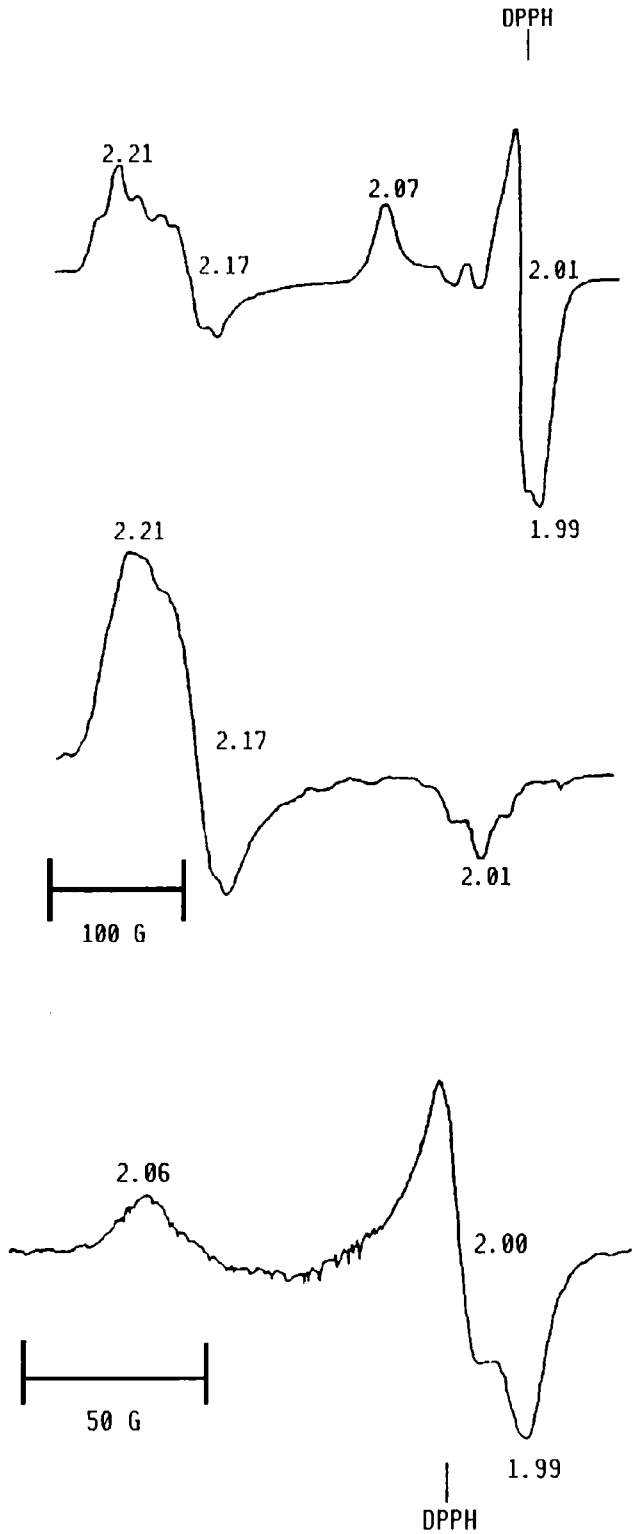

Figure 6. The Frozen Solution (4:1 $MeCl_2$/toluene) ESR Spectra of *28* (top), *29*, and *31* (bottom) at -196°C.

The variable-temperature ESR spectra support the trends observed in section A., that the green dppm-containing complexes have the lowest α-β transition temperature, i.e. the isomerization temperature for a given $Rh_2(I,II)(t\text{-BuNC})_2$ pyrazolate decreases in the order dpam > dapm > dppm. The spectra also offer resolution to the primary question posed in this section. This question was whether the decrease in the thermochromic transition temperature of the bromine-containing paramagnetic species was due (1) to a resonance interaction or (2) to an inductive effect of the bromine substituents on the pyrazolate. Incremental lowering of the α-β isomerization temperature in the mono- and bis(CF_3)-pyrazolate complexes, as in the μ-4b35pz- and μ-345bpz-bridged complexes, indicates that increasing the electronegativity of the pyrazole ring substituents lowers the transition temperature.

Further spectroscopic characterization of the CF_3-containing complexes included electronic spectroscopy in ultraviolet and visible wavelengths, as shown in Table IX. The UV-Vis spectra of the green dirhodium(I,II) isocyanide complexes, *28-31*, are dominated by an absorbance with a maximum around 430 nm. The lowest energy band present in UV-Vis spectra of the dirhodium(I,I) isocyanide compounds, *24-27*, is a peak with a maximum in the range of 485 to 500 nm. For the dirhodium(I,I) carbonyl species, (*16-19*), the wavelength of the analogous peak varies from 470 to 485 nm. Like the dpam complexes discussed in section A, this increase in the UV-Vis transition energy of the carbonyl versus the isocyanide species can be explained, assuming a LUMO

Table IX

UV-Vis-NIR Spectroscopic Data for Chapter 3, Section B.

Compound	λ_{max} (ε)	λ_{max} (ε)	λ_{max} (ε)
16.	485 nm (9×10^3)		
17.	480 nm (8×10^3)		
18.	478 nm (1.7×10^4)		
19.	470 nm (1.0×10^4)		
24.	500 nm (1.7×10^4)	305 nm (1.8×10^4)	
25.	495 nm (1.5×10^4)	300 nm (1.5×10^4)	
26.	496 nm (1.4×10^4)	304 nm (1.7×10^4)	
27.	485 nm (1.1×10^4)	299 nm (1.8×10^4)	
28.	428 nm (1.8×10^4)	588 nm (9×10^2)	865 nm (6×10^2)
29.	420 nm (1.5×10^4)	580 nm (1.4×10^4)	860 nm (6.4×10^3)
30.	425 nm (1.7×10^4)	580-650 nm (1.6×10^3)	870 nm (1.0×10^3)
31.	440 nm (1.1×10^4)	607 nm (1.5×10^3)	

of relatively constant energy in both types of dirhodium(I,I) complexes. This blue shift is due to the relative stabilization of the HOMO of the carbonyl-containing complexes, as seen in the CVs, by the enhanced backbonding capacity of the terminal ligand.

The ^{31}P NMR spectra were collected for the CF_3-containing dirhodium(I,I) compounds. Chemical shifts and rhodium-phosphorus coupling constants are listed in Table X. The spectra of the four dppm complexes, *16*, *17*, *24*, and *25*, displayed a standard AA'A"A'"XX' pattern, which is indicative of four magnetically non-equivalent phosphorus atoms split by two chemically equivalent rhodium atoms. Although the pattern was expected for the symmetric μ-btmp complexes, its observation for the asymmetric μ-mtmp complexes is indicative of the relative isolation of the magnetic environment of the phosphorus atoms from the effects of the substituents on the pyrazolate.

The dapm complexes, *18*, *19*, *26*, and *27*, display different ^{31}P NMR spectra. DePriest[5] demonstrated that a pair of doublets should be observed for symmetric μ-pyrazolate dapm-containing complexes due to the presence of two isomers. In the major species, the head-to-tail (HT) isomer, each rhodium is bonded to the phosphorus of one dapm ligand and the arsenic of the other dapm. In the minor head-to-head (HH) isomer one rhodium is bound to two phosphorus atoms and the other to two arsenic atoms. The rhodiums' splittings of magnetically equivalent phosphorus atoms give NMR doublets in both cases.

Table X

^{31}P NMR Spectroscopic Data for Chapter 3, Section B.

Compound		Chemical Shift δ, ppm	Coupling Constant J_{Rh-P}, Hz
16.		17.34	126.95
17.		18.45	124.51
18.	(HT)[a]	26.78	148.93, 9.77
	(HH)[a]	22.22	124.51, 9.77
19.	(HT)	26.16	146.48
	(HH)	20.10	122.07
24.		8.32	139.16
25.		16.36	139.16
26.	(HT)	26.39	168.46
	(HH)	25.28	141.61
27.	(HT)	25.82	156.01
	(HH)	24.14	151.36

[a] (HT) and (HH) represent head-to-tail and head-to-head bis(dapm) isomers, respectively.

The ^{31}P NMR spectra of compounds *19* and *27*, both of which contain the μ-btmp ligand, display the pair of doublets predicted for symmetrical bridgehead pyrazolates. The ratio of intensities for each pair varies as the ratio of the HH to the HT isomer present. The ^{31}P NMR spectra of *18*, and *26*, the dapm complexes containing the asymmetric μ-mtmp ligand, are shown in Figure 7. The spectrum of compound *18*, the carbonyl-containing species, depicts long range three-bond phosphorous-rhodium coupling as each pair of doublets are split into doublets-of-doublets. Surprisingly, the spectrum of the isocyanide-containing analog, *26*, does not indicate this long range coupling. The reason for the difference in the long range coupling constants is not clear but appears related to the terminal ligand present. The variation in long range coupling is perhaps dependent on the electron densities of the rhodium atoms, which is in turn dependent on the bonding and backbonding abilities of the terminal ligands.

C. Conclusion

A study of some dirhodium-μ-pyrazolato A-frame complexes was presented in this chapter. The relative effects of the modification of bridgehead, transoid-bridging, and terminal ligands and of single-electron oxidation on the chemical properties of the compounds were elucidated. The behavior of dpam-containing complexes was compared to that of the dapm and dppm analogs.

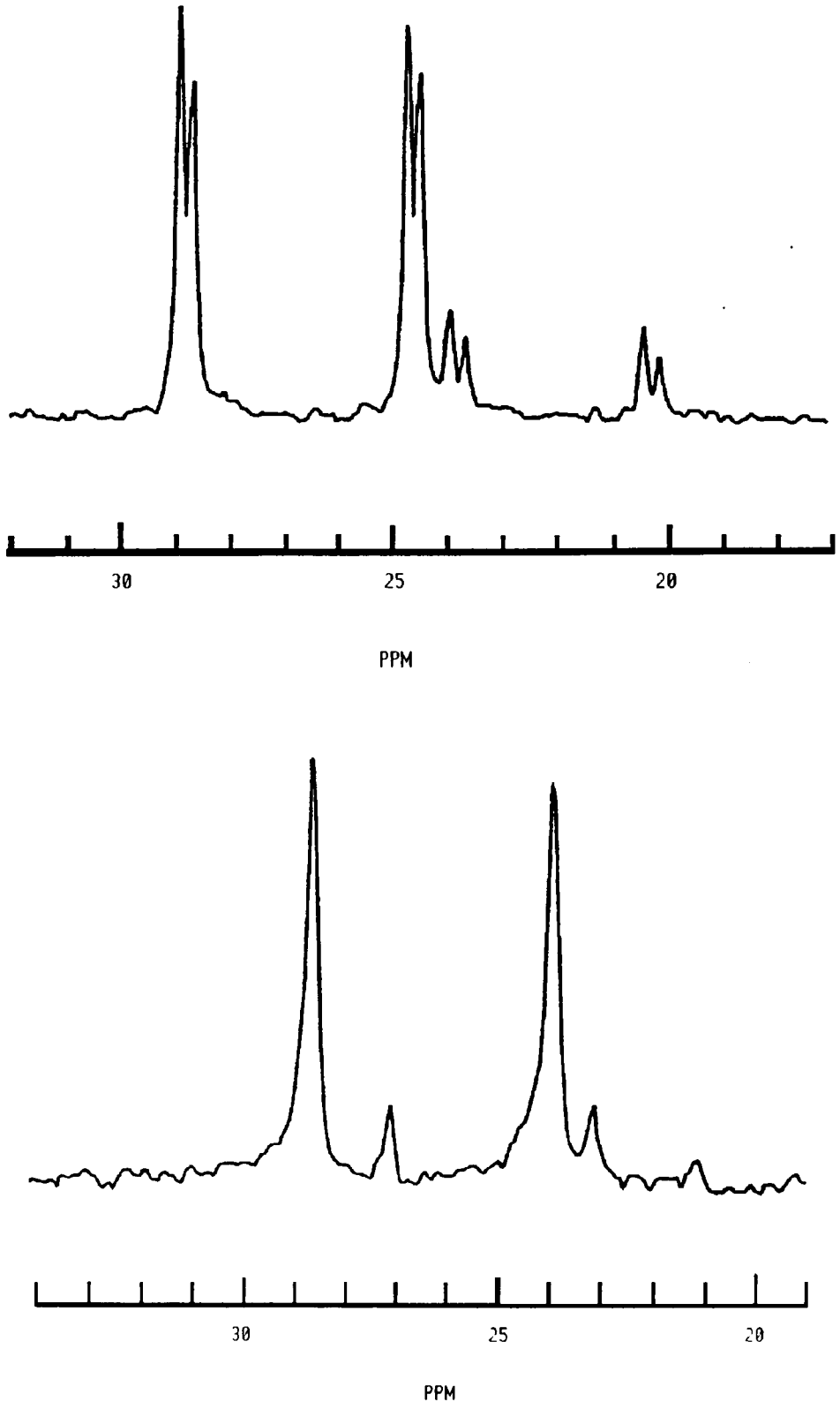

Figure 7. ^{31}P NMR Spectra of Compounds *22* (top) and *26*.

The unusual thermochromic property of the isocyanide-containing dirhodium(I,II) compounds was introduced. In order to examine further the nature of this thermochromic isomerism, btmp- and mtmp-containing dapm and dppm species were examined. ESR spectroscopy was again used to chart the temperature-dependence of the transition. It was determined that an increase in the electronegativity of the pyrazole ring substituents decreased the thermochromic isomerization temperature of the pyrazolate complexes. This study concludes the trilogy of dppm, dapm and dpam bis-bridged μ-pyrazolato-dirhodium complex studies initiated by Tortorelli[4] and continued by DePriest.[5]

CHAPTER 4

EXAMINATION OF 2-HYDROXYPYRIDINATO-BRIDGED DIRHODIUM COMPLEXES

The behavior of the μ-pyrazolato-complexes described in the previous chapter led to the search for ligands with similar apex bonding abilities. Anionic 2-hydroxypyridinate (hp) and its derivatives were selected because the donor atoms are involved in ring π systems similar to the pyrazolates and their use as bridging groups in dinuclear metal complexes had been demonstrated.[63,32] The 2-hydroxypyridinate derivatives with electron-donating 6-methyl- (mhp) and electron-withdrawing 6-chloro- substituents were also chosen to study substituent inductive effects on the ligand-metal interaction. Each of these ligands can bridge as either monodentate μ-O-bound or bidentate O- and N-bound species, as depicted below in Figure 8. Table XI lists the 2-hydroxy-

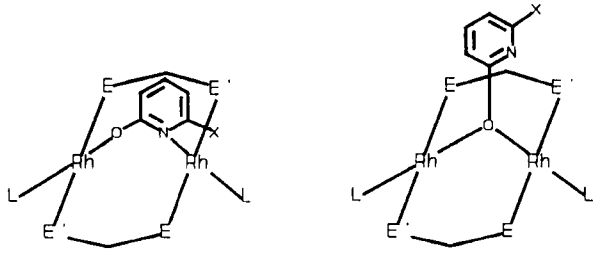

Figure 8. Possible Structures of the 2-hydroxypyridonato-bridged Dirhodium A-frame Complex (E^E' is the transoid bridge, X is H, Cl, or CH_3 and L is CO).

Table XI

2-Hydroxypyridinato-dirhodium Compounds Discussed in Chapter 4

32.	$[Rh_2(\mu\text{-dppm})_2(CO)_2(\mu\text{-mhp})](PF_6)$
33.	$[Rh_2(\mu\text{-dppm})_2(CO)_2(\mu\text{-chp})](PF_6)$
34.	$[Rh_2(\mu\text{-dppm})_2(CO)_2(\mu\text{-hp})](PF_6)$
35.	$[Rh_2(\mu\text{-dapm})_2(CO)_2(\mu\text{-mhp})](PF_6)$
36.	$[Rh_2(\mu\text{-dapm})_2(^{13}CO)_2(\mu\text{-mhp})](PF_6)$
37.	$[Rh_2(\mu\text{-dapm})_2(CO)_2(\mu\text{-chp})](PF_6)$
38.	$[Rh_2(\mu\text{-dapm})_2(CO)_2(\mu\text{-hp})](PF_6)$
39.	$[Rh_3(\mu\text{-dppm})_2(CO)_3(\mu\text{-CO})_3](PF_6)$

pyridinato-dirhodium complexes that contain either bis(dppm) or bis(dapm) transoid bridges and carbon monoxide terminal ligands. An examination of these dirhodium A-frame 2-hydroxypyridinate complexes is presented in this chapter in order to evaluate the spectroscopic and structural effects of bifunctional asymmetric bridgehead ligands.

The 2-hydroxypyridinate complexes were characterized using five analytical methods: infrared spectroscopy (IR) was used to monitor the infrared-active stretches of the complexes; proton-decoupled phosphorus nuclear magnetic resonance spectroscopy ($^{31}P\{H\}$ NMR) to examine the magnetic environment of the rhodium-bound phosphorus atoms of the dppm and dapm transoid bridges; cyclic voltammetry (CV) to study electrochemical behavior; ultraviolet-visible spectroscopy (UV-Vis) to probe electronic behavior; and single-crystal X-ray diffractometry to determine the crystal structures of selected compounds.

The complexes in this chapter were synthesized from a solution containing $[Rh_2(\mu\text{-dppm})_2(\mu\text{-Cl})(CO)_2](PF_6)$ and the potassium salt of the appropriate 2-hydroxypyridine via the method used to prepare the (CF_3)-pyrazolate complexes described in Chapter 3, section B. After several attempts under an inert gas, synthesis of the hp-containing complex, compound *34*, was attempted under a reducing atmosphere of carbon monoxide, as Oro et al.[38] detailed in a publication that appeared during this investigation. The red

crystalline compound *39*, $[Rh_3(\mu\text{-dppm})_2(CO)_3(\mu\text{-}CO)_3](PF_6)$, resulted from the attempt to grow crystals of *34* at approximately -25°C from a CO-saturated solution. A synthesis of the perchlorate salt of *39* from a solution containing analogous μ-OMe or μ-OEt (but not μ-OH) complexes under a CO pressure of 2.1 MPa had been reported by Deraniyagala and Grundy.[52] Although cell parameters for the perchlorate salt were reported, their attempts to determine a crystal structure were unsuccessful due to poorly diffracting crystals.

Infrared spectroscopy was used to examine the infrared-active CO stretches of the complexes. IR results are given in Table XII. Each spectrum revealed a pair of the expected $\nu_{(C\equiv O)}$ at approximately 1985 and 1967 cm^{-1}. In *36*, the dapm mhp ^{13}CO complex, the terminal $^{13}C\equiv O$ stretching frequencies are red shifted 40-50 cm^{-1} due to the isotope effect. Also present was the 2-hydroxypyridinate C-O stretch near 1602 cm^{-1}. The energy of this stretch might be expected to vary with the monodentate or bidentate coordination mode of 2-hydroxypyridinate. However, no significant difference in the energy of this stretch is observed among the spectra of different compounds or of a single complex when recorded either in a Nujol mull or a methylene chloride ($MeCl_2$) solution. This observation raises the question of whether the mode of bonding is constant or the energy of the hydroxypyridinate C-O stretch is insensitive to the mode of bridging.

Table XII

Infrared Data for Chapter 4

	Compound[a]	$\nu_{(C\equiv O)}$	$\nu_{(C-O)}$, cm^{-1}
32.	$[Rh_2(\mu\text{-dppm})_2(CO)_2(\mu\text{-mhp})](PF_6)$	1981 1968	1600
33.	$[Rh_2(\mu\text{-dppm})_2(CO)_2(\mu\text{-chp})](PF_6)$	1986 1964	1597
34.	$[Rh_2(\mu\text{-dppm})_2(CO)_2(\mu\text{-hp})](PF_6)$	1983 1966	1607
35.	$[Rh_2(\mu\text{-dapm})_2(CO)_2(\mu\text{-mhp})](PF_6)$	1991 1969	1604
36.	$[Rh_2(\mu\text{-dapm})_2(^{13}CO)_2(\mu\text{-mhp})](PF_6)$	1931 1913	1598
37.	$[Rh_2(\mu\text{-dapm})_2(CO)_2(\mu\text{-chp})](PF_6)$	1983 1966	1597
38.	$[Rh_2(\mu\text{-dapm})_2(CO)_2(\mu\text{-hp})](PF_6)$	1978 1959	1603

[a] Spectra taken as Nujol mulls sealed between polyethylene sheets.

Insight into this question may be gained by an examination of the ^{31}P NMR spectra. The NMR spectra will be discussed in two phases. Initially, the dppm bis-bridged complexes will be examined, followed by discussion of the dapm-containing complexes. Coupling constants and chemical shifts are given for these complexes in Table XIII.

Room-temperature spectra of complexes *32* and *33* (Figure 9) in $MeCl_2$ exhibit the AA'A"A'"XX' pattern expected for an A-frame complex containing four magnetically non-equivalent phosphorus atoms split by two chemically equivalent rhodium atoms. These species contain the asymmetric 2-hydroxypyridinate and there are three possible explanations for the equivalency of the phosphorus atoms. First and most obvious is the interpretation that the hp ligands are monodentate μ-O bridges. The second is that the hp is bidentate and the bonding through the O and N atoms is so similar that no detectable differences exist in the magnetic environments of the phosphorus atoms for dppm complexes with either the mhp or chp ligand. The third explanation involves bidentate bonding where the hp ligand 'flips' rapidly, i.e., the O and N exchange rhodium sites so rapidly that on the NMR time scale, only the average environment is depicted in the spectrum. For reasons to be presented, this third explanation is the most likely.

Fluxional behavior such as that alluded to above has been observed in two cases for dinuclear complexes bridged by two cisoid hp or 6-substituted-hp

Table XIII

^{31}P NMR Spectroscopic Data for Chapter 4

Compound		Chemical Shift δ, ppm	Coupling Constant J_{Rh-P}, Hz
32.		22.25	126.96
33.		22.05	126.95
34.		23.53	[a]
35.	(HT)[b]	29.35	148.95
	(HT)	26.36	146.45
	(HH)[b]	24.71	125.12
	(HH)	22.93	127.02
36.[c]	(HT)	28.95	148.96
	(HT)	27.17	151.42
37.[d]	(HT)	24.04	148.92
38.	(HT)	30.36	148.92
	(HH)	23.40	131.83

[a] Peak was a multiplet.

[b] (HT) and (HH) represent head-to-tail and head-to-head bis(dapm) isomers, respectively; these peaks are reported at -25 °C due to very poorly defined signal at 25 °C. All other data are from spectra taken at 25 °C.

[c] Product was recrystallized several times to remove HH isomer; $J_{P-^{13}C}$ = 14.7 Hz.

[d] Signal for the HH isomer was very poorly defined.

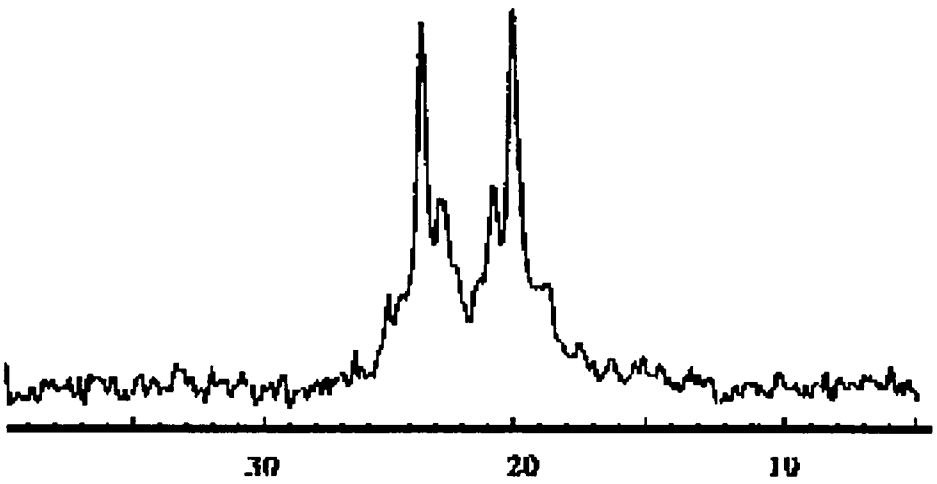

Figure 9. ^{31}P NMR spectrum of *33* at 25°C.

ligands: (a) diplatinum(III) species, for the exchange of the head-to-tail (HT) and head-to-head (HH) isomers;[64] (b) dirhodium(I) species, for the intramolecular exchange of the two bridging ligands.[65] One of two mechanisms proposed in these reports is likely responsible for this apex flip in these A-frame complexes. The first proceeds by way of an intermediate of the monodentate μ-O-bound apex:[64]

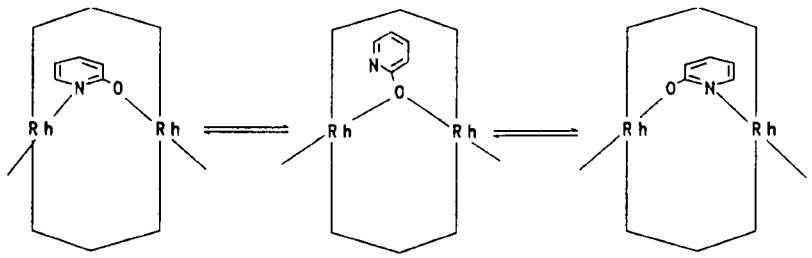

The intermediate of the second scheme contains a hydroxypyridinate chelate of only one rhodium center:[65]

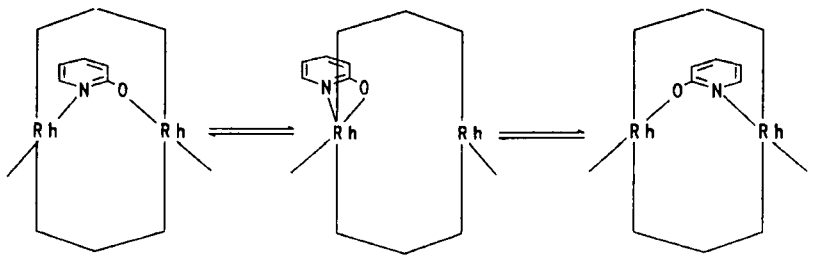

Given a rate that is faster than the NMR time scale, either mechanism would result in the observed AA'A"A"'XX' ^{31}P NMR pattern.

The room-temperature spectrum of compound *34* in $MeCl_2$, shown in Figure 10, is similar to that of a dppm dirhodium complex reported by Tortorelli et al.[66] with different rhodium environments and is interpreted as an AA'BB'XY

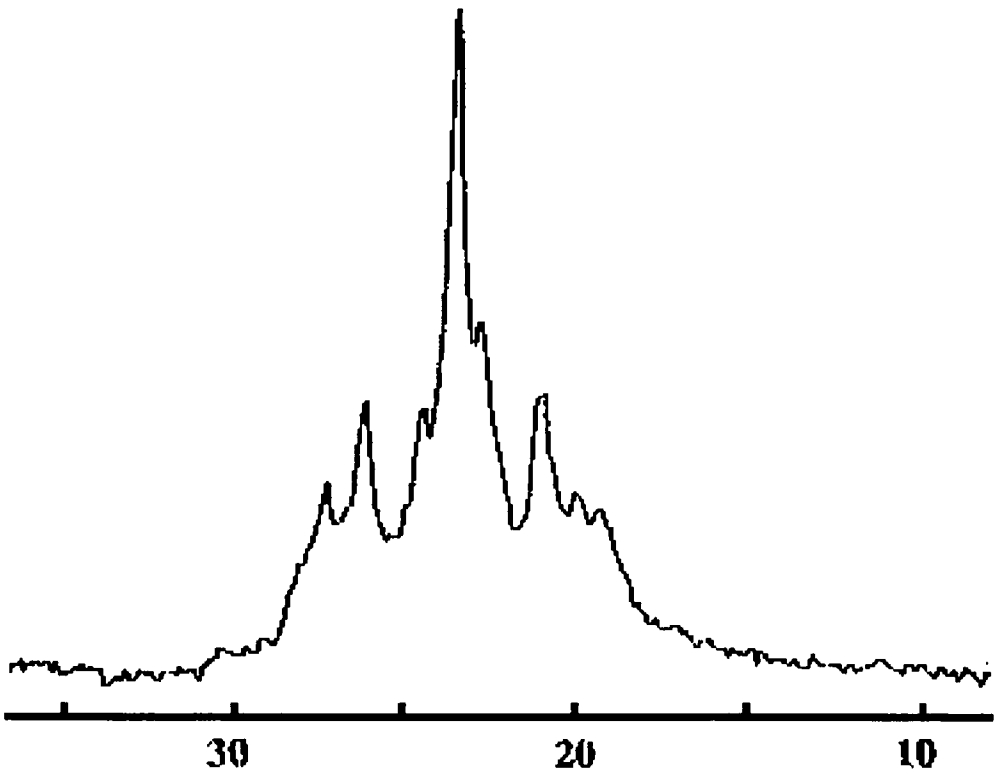

Figure 10. ^{31}P NMR spectrum of *34* at 25°C.

spectrum (two pairs of chemically non-equivalent phosphorus atoms, each pair split by a rhodium atom). In contrast to the above AA'A"A"'XX' spectra, this spectrum suggests that the apex hp is bidentate, and that there is a discernible difference between the Rh-O and Rh-N bonds. The spectrum also suggests the lack of rapid exchange of the hp ligand.

The obvious bidentate bonding of *34* suggested that this type of bonding might occur for the other two complexes containing dppm. In order to determine whether fluxional bidentate bonding is responsible for the AA'A"A"'XX' spectra of complexes *32* and *33*, variable-temperature ^{31}P NMR spectra were collected. If a chp or mhp flip occurred at room temperature and could be slowed at low temperature the resultant low-temperature ^{31}P NMR would give AA'BB'XY spectra. Conversely, the ^{31}P NMR of *34* at elevated temperature might be expected to result in an AA'A"A"'XX' spectrum due to possible fluxional behavior of the apex hp ligand.

Variable-temperature (VT) ^{31}P NMR spectra were collected for the dppm complexes and showed temperature dependence similar to that predicted above. Due to the low boiling point of $MeCl_2$, high temperature solution spectra were obtained in 1,1,2,2-tetrachloroethane, which has a boiling point of 146°C. The low temperature spectra of the chp-containing complex, *33*, are shown in Figure 11. In these spectra, the two main peaks of the room-temperature spectrum broaden at 0°C and coalesce into a broad multiplet at -25°C, and a

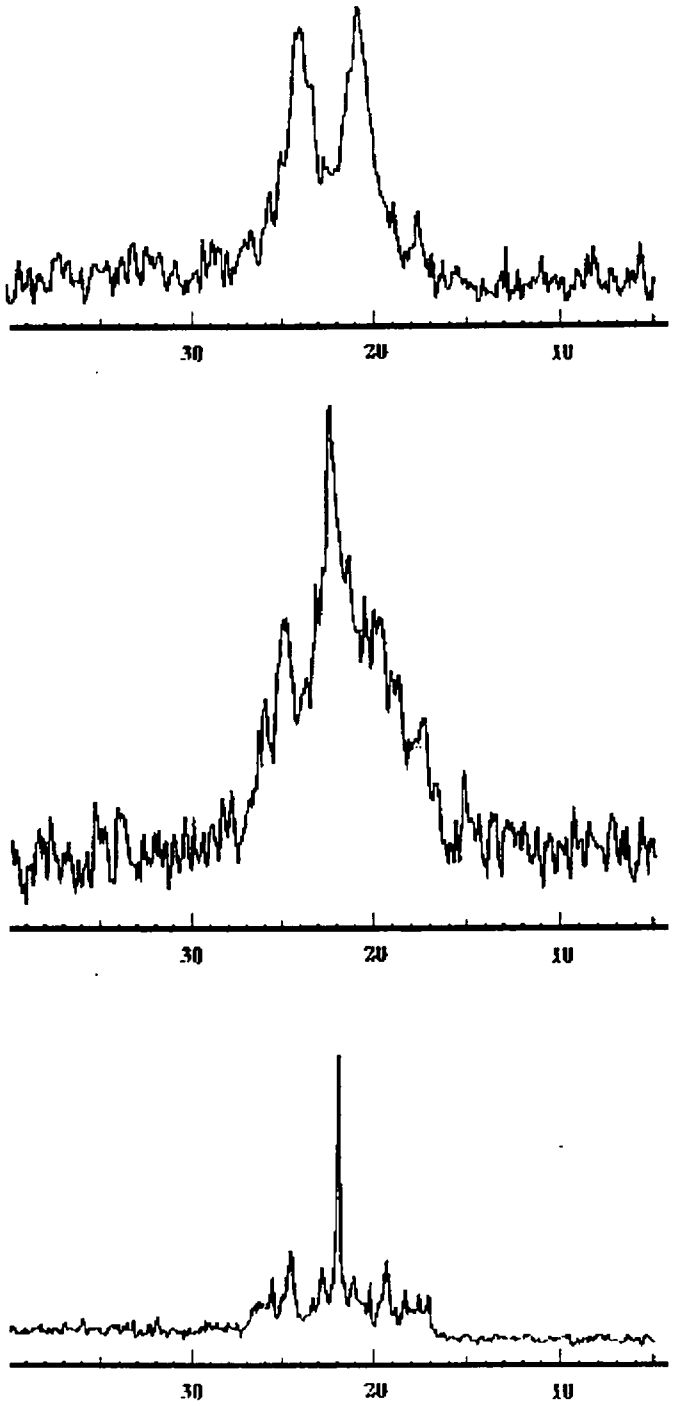

Figure 11. ^{31}P NMR spectra of *33* at 0°C (top), -25°C, and -50°C (bottom).

multiplet with a sharp center peak at -50°C. No significant change was noted on further cooling down to -100°C. This is consistent with a temperature-dependent flux of the apex chp, which stops or slows enough to appear static on the ^{31}P NMR time scale at low temperatures. While the spectrum of *32*, the mhp complex, remains an AA'A"A"'XX' spectrum from 75°C down to -95°C, the major peaks sharpen with increasing temperature and broaden with decreasing temperature. This implies that the mhp flip is more rapid than that of the chp complex. Coupled with the VT NMR results of the chp complex, the peak broadening in this spectrum suggests that an AA'BB'XY spectrum might be seen if solution spectra were obtainable at lower temperatures.

The VT ^{31}P NMR of *34* gave some unexpected information about the temperature-dependent bonding mode of the apex hp. Both high- (125°C) and low-temperature (-95°C) NMR spectra, displayed in Figure 12, showed an AA'A"A"'XX' pattern. This suggests that rapid exchange of the bidentate hp occurs at elevated temperatures and slows or stops at room temperature. At low temperature a change in the bonding mode from bidentate to monodentate would be consistent with the data. The formation of a somewhat more reactive monodentate μ-O-bridged complex at lower temperatures is consistent with the fact that the trirhodium species is obtained at low temperature. Also, only when the low-temperature NMR spectrum is taken, does a decomposition product of *34*, as shown in Figure 12, appear; this signal remains visible in the NMR spectrum upon returning to ambient temperature.

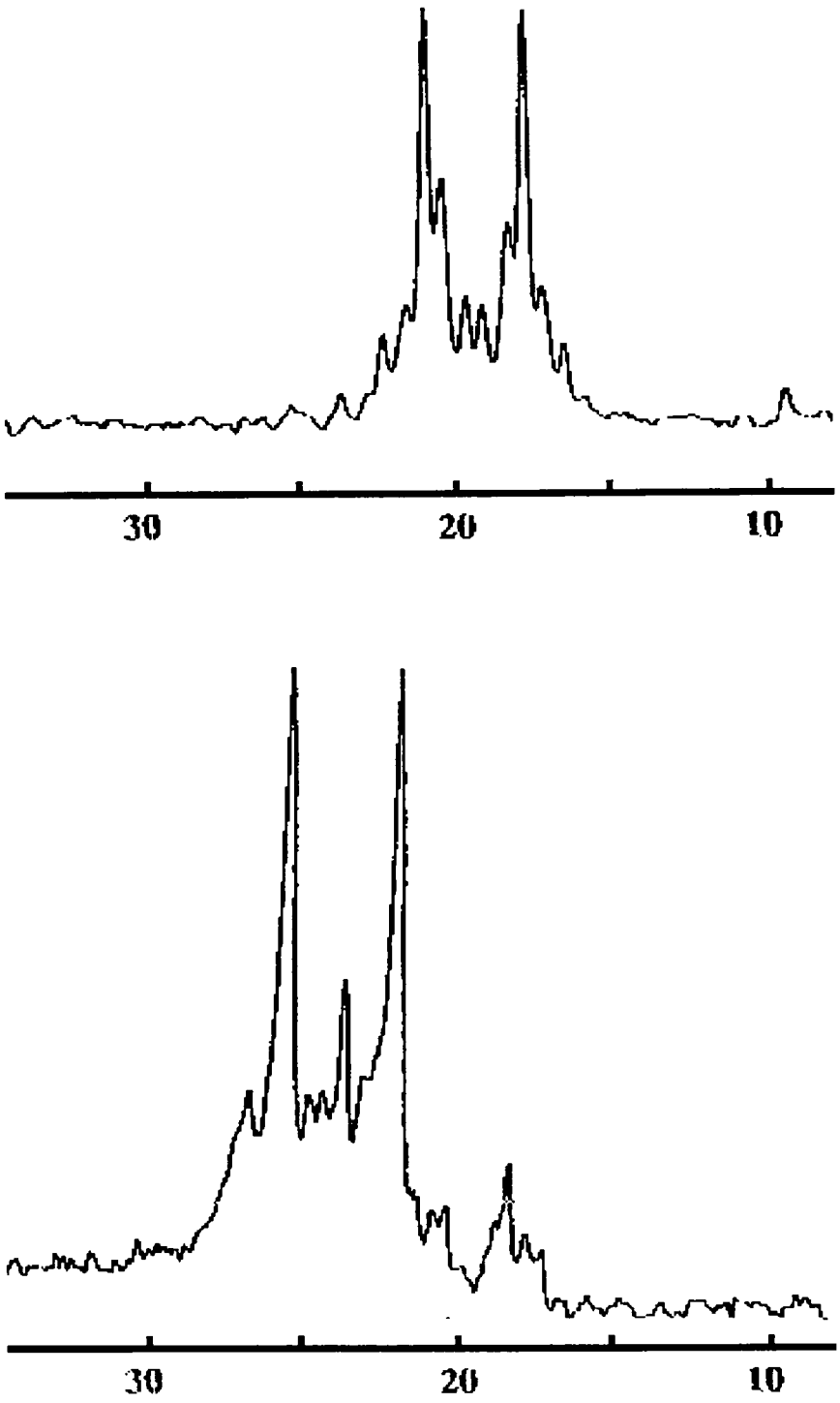

Figure 12. ^{31}P NMR spectra of *34* in $Cl_2CHCHCl_2$ at 125°C (top), and in $MeCl_2$ at -95°C.

^{31}P NMR results for the dapm-containing complexes *35*, *37*, and *38* are qualitatively similar and show a temperature dependence which suggests apex fluxional behavior at and above room temperature. The spectra contain peaks attributable to the HT and HH dapm isomers which are identified by the comparison of specific chemical shifts and coupling constants of the μ-pyrazolate dapm isomeric complexes discussed in Chapter 3. Generally, the chemical shifts and coupling constants of the HT isomer are 5 ppm and 25 Hz higher than the corresponding HH isomer. This correlation was reported initially by Guimerans and Balch who compared the chemical shifts and coupling constants of $Rh(CO)Cl(P\phi_3)_2$ and $Rh(CO)Cl(P\phi_3)(As\phi_3)$.[67]

The room-temperature spectrum of *35* is composed of very broad indistinguishable peaks, which suggests that the mhp ligand flip occurs at a frequency that averages the phosphorus environments. The low-temperature (-25°C) spectrum of *35*, shown in Figure 13, is composed of four doublets, labeled A-D: A and B are assigned to the nonequivalent phosphorus atoms of the major HT $(P\text{-}Rh\text{-}As)_2$ isomer and C and D are assigned to the two minor HH isomers, where the mhp nitrogen is bound to either the As-Rh-As or P-Rh-P side, as represented below.

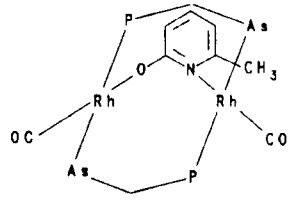

NMR: (d), A and B

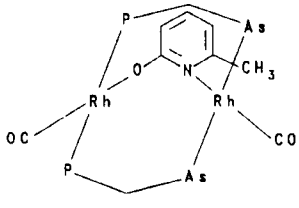

NMR: (d), C or D

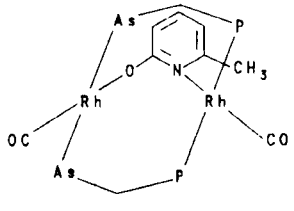

NMR: (d), D or C

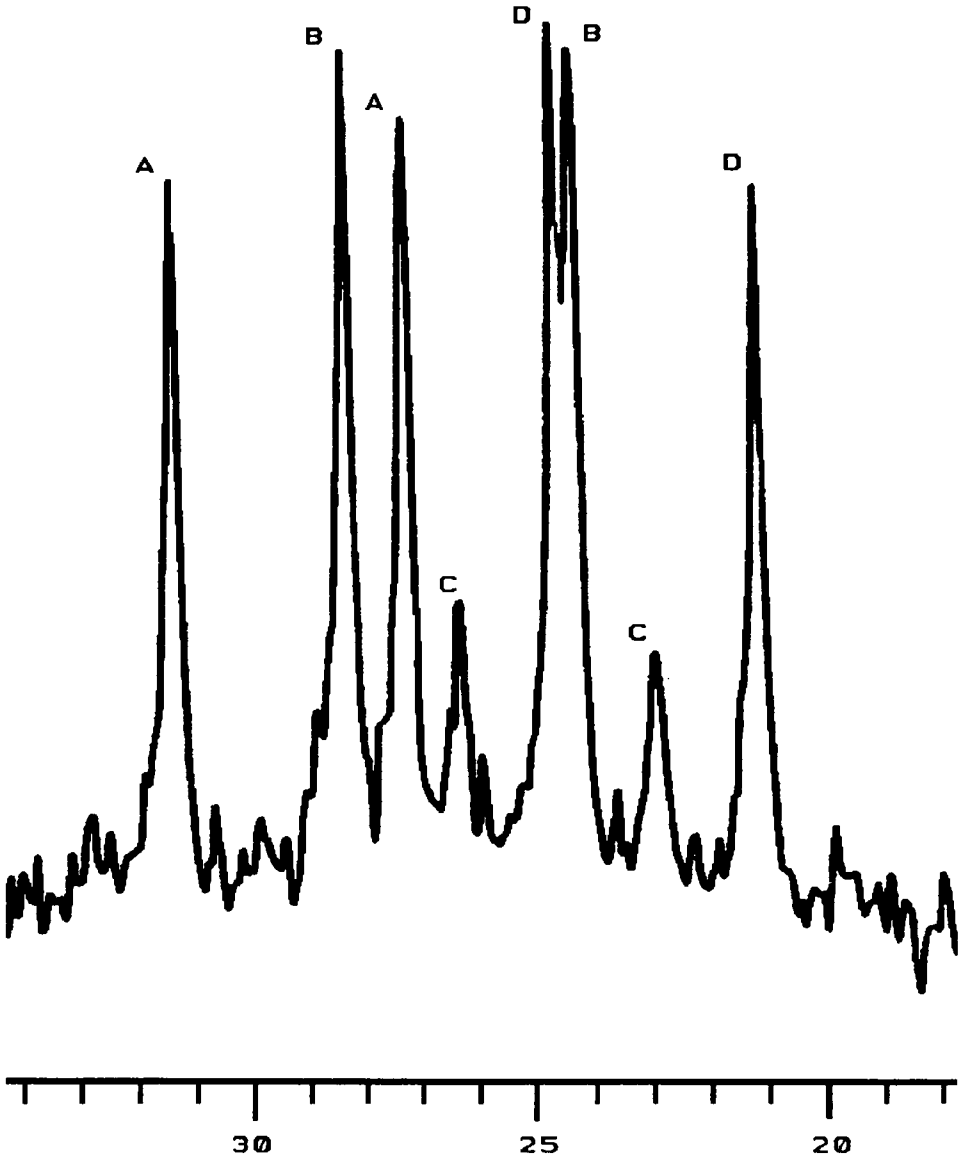

Figure 13. ^{31}P NMR spectrum of *35* at -25°C.

Compound *36*, the ^{13}C-enriched CO analog of *35*, was recrystallized many times in attempts to purify the compound. The final product was composed exclusively of the HT isomer. The ^{31}P NMR spectrum of *36* showed ^{13}C coupling and slightly different chemical shifts than those of *35* and lacked the peaks that could be assigned to the HH isomer.

Variable temperature ^{31}P NMR spectra of *37* were collected and are shown in Figure 14. The room-temperature NMR spectra for *37* clearly shows a pair of sharp peaks for the HT isomer and hints of a broad pair of peaks for the minor HH isomer slightly upfield. The spectrum at 0°C is noisy and only displays a broad doublet, which is attributable to the major HT isomer. The peaks for the HH isomer are apparently broadened beyond recognition at 0°C because cooling the dapm chp complex down to -50°C reveals four doublets that are characterized in the same manner as above for *35*.

The room-temperature ^{31}P NMR spectrum for *38* contains a doublet assigned to the major HT and also one of less intensity assigned minor HH isomer. This is predicted for either mhp-oxy-bridged or rapidly flipping mhp species, but is likely due to the fluxional behavior as described above.

Cyclic voltammograms of the dppm complexes are very similar to those of the dicarbonyl-containing pyrazolate complexes discussed in the previous chapter. The CVs each show a quasi-reversible one-electron couple at

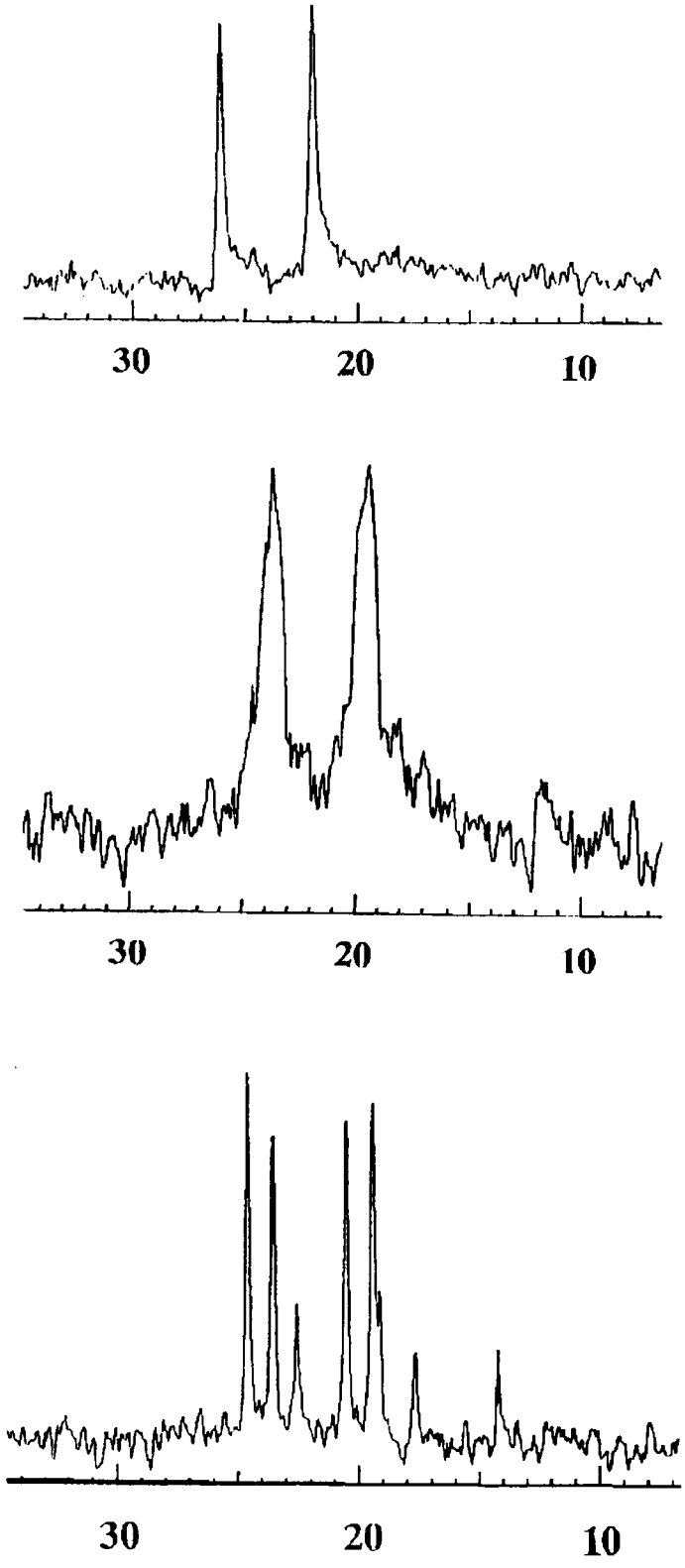

Figure 14. ^{31}P NMR spectra of *37* at 25°C (top), 0°C, -50°C (bottom).

approximately +700 mV (versus SCE) and a second quasi- or irreversible couple near +1200 mV. Peak potentials are listed in Table XIV. Attempts to isolate a single-electron oxidized product were unsuccessful, and the inability to synthesize any bis(isocyanide) complexes with hydroxypyridinate apex ligands reduced the likelihood of finding a thermochromic species.

The UV-Vis spectra are qualitatively the same as the previously examined pyrazolate-bridged dicarbonyl complexes. The UV-Vis data for the 2-hydroxypyridinate complexes, presented in Table XV, show the same absorbances near 490 and 390 nm as the pyrazolate-containing complexes. The absorbance at 490 nm is assigned similarly to the HOMO $\rightarrow$ LUMO transition.

Single-crystal X-ray structures for these complexes are of interest because of the various bonding modes possible and suggested by the ^{31}P NMR data. The structures of compounds *32* and *39* were determined and are presented here. Crystal data (Table XXXIII), non-hydrogen atomic coordinates (Table XXXIV, Table XXXVII), bond lengths (Table XXXV, Table XXXVIII), and bond angles (Table XXXVI, Table XXXIX) are presented in the Appendix.

The structure of complex *32*, illustrated in Figure 15, shows an A-frame complex with the mhp ligand as a bidentate apex bridge. Each d^8 Rh atom lies in a local square planar environment with trans dppm P atoms and with the CO trans to the mhp O or N atom. Although the environment of each rhodium is

Table XIV

Peak Potentials (mV vs. SCE) of Bis(dppm) 2-Hydroxypyridinate Dirhodium Complexes in 0.1 M TBAH/$MeCl_2$

Compound	$E_{p1,a}$ [a]	$E_{p1,c}$	$E_{p2,a}$	$E_{p2,c}$
32.	757	682	ca. 1300	ca. 1200
33.	728	663	1252	1143
34.	755	682	1225	ca. 1150

[a] $E_{pn,a/c}$ = Potential of peak **n**; a, c = anodic and cathodic peaks, respectively.

Table XV

UV-Vis Spectroscopic Data for Selected 2-Hydroxypyridinate-bridged Dirhodium Complexes

Compound	λ_{max} (ε)	λ_{max} (ε)
32.	496 nm (7.6×10^3)	302 nm (1.9×10^4)
33.	494 nm (8.0×10^3)	292 nm (1.5×10^4)
35.	488 nm (1.1×10^4)	298 nm (2.1×10^4)
37.	490 nm (1.1×10^4)	294 nm (2.3×10^4)

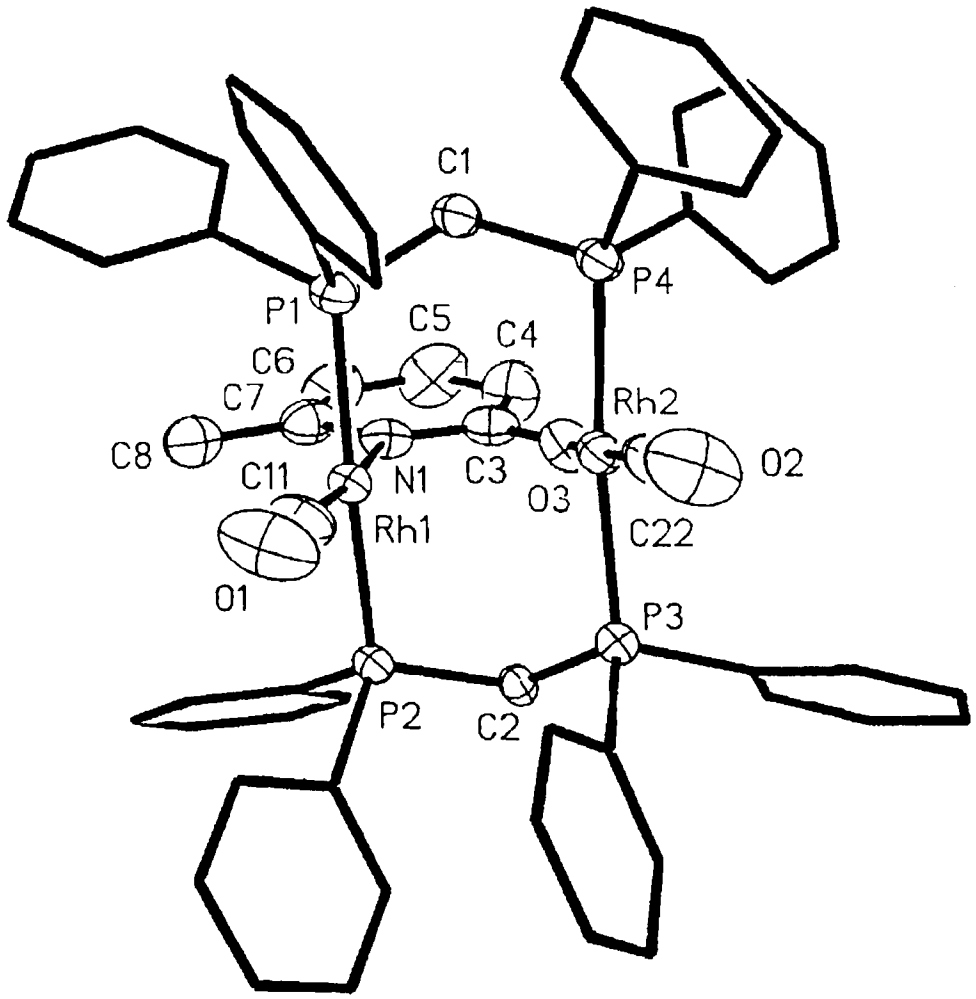

Figure 15. Perspective drawing of the cation of *32*. 50% thermal ellipsoids are shown except for the phenyl carbons.

different due to the bidentate bonding mode of the mhp ligand, other bonds to the rhodium atoms are quite similar. The Rh-P distances vary from 2.315(2) to 2.347(2) Å, the distances to the carbonyl carbons are 1.797(7) and 1.818(6) Å. This suggests that the Rh-N and Rh-O bonds are quite similar, and the distances from the rhodium to the apex O and N atoms, 2.067(4) and 2.139(4) Å, respectively, support this similarity. The Rh-Rh distance, 3.019(1) Å, verifies the expected Rh-Rh bond order of zero.[68]

As is generally the case, the methylene bridges of the transoid dppm ligands bend over towards the mhp ligand, pushing the dppm phenyl rings away from the apex ligand, creating a pocket into which the mhp ligand fits. The mhp ligand itself is undistorted, with all bond angles within 3° of the 120° angles predicted.

A crystal structure determination was also attempted for *35*. The bidentate bonding mode of the mhp ligand is the same as in *32*. The solution, however, would only refine to an R-value of around ten percent with corrections for absorption and other effects. Co-crystallization of HT and HH isomers may have contributed to this difficulty: while the bidentate apex mhp did not show disorder, there was disorder in the positions of the As and P in the dapm ligands. On average, there appears to be partial occupation of these positions by As and P atoms. Modeling of this disorder proved unsuccessful.

Collection of X-ray data for the determination of the crystal structure of *39*, the trirhodium complex that crystallized during an attempt to grow crystals of *34*, was quite difficult. Upon isolation from the crystallization solution, the crystal begins to deteriorate under inert or reducing atmospheres. Because of this, the X-ray data were collected at -100° C in a N_2 stream.

Figure 16 illustrates the structure determined for the cation of *39*. The structure can be thought of as a 14 electron fragment, $[Rh(CO)_3]^+$, bridging a $[Rh_2(\mu\text{-dppm})_2(\mu\text{-CO})(CO)_2]$ backbone.[52] There is a metal-metal bond and a bridging carbon monoxide joining pairs of rhodium atoms. The Rh-Rh distances are 2.785(2) and 2.752(2) Å, for the distances to the apex Rh, and 2.807(2) Å for the distance between the two dppm-bound rhodium atoms. While the longer distance may suggest the steric restraints imposed by the transoid dppm ligands, this distance is in agreement with the expected intermetallic bond order of one.[68] The bond distances of the bridging COs to the apex rhodium (1.95(2), 1.96(2) Å) are shorter than to the dppm-bound Rh atoms (2.45(2), 2.31(2) Å), while the Rh-C bond distances of the μ-CO between the dppm-bound Rh atoms are 2.07(2) and 2.09(2) Å. Another carbon monoxide is terminally bonded to each rhodium at a distance of 1.88(2), 1.90(2) and (apex) 1.86(2) Å. The three rhodium atoms and the bridging and terminal carbonyls are approximately coplanar (± 0.200 Å).

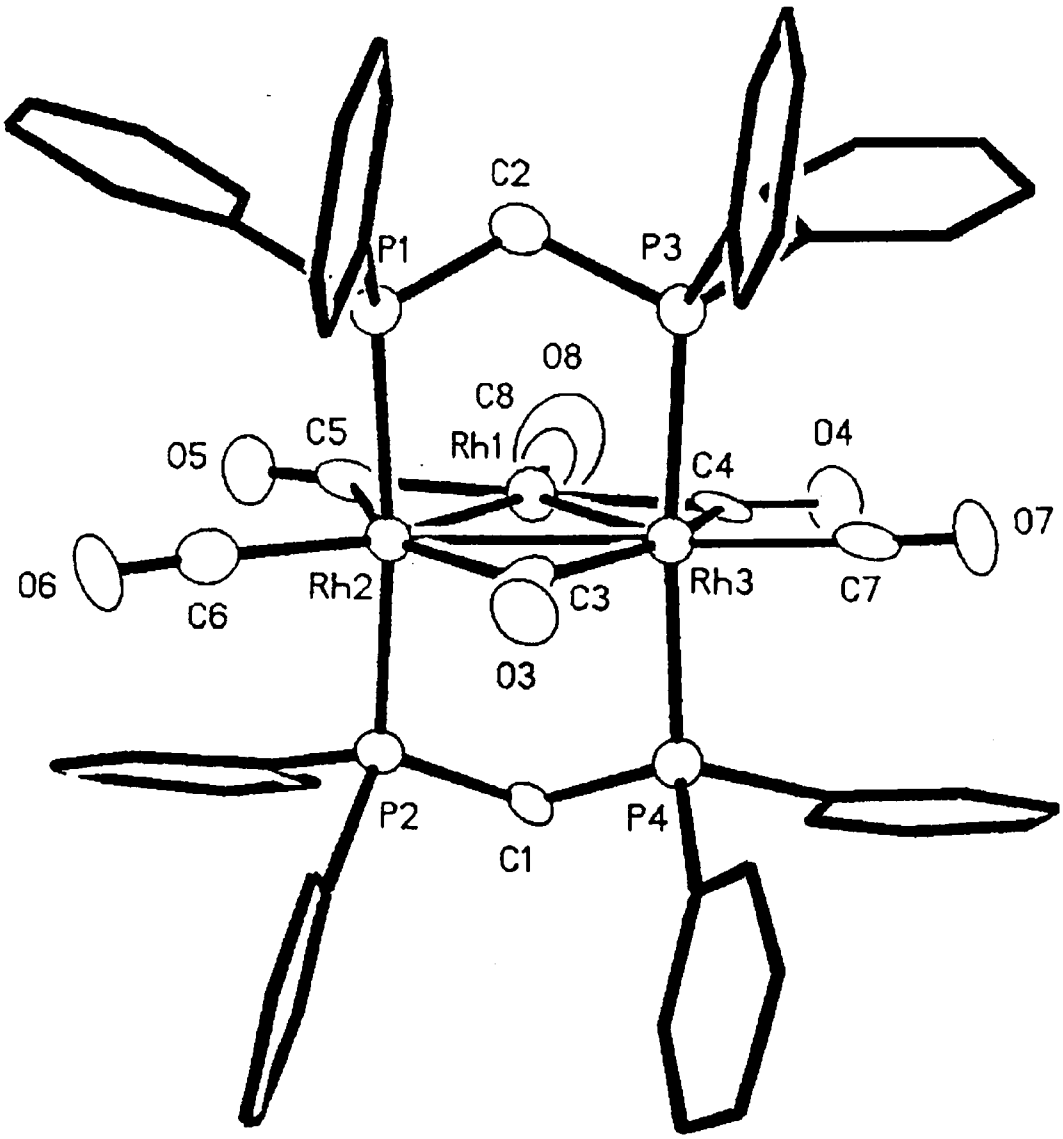

Figure 16. Perspective drawing of the cation of *39*. 50% thermal ellipsoids are shown except for the phenyl carbons.

The bond distances of the μ-dppm ligands are similar to those revealed in the structure of *32*, but the atom configurations are different: the methylene carbons are unusually folded away from the apex ligand.

The study of some dirhodium-μ-hydroxypyridinato A-frame complexes has been summarized in this chapter. Variations in chemical properties of these complexes resulting from the modification of the bridgehead hydroxypyridinate at the 6-position, and from exchanging the dppm and dapm transoid-bridging ligands were examined. General spectroscopic properties of these complexes are, in most cases, similar to the properties of the dirhodium-μ-pyrazolato A-frame complexes discussed in Chapter 3. The fluxional behavior of the apex hydroxypyridinate ligands was identified and characterized using ^{31}P NMR. This fluxional behavior has been shown to vary depending on the bis-transoid bridges and on the substituent in the 6-position of the hydroxypyridinate apex ligand.

CHAPTER 5

MASS SPECTROMETRY OF SELECTED PYRAZOLATO-BRIDGED DIRHODIUM COMPLEXES

This work was performed jointly with J. D. Reynolds and much of the data reported here, including tables and figures, have been previously reported.[8,69] The research was undertaken to assess the use of fast-atom-bombardment mass spectrometry, FAB, and collision-induced-dissociation mass spectrometry, CID, to analyze a series of dirhodium A-frame complexes containing various apex bridging pyrazolates.

FAB, a technique first reported in the early 1980's,[70] involves bombardment of the sample and matrix (solvent) with high energy atoms and detection of the resulting ions. An atom beam of eight keV xenon atoms, produced by focusing Xe ions into a chamber containing Xe gas, was used in this study. CID is a tandem mass spectrometric technique that involves further fragmentation of a FAB-generated ion by collisions with neutral gas molecules. The 'daughter' fragments from this second collision are then subjected to mass spectrometric analysis.

Mass spectrometry (MS) can be used to rapidly obtain structural information that might otherwise be obtainable mainly through single-crystal X-ray crystallography, which requires the preparation of a single crystal and more

time. The utility of FAB in studies is limited because of interference signals due to redox processes induced by the medium. Either the matrix (solvent) or the argon atom beam is responsible for these medium-induced redox processes. CID expands the application of FAB and allows further structural information about dirhodium pyrazolato complexes to be obtained without redox interferences.

The pyrazolate compounds, identified in Table XVI, were introduced in chapter 2 and references therein. The compound of primary focus in this study is *47*, *$[Rh_2(I,II)(\mu\text{-}dppm)_2(t\text{-}BuNC)_2(\mu\text{-}4b35pz)](PF_6)_2$*, which contains an apex 4-bromo-3,5-dimethylpyrazolate, 4b35pz, whose single bromine atom gives a unique and easily traceable isotopic pattern in the mass spectrum. Several related complexes were studied to assess the effects of ligand variation and of metal oxidation state on the mass spectra. Comparisons of the apex ligands were made using *47* and complexes containing the 3,5-dimethylpyrazolate (35dmpz) or 5-methyl-3-trifluoromethylpyrazolate (mtmp); comparisons of the terminal ligand effects were made using complexes containing pairs of *t*-BuNC and CO ligands. Changing the transoid bridging ligands from dppm to dapm or dpam allowed comparison of the effects of these ligands. Oxidation state comparisons involved the use of complexes containing $Rh_2(I,II)$ and $Rh_2(I,I)$ cores. The compounds in this chapter may be designated as $M(PF_6)_n$, where n = 1 or 2 and M^+ or M^{2+} represents the $Rh_2(I,I)$- or $Rh_2(I,II)$-containing cations, respectively. MPF_6^+ refers to the ion-pair that contains a $Rh_2(I,II)$ species.

Table XVI

Dirhodium Compounds Discussed in Chapter 5

4.	$[Rh_2(\mu\text{-dpam})_2(CO)_2(\mu\text{-4b35pz})](PF_6)$
9.	$[Rh_2(\mu\text{-dpam})_2(t\text{-BuNC})_2(\mu\text{-4b35pz})](PF_6)$
12.	$[Rh_2(\mu\text{-dpam})_2(t\text{-BuNC})_2(\mu\text{-35dmpz})](PF_6)_2$
14.	$[Rh_2(\mu\text{-dpam})_2(t\text{-BuNC})_2(\mu\text{-4b35pz})](PF_6)_2$
28.	$[Rh_2(\mu\text{-dppm})_2(t\text{-BuNC})_2(\mu\text{-mtmp})](PF_6)_2$
30.	$[Rh_2(\mu\text{-dapm})_2(t\text{-BuNC})_2(\mu\text{-mtmp})](PF_6)_2$
44.	$[Rh_2(\mu\text{-dppm})_2(CO)_2(\mu\text{-4b35pz})](PF_6)$
45.	$[Rh_2(\mu\text{-dppm})_2(t\text{-BuNC})_2(\mu\text{-4b35pz})](PF_6)$
46.	$[Rh_2(\mu\text{-dppm})_2(CO)_2(\mu\text{-4b35pz})](PF_6)_2$
47.	$\mathbf{[Rh_2(\mu\text{-dppm})_2(t\text{-BuNC})_2(\mu\text{-4b35pz})](PF_6)_2}$
48.	$[Rh_2(\mu\text{-dppm})_2(t\text{-BuNC})_2(\mu\text{-35pz})](PF_6)_2$
49.	$[Rh_2(\mu\text{-dapm})_2(CO)_2(\mu\text{-4b35pz})](PF_6)$
50.	$[Rh_2(\mu\text{-dapm})_2(t\text{-BuNC})_2(\mu\text{-4b35pz})](PF_6)$
51.	$[Rh_2(\mu\text{-dapm})_2(CO)_2(\mu\text{-4b35pz})](PF_6)_2$
52.	$[Rh_2(\mu\text{-dapm})_2(t\text{-BuNC})_2(\mu\text{-4b35pz})](PF_6)_2$
53.	$[Rh_2(\mu\text{-dapm})_2(t\text{-BuNC})_2(\mu\text{-35pz})](PF_6)_2$

FAB experiments were performed using *meta*-nitrobenzyl alcohol (NBA) solutions of the appropriate compounds. NBA was selected as the matrix based on relative analyte sensitivities.[71] The FAB spectrum for *45*, which is representative of all compounds studied, is illustrated in Figure 17, and its major peaks are identified in Table XVII. Bromine's unique isotopic pattern is seen in the molecular ion cluster, shown enlarged in the upper left of Figure 17.

The major cluster of peaks in the FAB spectra of all compounds corresponds to M^+, the singly-charged molecular cation containing a $Rh_2(I,I)$ core. This indicates that reduction of the M^{2+} species with the $Rh_2(I,II)$ core occurs. Conversely, oxidation of a small percentage of the MPF_6 ion pair occurs for all $Rh_2(I,I)$ species as indicated by the presence of MPF_6^+ (Table XVIII). These are both examples of medium-induced redox processes.

In order to verify NBA-induced reduction/oxidation of the dirhodium species, UV-vis spectra for the compounds discussed in this chapter were obtained in degassed $MeCl_2$ and NBA. The λ_{max} values for the compounds are reported in Table XIX. Although NBA absorbs strongly below about 420 nm, this band does not hinder identification of the $Rh_2(I,II)$ and $Rh_2(I,I)$ complexes. In complexes containing *t*-BuNC, the maximum absorbances for each oxidation state are unique and are not solvent dependent. Since the absorbance maxima for the $Rh_2(I,II)(t\text{-BuNC})_2$ species are identical in both solvents, it follows that the reduction of a $Rh_2(I,II)$ species during the MS experiment is beam-induced. The

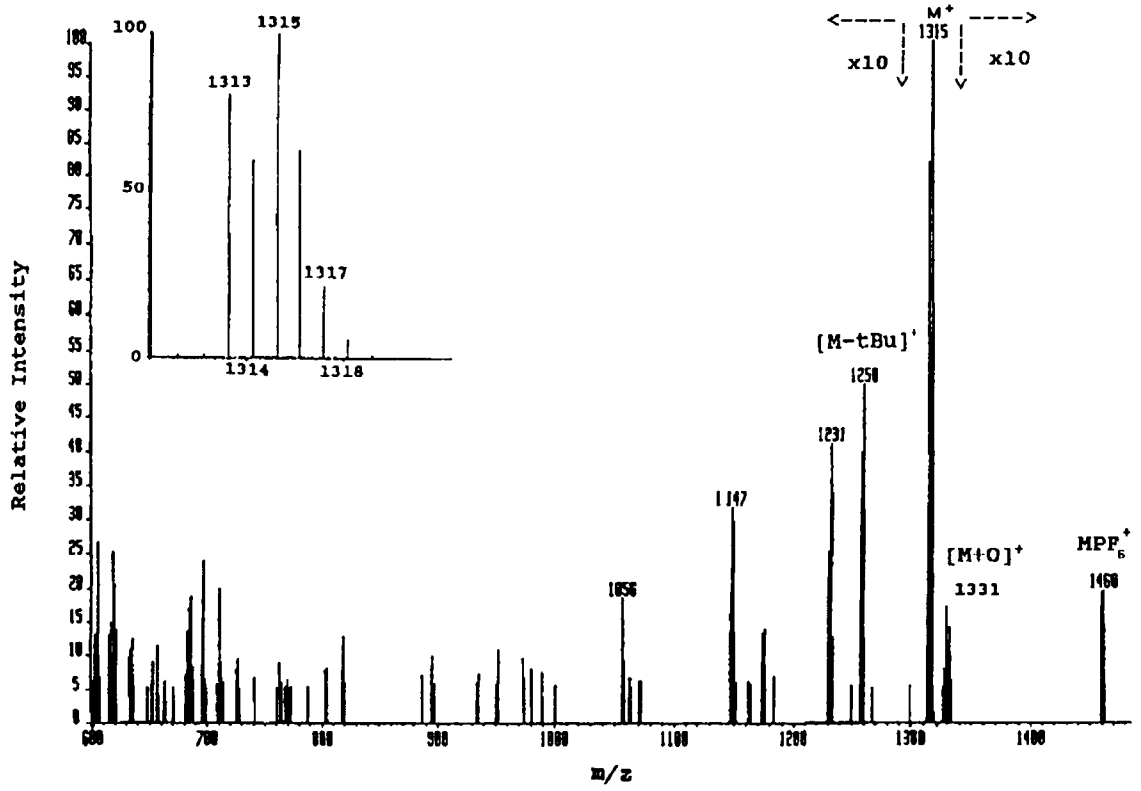

Figure 17. FAB spectrum of compound *45* in NBA.

Table XVII

Ions Detected in the FAB MS of *45* and *47*.

m/z	Relative Intensity[a] *45*	*47*	Ion[b]
1460	2	6	$[MPF_6]^+$
1365	-	2	unID'd
1331	2	4	$[M+O]^+$
1315	100	100	$[M]^+$
1258	5	8	[M-*t*-Bu]$^+$
1231	4	6	[M-*t*-BuNC]$^+$
1175	1	-	[M-(*t*-Bu+*t*-BuNC)]$^+$
1147	3	4	[M-2*t*-BuNC]$^+$
1057	2	4	[M-(*t*-BuNC+Z)]$^+$
973	1	5	[M-(2*t*-BuNC+Z)]$^+$
896	1	4	unID'd
658	-	4	$[M]^{2+}$

[a] Intensity is relative to the most abundant ion in the spectrum and refers to the most abundant ion in each isotope cluster.

[b] M = molecular cation; O = oxygen; unID'd = unidentified ion fragments; t-Bu = *tert*-butyl; and Z refers to 4-bromo-3,5-dimethylpyrazolate.

Table XVIII

Relative Intensities of Selected Ions Detected in FAB Spectra

Compound	Relative Intensity of Detected Ion (ox)[a]		
	MPF_6^+(I,II)	M^+(I,I)	M^{2+}(I,II)
4	6	100	0
9	5	100	0
12	6	100	3
14	14	100	7
28	6	100	2
30	6	100	2
44	8	100	0
45	2	100	0
46	0	100	0
47	6	100	4
48	31	100	6
49	6	100	0
50	3	100	0
51	0	100	0
52	6	100	3
53	7	100	4

[a] Intensity of the most abundant ion in each isotopic cluster.

Table XIX

UV-Vis λ_{max} (nm) Values in NBA and $MeCl_2$ and Redox Potentials in $MeCl_2$

Compound	Redox Conjugate	$MeCl_2$	NBA	$E_{1/2}$ (mV)[a]
4	-[b]	473	473	948
9	*14*	495	497	220
12	-[c]	436	438	220
14	*9*	436	438	-
28	-[c]	426	430	266
30	-[c]	428	431	163
44	*46*	492	494	780
45	*47*	513	430, 514	116
46	*44*	430	494	-
47	*45*	427	430	-
48	-[c]	429	431	55
49	*51*	484	486	886
50	*52*	502	436, 504	184
51	*49*	432	486	-
52	*50*	433	436	-
53	-[c]	435	438	146

[a] $E_{1/2} = (E_{p,a}+E_{p,c})/2$ vs. SCE (0.1 M TBAH/$MeCl_2$) for the $Rh_2(I,I)/(I,II)$ couple. Couple only listed for first occurrence of the conjugate. Values are from Chapter 3 or the synthetic reference listed in Chapter 2.

[b] Not isolable.

[c] Not investigated.

UV-vis spectra of the $Rh_2(I,I)$ species, *45* and *50*, in NBA reveal the presence of some oxidation products; thus *9* is the only $Rh_2(I,I)$ species containing *t*-BuNC that is not oxidized by NBA.

The $Rh_2(I,II)(CO)_2$ species *46* and *51* are shown to be reduced by NBA since the UV-Vis absorbance maxima in NBA are identical to those of the corresponding $Rh_2(I,I)(CO)_2$ species in either NBA or $MeCl_2$. This is indicative of NBA-induced reduction of the $Rh_2(I,II)(CO)_2$ species. Since oxidation of the corresponding $Rh_2(I,I)(CO)_2$ species in NBA is not observed, the presence of the $Rh_2(I,I)$ product in the mass spectrum must be due to beam-induced oxidation. While beam-induced reduction reactions are common in FAB MS,[72] beam-induced oxidation reactions are rare.[73] Inexplicably, the FAB spectra of *46* and *51* are the only ones that do not show ions corresponding to MPF_6^+ or M^{2+} (see Table XVIII). This is surprising since it has been demonstrated that the NBA solvent reduces the $Rh_2(I,II)(CO)_2$ species to $Rh_2(I,I)$, and the beam oxidizes the $Rh_2(I,I)(CO)_2$ species to $Rh_2(I,II)$.

An important observation made in Chapter 3 should be reiterated here: the rhodium(I,II) species containing carbon monoxide are more easily reduced than those containing *tert*-butylisocyanide due to the superior σ-donating ability of the isocyanide which stabilizes the higher oxidation state. This causes the $E_{1/2}$ value of the $Rh_2(I,I)/(I,II)$ couple of the carbon monoxide-containing $Rh_2(I,I)$

complexes, listed in the right column of Table XIX, to be approximately 600 mV higher than the isocyanide-containing compounds.

There appears to be a correlation between the NBA-induced redox reactions and the reduction potentials of the compounds studied. An examination of the electrochemical properties of NBA was thus performed. Cyclic voltammetry (CV) (± 2000 mV) of NBA with 0.1 M TBAH exhibited three poorly defined oxidation processes at approximately -500, 300, and 1400 mV versus SCE, while cyclic voltammetry of a solution of 5×10^{-4} M NBA in $MeCl_2$ and 0.1 M TBAH displayed one quasireversible couple centered at 1160 mV versus SCE. While cyclic voltammetry of the dirhodium complexes in NBA were unsuccessful due to solvent redox processes that overwhelmed the analyte signal, following the example of Callahan,[74] the above UV-vis data allow 'bracketing' or estimating the reduction and oxidation potentials of NBA based on the dirhodium species reduced and oxidized. The data in Table XX summarize the estimations of the reduction potential of NBA, between 314 and 222 mV versus SCE, and the oxidation potential of NBA, between 715 and 314 mV versus SCE. These bracketing estimations require the assumption that the redox potentials of the dirhodium complexes are solvent independent.

Although FAB has been shown to be a useful tool for general molecular weight determinations of the cationic complexes, the spectra are littered with fragments due to the medium-induced redox reactions. Further MS analysis of

Table XX

Selected Redox Reactions and Potentials

Half Reaction	Potential[a] (mV vs SCE)	Source[b]
51 + e^- -> *49*	841	red_{NBA}
46 + e^- -> *44*	715	red_{NBA}
NBA -> NBA_{ox} + ne^-	715 > E_{ox} > 231	
14 + e^- -> *9*	231	red_{beam}
9 -> *14* + e^-	314	ox_{beam}
NBA + ne^- -> NBA_{red}	314 > E_{red} > 222	
50 -> *52* + e^-	222	ox_{NBA}
45 -> *47* + e^-	188	ox_{NBA}

[a] Cathodic and anodic peak potentials are given for reduction and oxidation half reactions, respectively. Values are from Chapter 3 or the synthetic reference listed in Chapter 2.

[b] Source of reduction/oxidation is either NBA or the atom beam.

an individual ion from an identified ion cluster in the primary mass spectrum yields more identifiable structural information and also gives an estimate of relative bond strengths within the isolated ion. This tandem MS may be accomplished using CID.

M^+, M^{2+}, and MPF_6^+ ions were selected for CID in an attempt to further characterize the fragmentation patterns of these dirhodium compounds. The CID of M^{2+} was not obtainable, likely due to the ion's low abundance. In general, detection of doubly-charged ions in FAB is uncommon.[75] This may be related to the low intensity of the M^{2+} ion. Attempts to increase the signal intensity of the M^{2+} ion proved unsuccessful.

The only successfully characterized CID of MPF_6^+ ions were those generated from the isocyanide-containing complexes. The only ion detected in the CID mass spectrum of the Rh_2(I,II) ion-paired molecular cation, MPF_6^+, was the ion corresponding to loss of both the hexafluorophosphate anion and a *tert*-butyl radical cation, $[M-(PF_6^-+t\text{-}Bu^+)]^+$. This fragmentation is not readily explicable, but the concurrent loss of PF_6^- and t-Bu^+ suggest an ion pairing or the formation of the three neutrals: PF_5°, HF, and isobutene. Formation of the neutrals is favored in the gas phase by approximately 90.1 kcal/mol.[76] Similarly, the loss of HF and PF_5° (and other neutral losses) from the ion-paired $[Ru(bdmt)(bpy)_2PF_6]^+$ complex (bdmt = 3,3':5,3"-bis(dimethylene)-2,2':6,2"-terpyridine; bpy = 2,2'-bypyridine) has been observed using CID.[77]

The intensity of the $[M-(PF_6^- + t\text{-}Bu^+)]^+$ signal is virtually identical in both the CID of the MPF_6^+ species arising from the dissociation of $M(PF_6)_2$ with the $Rh_2(I,II)$ core (*14*, *47*, and *52*) and the CID of MPF_6^+ arising from the medium-induced oxidation of $M(PF_6)$ with the $Rh_2(I,I)$ core (*9*, *45*, and *50*). This demonstrates that medium-induced oxidation arising from the primary atom beam or NBA does not change the structure/internal energy enough to alter the collision-induced fragmentation.

Much more can be learned by examination of the CID of the M^+ cation derived from these dirhodium compounds than from FAB or the CID of MPF_6^+ species. A representative spectrum is illustrated in Figure 18 which shows the CID spectrum of M^+ for *45*. Data tabulated from the CID spectrum of the M^+ ions of the compounds examined are listed in Tables XXI-XXX. The mass determinations from the CID results reported are within two amu.

Comparison of the M^+ species generated from the dissociation of the $Rh_2(I,I)$-containing MPF_6 and the M^+ species generated from medium-induced reduction of $Rh_2(I,II)$-containing species shows the effect of the reductions on the CID process. The M^+ ions from reduced $Rh_2(I,II)$ species show less fragmentation than the M^+ ions from $Rh_2(I,I)$ complexes. Specifically, the CID spectra of M^+ from $Rh_2(I,I)$ complexes show a greater abundance of daughter ions missing a phenyl ring from one of the transoid dppm, dapm, or dpam ligands. Furthermore, in the CID spectra of M^+ ions from the isocyanide-

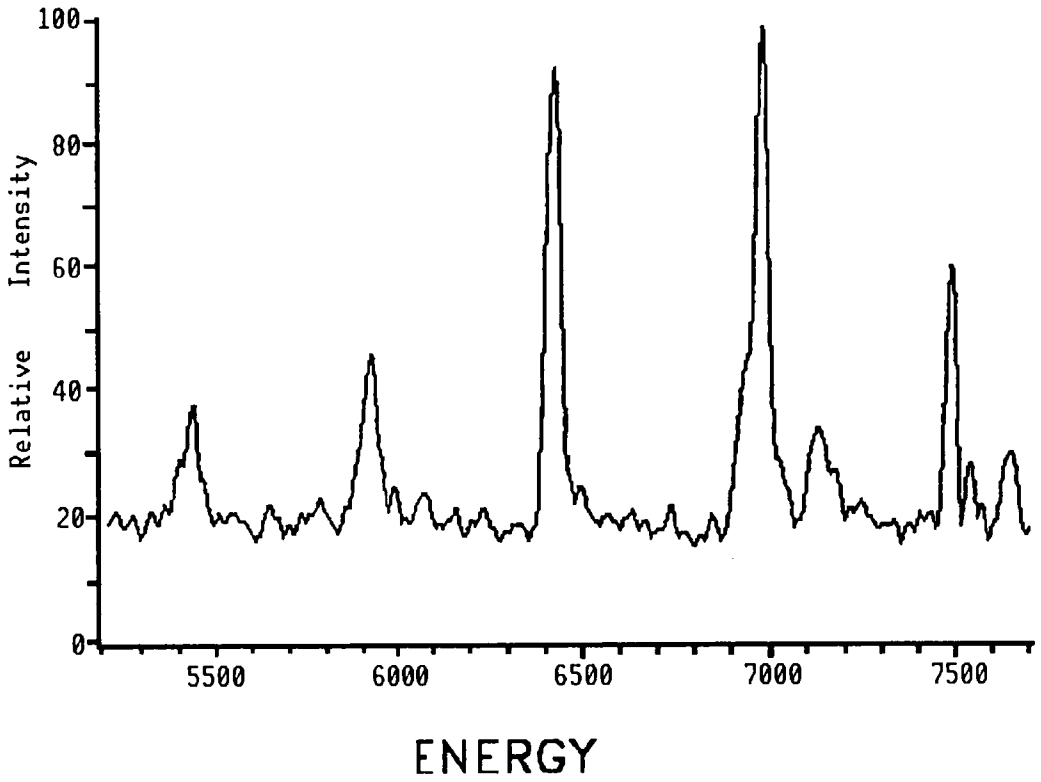

Figure 18. CID Spectrum (Energy, V, vs. Relative Intensity) for M^+ (m/z = 1313) of Compound *45* in NBA.

Table XXI

Ions Detected in the CID Spectrum of the Molecular Cation (M^+; m/z = 1313) for Compound *45*.

Energy (Volts)	m/z	Relative Intensity[a]	Ion[b]
7653	1256	31	[M-*t*-Bu]$^+$
7530	1236	28	[M-ϕ]$^+$
7494	1230	61	[M-*t*-BuNC]$^+$
7147	1173	39	[M-(*t*-Bu+*t*-BuNC)]$^+$
6988	1147	100	[M-2*t*-BuNC]$^+$
6934	1138	49	[M-Z]$^+$
6428	1055	89	[M-(Z+*t*-BuNC)]$^+$
5922	972	44	[M-(Z+2*t*-BuNC)]$^+$
5435	895	44	[M-(Z+2*t*-BuNC+ϕ)]$^+$

[a] Intensity is measured at maximum peak height and is relative to the most abundant ion in the spectrum.

[b] M = molecular cation; *t*-Bu = *tert*-butyl radical; ϕ = phenyl radical; Z = neutral 4-bromo-3,5-dimethylpyrazole radical.

Table XXII

Ions Detected in the CID Spectrum of the Molecular Cation (M^+) for Compounds *44*, *49*, and *4*.

Energy (Volts)	m/z	Relative Intensity[a]	Ion[b]
	1205	**Compound *44***	**M^+**
7814	1177	44	$[M\text{-}CO]^+$
7628	1149	100	$[M\text{-}2CO]^+$
7100	1072	11	$[M\text{-}(2CO+\phi)]^+$
6612	996	56	$[M\text{-}(pz+CO)]^+$
6452	972	28	$[M\text{-}(pz+2CO)]^+$
5595	897	34	$[M\text{-}(pz+2CO+\phi)]^+$
	1291	**Compound *49***	**M^+**
7826	1263	26	$[M\text{-}CO]^+$
7652	1235	100	$[M\text{-}2CO]^+$
7158	1158	54	$[M\text{-}(2CO+\phi)]^+$
6580	1062	33	$[M\text{-}\phi_2As]^+$
5750	928	48	$[M\text{-}(\phi_2As+2CO+\phi)]^+$
	1379	**Compound *4***	**M^+**
7837	1351	45	$[M\text{-}CO]^+$
7760	1335	37	$[M\text{-}(CO+O)]^+$
7675	1323	100	$[M\text{-}2CO]^+$
7390	1274	56	$[M\text{-}(\phi+CO)]^+$
7228	1246	54	$[M\text{-}(\phi+2CO)]^+$
6753	1164	54	$[M\text{-}(2\phi+2CO)]^+$
6672	1150	31	$[M\text{-}\phi_2As]^+$
6265	1080	63	$[M\text{-}(\phi_2As+2CO)]^+$

[a] Intensity is measured at maximum peak height and is relative to the most abundant ion in the spectrum.

[b] M = molecular cation; ϕ = phenyl radical; pz = 4-bromo-3,5-dimethylpyrazole radical.

Table XXIII

Ions Detected in the CID Spectrum of the Molecular Cation (M^+; m/z = 1401) for Compound *50*.

Energy (Volts)	m/z	Relative Intensity[a]	Ion[b]
7675	1344	36	$[M\text{-}t\text{-Bu}]^+$
7526	1318	85	$[M\text{-}t\text{-BuNC}]^+$
7180	1261	26	$[M\text{-}(t\text{-Bu}+t\text{-BuNC})]^+$
7052	1235	100	$[M\text{-}2t\text{-BuNC}]^+$
6692	1172	54	$[M\text{-}\phi_2As]^+$
6612	1158	23	$[M\text{-}\phi_2AsCH_2]^+$
6367	1115	15	$[M\text{-}(\phi_2As+t\text{-Bu})]^+$
6253	1095	8	$[M\text{-}(\phi_2As+\phi)]^+$
6218	1089	12	$[M\text{-}(\phi_2As+t\text{-BuNC})]^+$
5893	1032	15	$[M\text{-}(\phi_2As+t\text{-Bu}+t\text{-BuNC})^+$
5744	1006	10	$[M\text{-}(\phi_2As+2t\text{-BuNC})]^+$
5556	973	14	$[M\text{-dapm}]^+$
5110	896	8	$[M\text{-}(dapm+\phi)]^+$

[a] Intensity measured at maximum peak height and is relative to the most abundant ion in the spectrum.

[b] M = molecular cation; *t*-Bu = *tert*-butyl radical; ϕ = phenyl radical; dapm = (diphenylarsino)(diphenylphosphino)methane.

Table XXIV

Ions Detected in the CID Spectrum of the Molecular Cation (M^+; m/z = 1489) for Compound *9*.

Energy (Volts)	m/z	Relative Intensity[a]	Ion[b]
7694	1432	64	$[M\text{-}t\text{-Bu}]^+$
7554	1406	34	$[M\text{-}t\text{-BuNC}]^+$
7108	1323	11	$[M\text{-}2t\text{-BuNC}]^+$
6769	1260	80	$[M\text{-}\phi_2As]^+$
6694	1246	24	$[M\text{-}\phi_2AsCH_2]^+$
6463	1203	14	$[M\text{-}(\phi_2As+t\text{-Bu})]^+$
6248	1163	20	$[M\text{-}(\phi_2As+t\text{-BuNC})]^+$
5803	1080	8	$[M\text{-}(\phi_2As+2t\text{-BuNC})]^+$
5464	1017	47	$[M\text{-dapm}]^+$
5018	934	65	$[M\text{-}(dapm+t\text{-BuNC})]^+$
4712	877	50	$[M\text{-}(dapm+t\text{-BuNC}+t\text{-Bu})]^+$
4572	851	100	$[M\text{-}(dapm+2t\text{-BuNC})]^+$
4158	774	74	$[M\text{-}(dapm+\phi_2AsCH_2)]^+$

[a] Intensity is measured at maximum peak height and is relative to the most abundant ion in the spectrum.

[b] M = molecular cation; *t*-Bu = *tert*-butyl radical; ϕ = phenyl radical; dapm = bis(diphenylarsino)methane.

Table XXV

Ions Detected in the CID Spectrum of the Molecular Cation (M^+) for Compounds *47*, *48*, and *28*.

Energy (Volts)	m/z	Relative Intensity[a]	Ion[b]
	1313	**Compound *47***	**M^+**
7653	1256	27	[M-*t*-Bu]$^+$
7494	1230	62	[M-*t*-BuNC]$^+$
7147	1173	19	[M-(*t*-Bu+*t*-BuNC)]$^+$
6988	1147	100	[M-2*t*-BuNC]$^+$
6934	1138	34	[M-Z]$^+$
6428	1055	104	[M-(Z+*t*-BuNC)]$^+$
5922	972	11	[M-(Z+2*t*-BuNC)]$^+$
	1235	**Compound *48***	**M^+**
7630	1178	36	[M-*t*-Bu]$^+$
7462	1152	89	[M-*t*-BuNC]$^+$
7094	1095	51	[M-(*t*-Bu+*t*-BuNC)]$^+$
7925	1069	100	[M-2*t*-BuNC]$^+$
6866	1060	145	[M-Z]$^+$
6330	977	73	[M-(Z+*t*-BuNC)]$^+$
5791	894	53	[M-(Z+2*t*-BuNC)]$^+$
	1289	**Compound *28***	**M^+**
7646	1232	43	[M-*t*-Bu]$^+$
7485	1206	72	[M-*t*-BuNC]$^+$
7130	1149	51	[M-(*t*-Bu+*t*-BuNC)]$^+$
6970	1123	100	[M-2*t*-BuNC]$^+$
6914	1114	25	[M-Z]$^+$
6400	1031	76	[M-(Z+*t*-BuNC)]$^+$
5884	948	37	[M-(Z+2*t*-BuNC)]$^+$

[a] Intensity is measured at peak maximum and is relative to the intensity of [M-2*t*-BuNC].

[b] M = molecular ion; *t*-Bu = *tert*-butyl radical; Z = 4-bromo3,5-dimethyl-pyrazole (*47*), 3,5-dimethylpyrazole (*48*), or 3-methyl-5-trifluoromethyl-pyrazole (*28*) radical.

Table XXVI

Ions Detected in the CID Spectrum of the Molecular Cation (M^+) for Compounds *46* and *51*.

Energy (Volts)	m/z	Relative Intensity[a]	Ion[b]
	1205	Compound *46*	M^+
7814	1177	64	$[M\text{-}CO]^+$
7628	1149	100	$[M\text{-}2CO]^+$
7100	1070	13	$[M\text{-}(2CO+Br)]^+$
6612	996	61	$[M\text{-}(Z+CO)]^+$
6452	972	42	$[M\text{-}(Z+2CO)]^+$
	1291	Compound *51*	M^+
7826	1263	12	$[M\text{-}CO]^+$
7652	1235	100	$[M\text{-}2CO]^+$
7158	1156	20	$[M\text{-}(2CO+Br)]^+$
6580	1062	10	$[M\text{-}\phi_2As]^+$

[a] Intensity is measured at maximum peak height and is relative to the most abundant ion in the spectrum.

[b] M = molecular cation; ϕ = phenyl radical; Z = 4-bromo-3,5-dimethylpyrazole radical.

Table XXVII

Ions Detected in the CID Spectrum of the Molecular Cation (M^+; m/z = 1401) for Compound *52*.

Energy (Volts)	m/z	Relative Intensity[a]	Ion[b]
7675	1344	23	$[M\text{-}t\text{-Bu}]^+$
7526	1318	100	$[M\text{-}t\text{-BuNC}]^+$
7180	1261	26	$[M\text{-}(t\text{-Bu}+t\text{-BuNC})]^+$
7052	1235	87	$[M\text{-}2t\text{-BuNC}]^+$
6692	1172	76	$[M\text{-}\phi_2\text{As}]^+$
6612	1158	20	$[M\text{-}\phi_2\text{AsCH}_2]^+$
6367	1115	20	$[M\text{-}(\phi_2\text{As}+t\text{-Bu})]^+$
6218	1089	17	$[M\text{-}(\phi_2\text{As}+t\text{-BuNC})]^+$
5893	1032	17	$[M\text{-}(\phi_2\text{As}+t\text{-Bu}+t\text{-BuNC})]^+$
5744	1006	19	$[M\text{-}(\phi_2\text{As}+2t\text{-BuNC})]^+$
5556	973	16	$[M\text{-dapm}]^+$

[a] Intensity measured at maximum peak height and is relative to the most abundant ion in the spectrum.

[b] M = molecular cation; *t*-Bu = *tert*-butyl radical; ϕ = phenyl radical; dapm = (diphenylarsino)(diphenylphosphino)methane.

Table XXVIII

Ions Detected in the CID Spectrum of the Molecular Cation (M^+; m/z = 1489) for Compound *14*.

Energy (Volts)	m/z	Relative Intensity[a]	Ion[b]
7694	1432	71	[M-*t*-Bu]$^+$
7554	1406	51	[M-*t*-BuNC]$^+$
7108	1323	28	[M-2*t*-BuNC]$^+$
6769	1260	100	[M-ϕ_2As]$^+$
6694	1246	36	[M-ϕ_2AsCH$_2$]$^+$
6248	1163	43	[M-(ϕ_2As+*t*-BuNC)]$^+$
5803	1080	17	[M-(ϕ_2As+2*t*-BuNC)]$^+$
5464	1017	63	[M-dpam]$^+$
5018	934	14	[M-(dpam+*t*-BuNC)]$^+$
4712	877	15	[M-(dpam+*t*-BuNC+*t*-Bu)]$^+$
4572	851	23	[M-(dpam+2*t*-BuNC)]$^+$

[a] Intensity is measured at maximum peak height and is relative to the most abundant ion in the spectrum.

[b] M = molecular cation; *t*-Bu = *tert*-butyl radical; ϕ = phenyl radical; dpam = bis-(diphenylarsino)methane.

Table XXIX

Ions Detected in the CID Spectrum of the Reduced Molecular Cation (M^+) for Compounds *53* and *30*.

Energy (Volts)	m/z	Relative Intensity[a]	Ion[b]
	1323	**Compound *53***	**M^+**
7655	1266	53	[M-*t*-Bu]$^+$
7498	1240	100	[M-*t*-BuNC]$^+$
7153	1183	42	[M-(*t*-Bu+*t*-BuNC)]$^+$
6996	1157	106	[M-2*t*-BuNC]$^+$
6615	1094	53	[M-ϕ_2As]$^+$
6531	1080	30	[M-ϕ_2AsCH$_2$]$^+$
6270	1037	23	[M-(ϕ_2As+*t*-Bu)]$^+$
6113	1011	12	[M-(ϕ_2As+*t*-BuNC)]$^+$
5768	954	19	[M-(ϕ_2As+*t*-Bu+*t*-BuNC)]$^+$
5611	928	7	[M-(ϕ_2As+2*t*-BuNC)]$^+$
5411	895	14	[M-dapm]$^+$
	1377	**Compound *30***	**M^+**
7669	1320	26	[M-*t*-Bu]$^+$
7518	1294	100	[M-*t*-BuNC]$^+$
7187	1237	13	[M-(*t*-Bu+*t*-BuNC)]$^+$
7036	1211	67	[M-2*t*-BuNC]$^+$
6669	1148	36	[M-ϕ_2As]$^+$
6588	1134	18	[M-ϕ_2AsCH$_2$]$^+$
6338	1091	9	[M-(ϕ_2As+*t*-Bu)]$^+$
6187	1065	13	[M-(ϕ_2As+*t*-BuNC)]$^+$
5804	999	7	[M-(ϕ_2As+*t*-Bu+*t*-BuNC)]$^+$
5705	982	16	[M-(ϕ_2As+2*t*-BuNC)]$^+$
5513	949	8	[M-dapm]$^+$

[a] Intensity is measured at peak maximum and is relative to the intensity of [M-*t*-BuNC]$^+$.

[b] M = molecular cation; *t*-Bu = *tert*-butyl radical; ϕ = phenyl radical.

Table XXX

Ions Detected in the CID Spectrum of the Molecular Cation (M^+; m/z 1410) for Compound *12*.

Energy (Volts)	m/z	Relative Intensity[a]	Ion[b]
7676	1353	200	$[M\text{-}t\text{-Bu}]^+$
7529	1327	100	$[M\text{-}t\text{-BuNC}]^+$
7205	1270	15	$[M\text{-}(t\text{-Bu}+t\text{-BuNC})]^+$
7058	1244	60	$[M\text{-}2t\text{-BuNC}]^+$
6700	1181	140	$[M\text{-}\phi_2\text{As}]^+$
6621	1167	88	$[M\text{-}\phi_2\text{AsCH}_2]^+$
6378	1124	15	$[M\text{-}(\phi_2\text{As}+t\text{-Bu})]^+$
6230	1098	42	$[M\text{-}(\phi_2\text{As}+t\text{-BuNC})]^+$
5758	1015	80	$[M\text{-}(\phi_2\text{As}+2t\text{-BuNC})]^+$
5321	938	82	$[M\text{-dapm}]^+$
4851	855	85	$[M\text{-}(\text{dapm}+t\text{-BuNC})]^+$
4380	772	68	$[M\text{-}(\text{dapm}+2t\text{-BuNC})]^+$

[a] Intensity is measured at maximum peak height and is relative to [M-*t*-BuNC].

[b] M = molecular cation; *t*-Bu = *tert*-butyl radical; ϕ = phenyl radical; dapm = (diphenylarsino)(diphenylphosphino)methane.

containing Rh_2(I,II) complexes, no daughter ions showing the loss of a phenyl ring were observed. This behavior implies that beam-induced reduction stabilizes the species being fragmented, perhaps by decreasing the amount of collision energy available for fragmentation. In the case of matrix-induced reduction of the dirhodium (I,II) carbonyl species (*46* and *51*), less fragmentation is observed in the spectra than in the CID M^+ spectra of the $Rh_2(I,I)(CO)_2$ compounds (*44* and *49*). Thus, these solvent-solute redox reactions that are manifested in the mass spectra must lead to subtle changes in the structure or electronic nature of the reduced solutes.

A comparison of analogous compounds containing a pair of bridging dppm (*47*), dapm (*52*), and dpam (*14*) ligands shows a variation in the fragmentation patterns. For compounds containing bis(dppm) bridges, CID spectra of the M^+ species display signals due to loss of the apex pyrazolate (as a neutral pyrazole radical). Since signals due to the neutral loss of the apex ligand are not present in the CID spectra of the bis(dapm) and bis(dpam) complexes, this suggests that the relative strength of the Rh_2-$(N_{pz})_2$ interaction is intermediate to the strengths of the Rh-P (stronger) and Rh-As (weaker) bonds of the transoid ligands. Literature discussions of the relative strengths (strong to weak) of the Rh-P, Rh-$C_{(RNC)}$, and Rh-As bonds were presented in Chapter 1. In addition, CID spectra of the M^+ ions of the bis(dppm)-containing species do not display signals due to the loss of any part of a dppm ligand. This behavior further illustrates the relative strength of the Rh-P bond.

Conversely, only when the transoid bridging ligand contains an As atom (dapm or dpam), do the CID spectra of the M^+ species display signals due to loss of all or any identifiable part of the transoid bridging ligands.

In the dapm-containing compound *50* for example, certain of the signals from the fragmentation of M^+ can be attributed to the loss of one of three different neutrals originating from the dapm ligand (see Table XXIII). These three neutrals are a diphenylarsine radical ($\phi_2As\cdot$), a methylenediphenylarsine radical ($\phi_2AsCH_2\cdot$), and the bridging dapm ligand itself ($\phi_2AsCH_2P\phi_2$). Similar fragmentation patterns are noted for the other dapm-bridged compounds *30* (Table XXIX), *52* (Table XXVII), and *53* (Table XXIX).

For a dapm-containing molecular cation to lose an entire bridging ligand, a single Rh-P bond must be broken. These daughter ions are the only examples in this study that illustrate cleavage of the Rh-P bond. Thus, when a dapm-containing M^+ species loses part of the bridge, only As-containing neutrals are lost. The predominance of daughter ions missing the $\phi_2As\cdot$ fragment compared to those that lost the $\phi_2AsCH_2\cdot$ indicates that the $P\text{-}C_{dapm}$ (methylene) bonds are stronger than the corresponding $As\text{-}C_{dapm}$ (methylene) bonds. It is possible that collision-induced-dissociation imparts enough velocity to a partially dissociated dapm ligand that the mass of the As-containing free end of the ligand acts as a slingshot and provides enough energy to occasionally break the Rh-P bond.

The CID spectra of M^+ ions for compounds containing bis(dpam) bridges display the most signals at lower mass-to-charge ratio. This indicates greater fragmentation or loss of heavier fragments. A comparison of the dapm-containing *52* (Table XXVII) with the dpam-containing *14* (Table XXVIII) shows that the CID spectrum of *14* displays peaks of greater intensities for lower molecular weight daughters than does *52*. Also, the relative signal strengths of daughters formed by the loss of a single transoid bridge were greater in the dpam-containing complexes (Table XXVII and Table XXVIII). Experimentally, the bridging ligand becomes more labile under CID conditions as arsenic replaces phosphorus, and this reconfirms that the Rh-P bond is stronger than the Rh-As bond.

As previously noted, the apex pyrazolate is subject to loss (as a pyrazole radical) from only the M^+ ion of the dppm-containing complexes under CID conditions. There is a correlation between the intensity of daughter ions displaying the loss of the pyrazole radical and the basicity of the apex pyrazolate. The CID fragmentation of M^+ of the bis(dppm) bridged complexes *47*, *48*, and *28* (Table XXV) reveal that each displays three signals due to daughters that have lost the pyrazole radical ($[M\text{-}Z]^+$, $[M\text{-}(Z+t\text{-BuNC})]^+$, and $[M\text{-}(Z+2t\text{-BuNC})]^+$, where Z = the specific pyrazole lost). Relative pyrazolate basicities can be estimated based on the electronegativities of the ring substituents (the greater the substituent electronegativity, the less electron density available for donation to the rhodium centers). Thus, the relative

basicity of the pyrazolates increases as mtmp < 4B35pz < 35dmpz. AM1 semi-empirical calculations[78] of the gas-phase acidities of the pyrazoles (HZ), listed in Table XXXI, conform to this trend. Both the intensity of fragments resulting from the loss of the neutral pyrazole radical ($[M\text{-}pz]^+$) and a summation of the intensities for the three signals that exhibit the loss of pyrazole radical follow this trend. The most basic apex ligand (35mpz) shows the greatest loss because it is the pyrazolate most likely to leave as a neutral radical.

The CID of *t*-BuNC-containing complexes display spectra that are more complex than those of the CO-containing complexes, due to the increased fragmentation of the isocyanide ligand. The CID MS results for the dicarbonyl-dirhodium cations containing arsenic (*4*, *49*, and *51*) show fewer daughters that have lost part of their dapm or dpam ligands than have their isocyanide containing analogs (*9*, *50*, and *52*). This observation implies that the bonds of the transoid ligands are stronger in the carbonyl-containing complexes than in the isocyanide-containing complexes. This likely involves the greater π-acidity of CO (relative to *t*-BuNC) resulting in withdrawal of π-electron density from the rhodium, inductively strengthening the Rh-P and/or Rh-As bond compared to the *t*-BuNC terminal ligand.

Dirhodium complexes can be readily characterized by MS. The medium, specifically the primary atom beam or NBA, may induce both oxidation and reduction reactions. FAB spectra of these dirhodium(I,I) and (I,II) complexes

Table XXXI

Pyrazole Acidity and Loss Information for Compounds *28*, *47*, and *48*.

Pyrazolate Ligand	Gas-Phase Acidity[a]	Compound #	Relative Intensity[b] $[M-Z]^+$	Relative Intensity[b] SUM
35dmpz	339.1	*48*	145	271
4b35pz	330.8	*47*	34	149
mtmp	320.5	*28*	25	138

[a] Estimated enthalpy based upon AM1 semi-empirical calculation for HX (g) -> H^+ (g) + X^- (g) in kcal/mol.

[b] Intensity relative to $[M-2t\text{-BuNC}]^+$. SUM is the sum of intensities for all ions that have lost the pyrazole radical: $[M-Z]^+$, $[M-(Z+t\text{-BuNC})]^+$, $[M-(Z+2t\text{-BuNC})]^+$.

are dominated by signal from an intact $Rh_2(I,I)$ cation. FAB is thus useful for mass determinations. Identification of important fragmentation reactions is complicated by the signals due to additional fragmentation patterns of species formed by the beam- and/or matrix-induced damage.

The use of CID insures that spectra display only daughter fragments originating from a particular parent species of known mass. This allows proper assignment of the fragmentation reactions which reveal information about relative bond strengths within the selected ion. CID spectra arising from $Rh_2(I,I)$ cations reveal much about the differences in relative bond strengths due to differences in the ligands present. In general, relative rhodium bond strengths were observed to vary as Rh-P > $Rh\text{-}N_{(pz)}$ > $Rh\text{-}C_{(RNC)}$ > Rh-As > $Rh\text{-}C_{(CO)}$ within the various dirhodium species presented here. Further, the loss of a neutral pyrazole radical (from the dppm complexes) as in the CID spectrum is greatest for the complex containing the most basic pyrazole. The CID spectra arising from the isocyanide-containing $Rh_2(I,II)$ species ion-paired with PF_6^- show only a signal due to the loss of both PF_6^- and $t\text{-}Bu^+$. The mass spectral fragmentation patterns for these dirhodium pyrazolates can be understood by correlating them with reactivities of similar rhodium complexes. CID experiments reveal valuable chemical information about dirhodium A-frames and are complementary to FAB for their characterization.

CHAPTER 6

AN EXAMINATION OF THE KINETICS OF A DIRHODIUM DISPROPORTIONATION REACTION

The final topic to be discussed involves an examination of the kinetics and possible mechanism of the disproportionation of the green dirhodium (I,II) bis(isocyanide) complexes with halide or pseudohalide in methylene chloride, $MeCl_2$. The reaction of interest is the disproportionation of a $Rh_2(I,II)$ species in the presence of chloride ion, Cl^-:

$$[Rh_2(I,II)(\mu\text{-}E\hat{}E')_2(\mu\text{-}Xpz)(t\text{-}BuNC)_2](PF_6)_2 + Cl^- \rightarrow$$

$$\tfrac{1}{2}\,[Rh_2(II)(\mu\text{-}E\hat{}E')_2(\mu\text{-}Xpz)(t\text{-}BuNC)_2Cl_2](PF_6) +$$

$$\tfrac{1}{2}\,[Rh_2(I,I)(\mu\text{-}E\hat{}E')_2(\mu\text{-}Xpz)(t\text{-}BuNC)_2](PF_6),$$

where E^E' represents the transoid bridging ligand dppm, dapm or dpam, and Xpz represents the bridgehead pyrazolate or substituted pyrazolate.

In general, the thermodynamic impetus for the disproportionation of $Rh_2(I,II)$ d^7-d^8 radicals has been shown to originate in the energetically favorable axial coordination of ligands to form $Rh_2(II,II)$ d^7-d^7 species.[79] In the initial report of this reaction by Tortorelli et al.,[80] it was shown that the $Rh_2(II,II)$ species is greatly stabilized by the presence of halide or pseudohalide. In the presence of a coordinating halide or pseudohalide the oxidation wave in the cyclic

voltammogram of the $Rh_2(I,I)$ species becomes a two-electron process at less positive potential.

A spectroelectrochemical examination of the oxidation of the $Rh_2(I,I)$ species in the presence of the $Rh_2(II,II)Cl_2$ species and excess chloride confirms the direct formation of the $Rh_2(II,II)Cl_2$ species from the $Rh_2(I,I)$ species. The isosbestic point near 445 nm in Figure 19 gives evidence for lack of a discernible intermediate.

A prior report noted a similar chloride-induced disproportionation of the $Rh_2(I,II)(dppm)_2(dimen)_2$ (dimen is 1,8-diisocyanomenthane) species in solution.[81] This mixed-valence bis(dimen) species was shown to be stable in the presence of bulky anions such as ClO_4^-. The $Rh_2(I,II)(dppm)(dimen)_3$ and $Rh_2(I,II)(dimen)_4$ species disproportionate in perchlorate solutions as well as in chloride-containing solutions. This suggests that the phenyl rings of trans dppm ligands interfere with the axial binding of bulky ligands.[82] Thus the $Rh_2(I,II)$ oxidation state is stabilized in bis(dppm) complexes by steric protection of the axial sites.

The study presented here involves three representative dirhodium(I,II) compounds: $[Rh_2(\mu\text{-dpam})_2(t\text{-BuNC})_2(\mu\text{-35dmpz})](PF_6)_2$, *12*, $[Rh_2(\mu\text{-dapm})_2(t\text{-BuNC})_2(\mu\text{-mtmp})](PF_6)_2$, *30*, and $[Rh_2(\mu\text{-dppm})_2(t\text{-BuNC})_2(\mu\text{-35dmpz})](PF_6)_2$, *48*. Generally, the results of the reaction of bis(dppm)- and bis(dpam)-bridged species were compared, with the results from the bis(dapm)-bridged complex

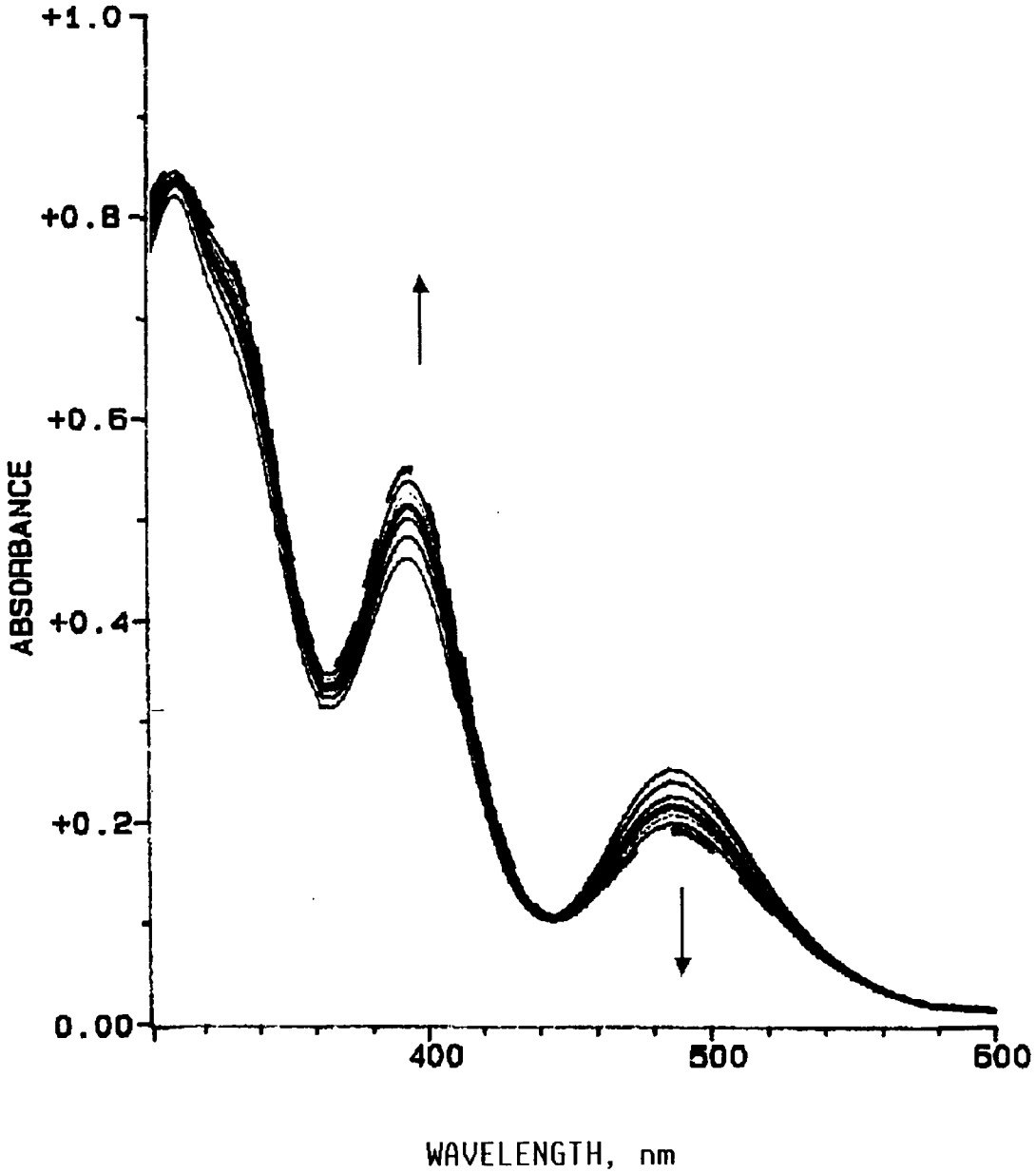

Figure 19. Spectroelectrochemical oxidation of *7* (2.6 X 10^{-5} M in 0.1 M TBAH/$MeCl_2$) at 500 mV in the presence of the $Rh_2(II,II)Cl_2$ product and Cl^- (7 scans 15 seconds apart).

30 used only to verify observed trends among the three types of bridged complexes. Solutions of both reactants were prepared in concentrations that varied by at least an order of magnitude except in the case of *30*, where the concentration of Rh_2(I,II) remained fixed. Neutral density filters (0.5, 1.0) were used for the bis(dppm) complex to examine the influence of photon flux.

The above reaction was carried out at room temperature (23 ± 2° C) using an Aminco Morrow stopped-flow apparatus (model J4) adapted with machined teflon inserts to accept luer-tipped syringes. All glass luer-tipped syringes (non-gas-tight) were used. While no reactants or products exhibited air sensitivity, all solutions were degassed with Ar thoroughly before use. The syringes were filled without any headspace gas by positive Ar pressure, and no further precautions were made to exclude trace amounts of oxygen. Small amounts of O_2 could have been introduced through a loosely fitting syringe barrel, through the luer tip, or through the fittings of the apparatus.

UV-Vis spectroscopy was chosen to monitor the reaction kinetics because the dirhodium reactant and product species each have unique absorbance maxima: Rh_2(I,II) (near 430 nm); Rh_2(II,II) (near 390 nm); and Rh_2(I,I) (near 490 nm). Initially, however, when the concentration of the starting material is much greater than that of the products, the absorbance of the Rh_2(I,II) overwhelms the absorbances of the products, even at their absorbance maxima. Thus, early in

the reaction, UV-Vis spectroscopy is suitable for monitoring only the disappearance of the Rh_2(I,II) starting material.

Preliminary data (using excess chloride) were collected at fixed wavelength using a UV-Vis spectrophotometer (Beckman DU). The disappearance of the Rh_2(I,II) species was monitored and did not follow simple kinetic behavior. A plot of absorbance versus time at 436 nm for the reaction of *48* (4.32×10^{-5} M) with Cl^- (1.14×10^{-3} M) is shown in Figure 20 (time dependent plots of this reaction will be used further as illustration). Both a plot of $\log(A_t - A_\infty)$ versus time (Figure 21) and a plot of $(A_t - A_\infty)^{-1}$ (Figure 22) show curvature indicating that the reaction does not obey either simple first- or second-order behavior (A_t is the absorbance at time *t*, and A_∞ is the final absorbance at time infinity).

A $MeCl_2$ solution of compound *30* was titrated with ¼ equivalents of chloride (four 4.4 μL additions of 7.44×10^{-3} M TBACl to 1.0 mL of 1.30×10^{-4} M *30*), as shown in Figure 23. The failure to observe an isosbestic point near 460 nm and the preliminary kinetic measurements above imply that the kinetics are not straightforward and a relatively long life may be present.

In order to investigate what effect chloride had on the redox properties of the green Rh_2(I,II) species, several spectroelectrochemical experiments were undertaken in the absence of chloride or any other readily coordinating anion. The electrochemical reduction (at 0 V) and oxidation (at 1 V) of *12* were separately examined by UV-Vis spectroscopy. In Figure 24, the UV-Vis

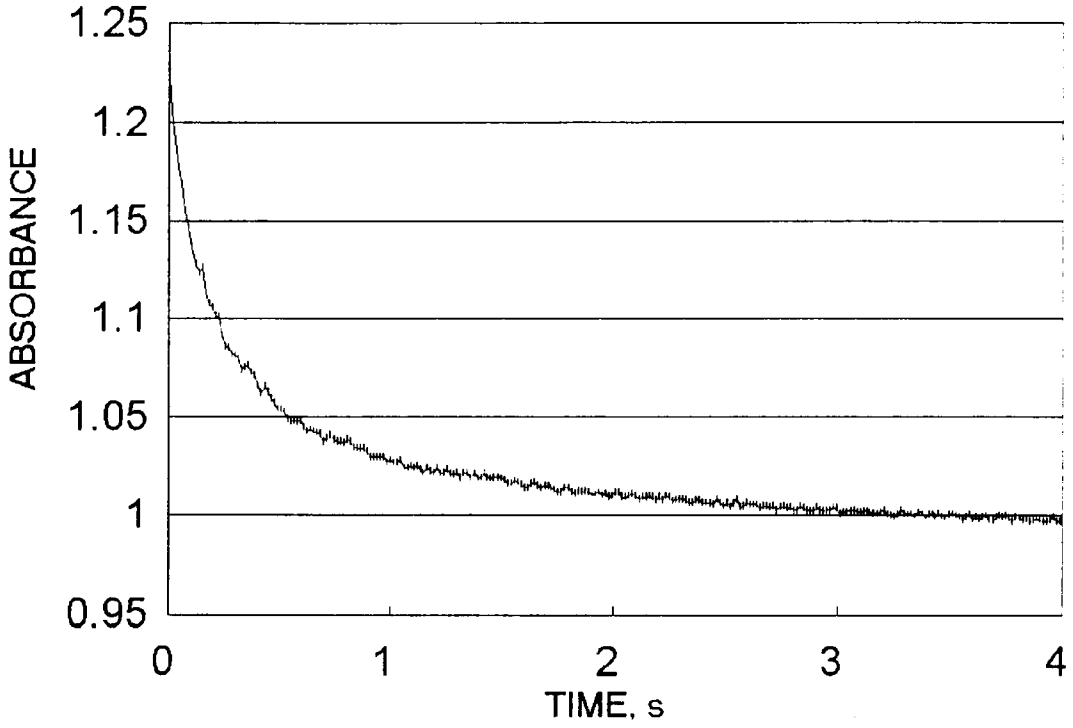

Figure 20. Absorbance versus time (seconds) at 436 nm for the reaction of *48* (4.32×10^{-5} M) with Cl^- (1.14×10^{-3} M).

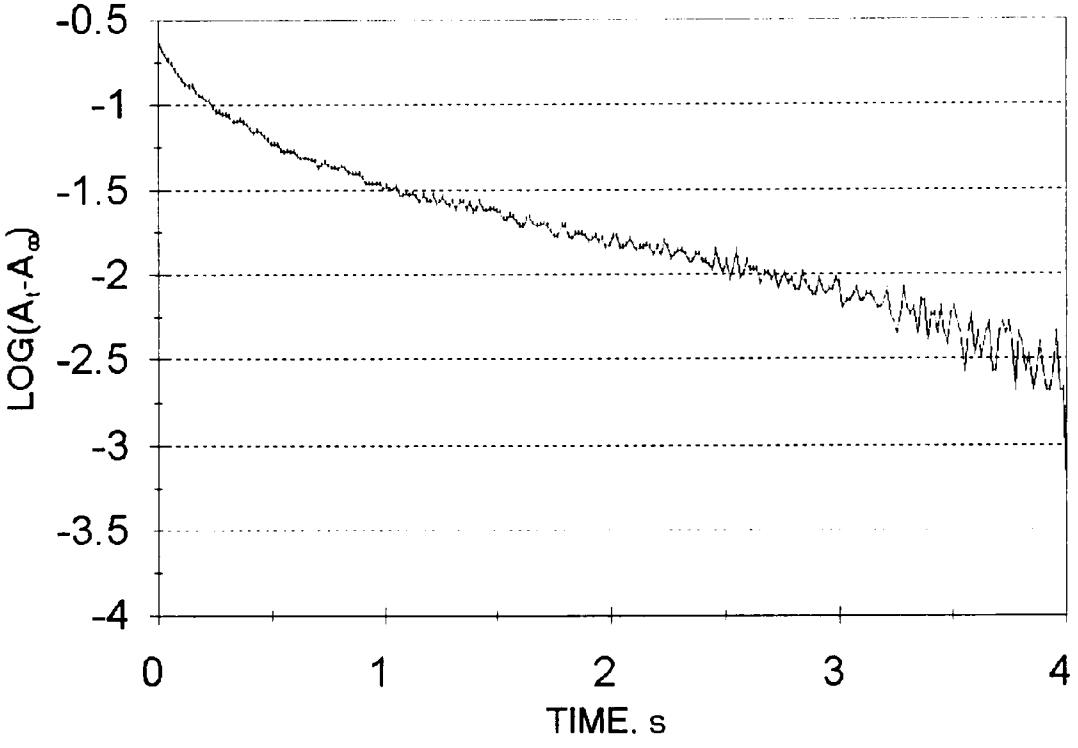

Figure 21. Log(A_t-A_∞) versus time (s) plot to test for first order dependence on [Rh_2(I,II)] at 436 nm for the reaction of *48* (4.32 X 10^{-5} M) with Cl^- (1.14 X 10^{-3} M).

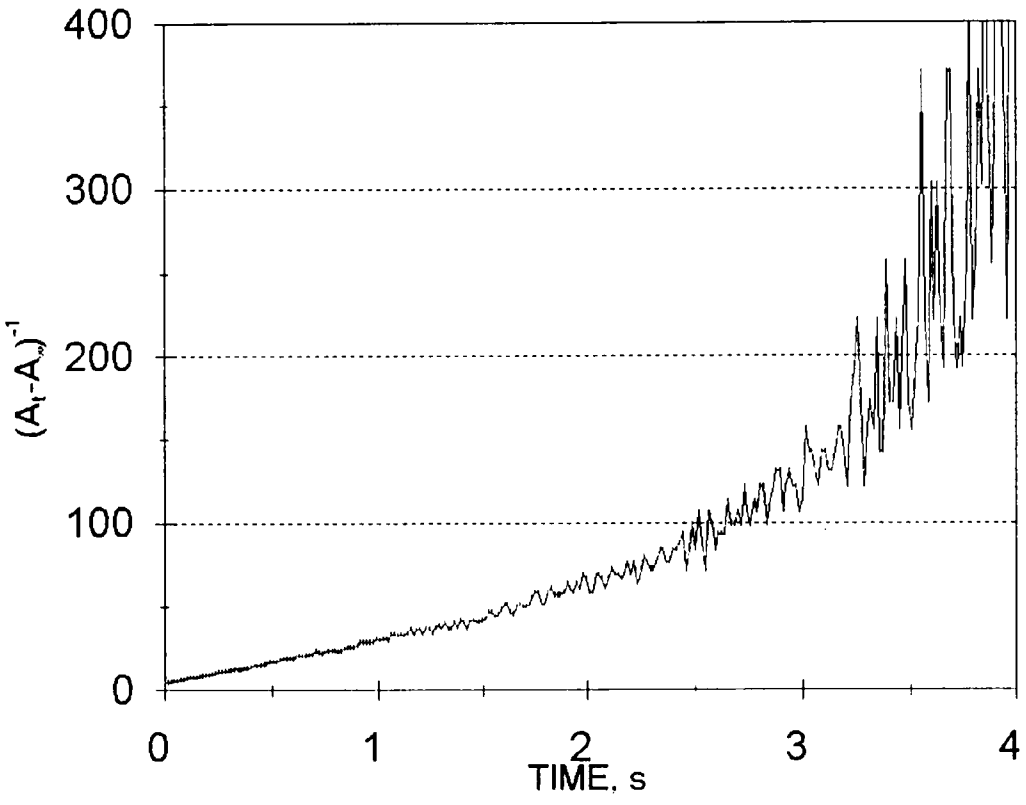

Figure 22. $(A_t-A_\infty)^{-1}$ versus time (s) plot to test for second order dependence on $[Rh_2(I,II)]$ at 436 nm for the reaction of *48* (4.32×10^{-5} M) with Cl^- (1.14×10^{-3} M).

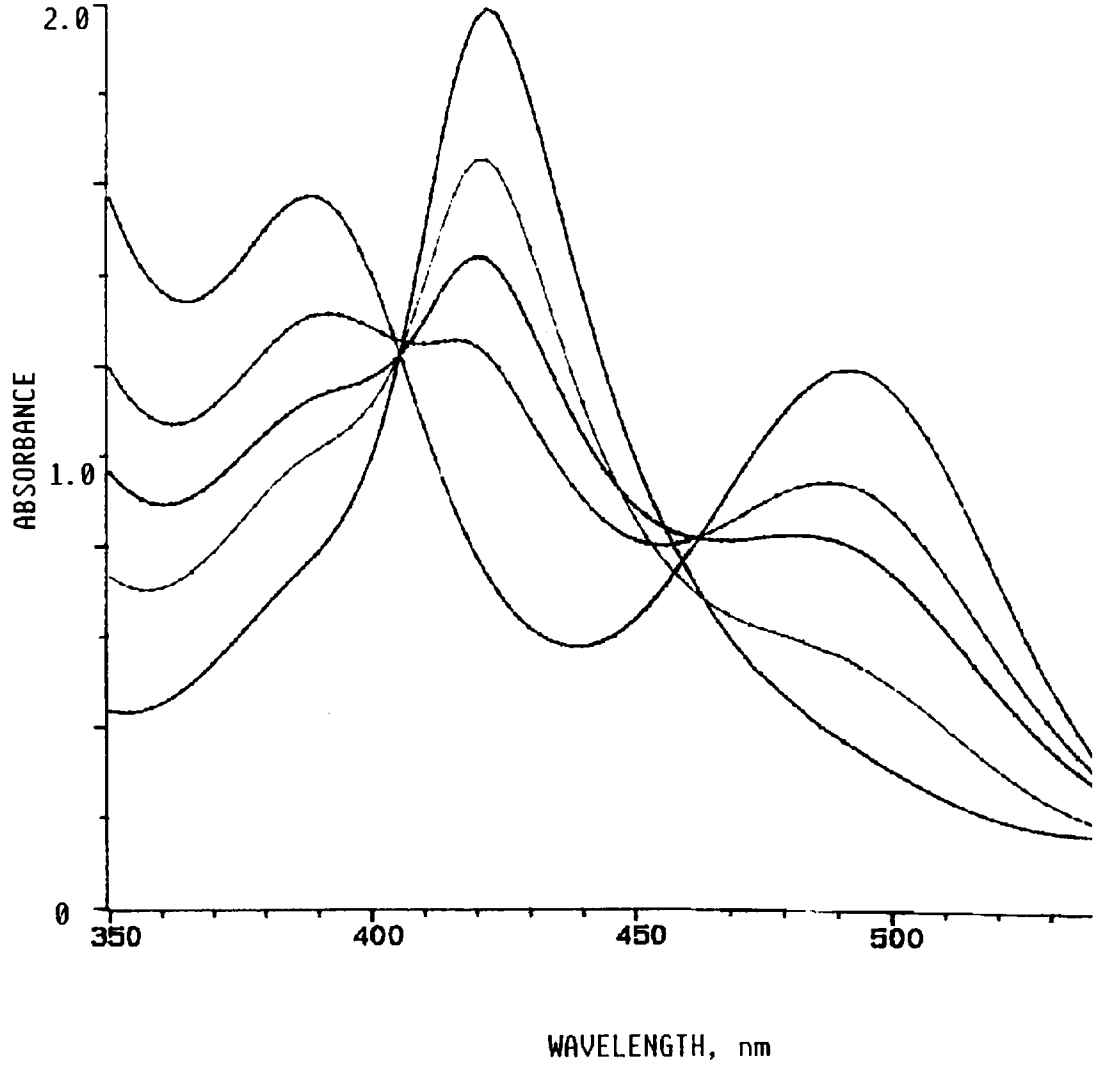

Figure 23. Equilibrium UV-Vis spectra in $MeCl_2$ of the reaction of ¼ equivalent of Cl^- (4.4 µl of 7.44 X 10^{-3} M TBACl) with *30* (1.0 ml of 1.30 X 10^{-4} M solution).

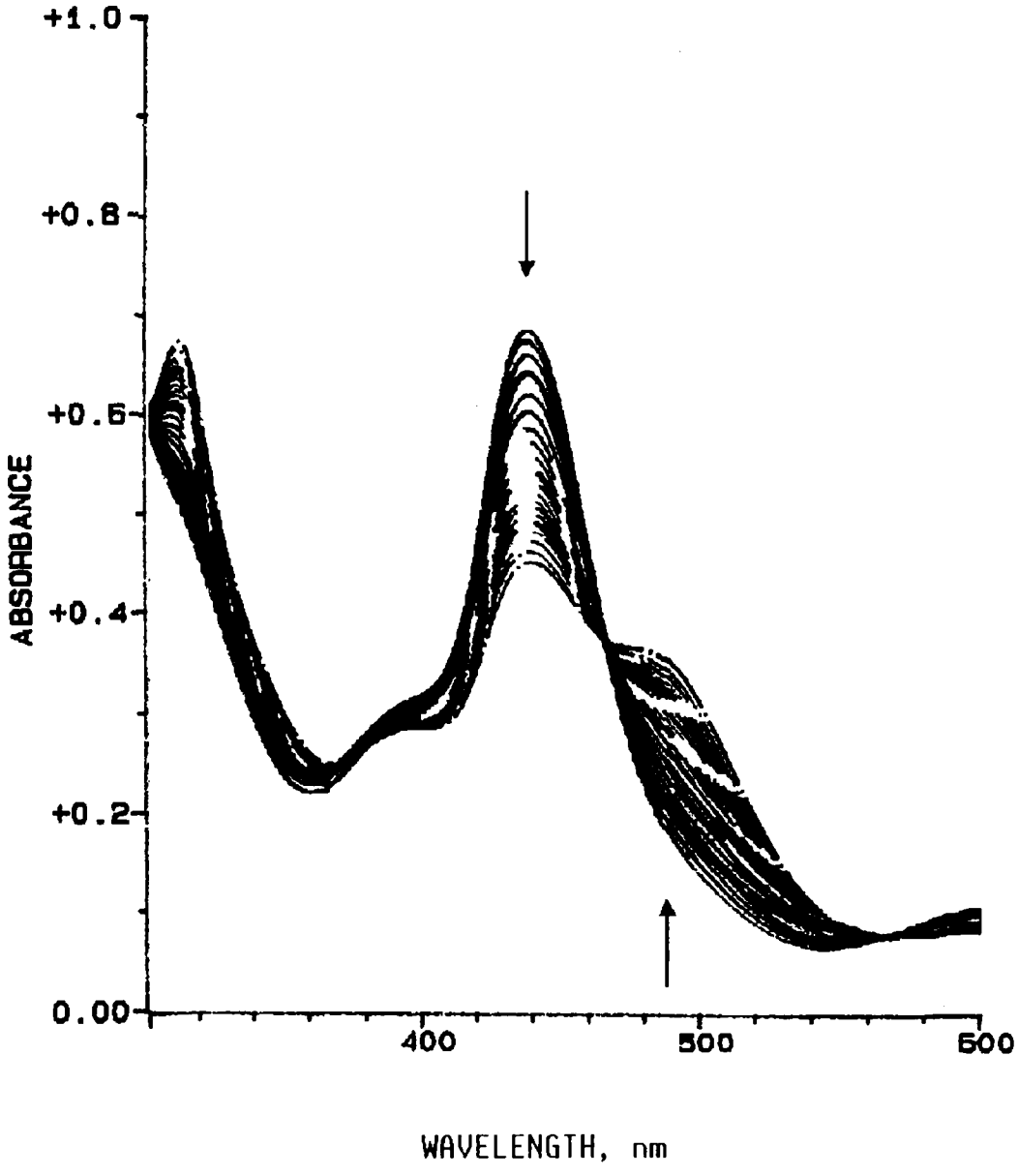

Figure 24. Spectroelectrochemical reduction of *12* (3.9 X 10^{-4} M in 0.1 M TBAH/$MeCl_2$) at 0 V (1 scan every 15 seconds for a total of 19 scans).

spectrum of the reduction of the $Rh_2(I,II)$ to the $Rh_2(I,I)$ species, the presence of a clear isosbestic point near 460 nm confirms the direct nature of the electron transfer. The UV-Vis spectrum of the oxidation of the $Rh_2(I,II)$ to the $Rh_2(II,II)$ species also reveals an isosbestic point (near 415 nm), as illustrated in Figure 25. The $Rh_2(II,II)$ triply-charged species is unstable and the absorbance near 380 nm due to the $Rh_2(II,II)$ decays into an unidentified band at higher energy. The d^7-d^7 cation prefers an octahedral geometry but is lacking a suitable axial ligand, and this causes an uncharacterized degradation (the $Rh_2(II,II)$ species was stabilized, however, by a potential of 1500 mV). These spectroelectrochemical studies showed that electrochemical oxidation and reduction of the $Rh_2(I,II)$ species alone were straightforward.

The kinetic data presented here were collected via an UV-Vis diode array spectrophotometer (Tracor-Northern TN-6500) through a flow-through mixing cell of 1.0 cm path length. The resultant data files were manually formatted for and used with Kinfit kinetics fitting routine (On Line Instrument Systems). Examination of data using the Kinfit routine also suggested that the decay curves are complex and not readily attributable to a specific rate equation. The data could be fit fairly well to the sum of three exponential decays:

$$(A_t - A_\infty) = \sum_{I=1}^{3} \alpha_I \, e^{(-k_I t)}$$

where A_t and A_∞ have been previously defined, the α_I are the rate amplitudes and the k_I are the rate constants.

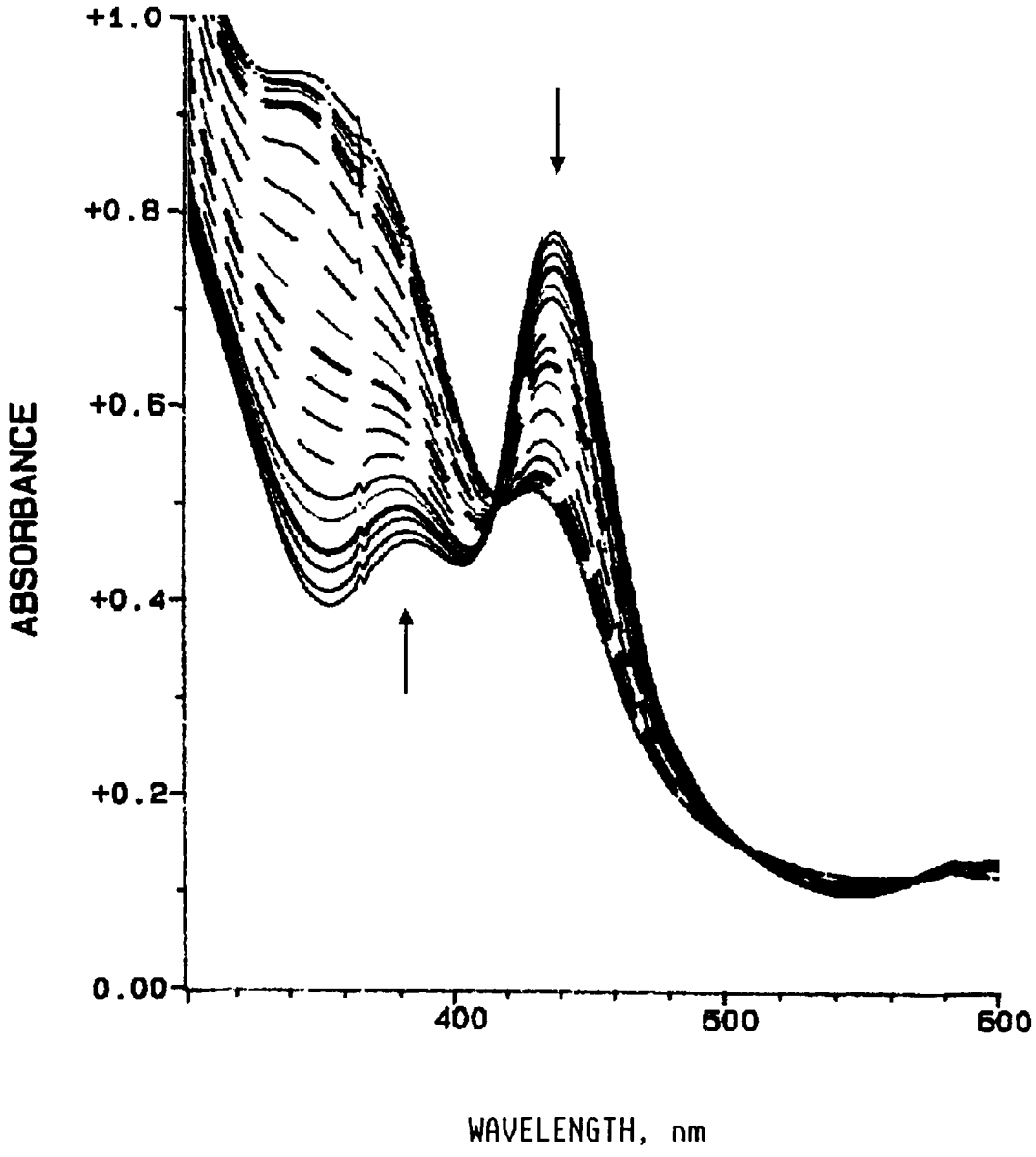

Figure 25. Spectroelectrochemical oxidation of *12* (3.9 X 10^{-4} M in 0.1 M TBAH/$MeCl_2$) at 1 V (1 scan every 15 seconds for a total of 19 scans).

A comparison of the initial rates as a function of [Cl^-] and [Rh_2(I,II)] was thus undertaken. The initial pseudo-first-order rate constant was taken from a fit (Kinfit) of a single exponential decay during the first several half-lives of the reaction. The initial rate was determined by multiplying this rate constant by the initial concentration of the Rh_2(I,II) species.

Rates as a function of the concentration of Cl^- and the Rh_2(I,II) species are listed in Table XXXII. The use of the neutral density filters did not influence the reaction rates, and thus photochemical reactions induced by the analyzing lamp can be neglected. Although the initial rates cannot be accounted for in detail, several general trends in the observed rates were apparent: (a) the rate of reaction generally decreases when changing the transoid bridge in the order dppm > dapm > dpam; (b) at constant [Rh_2(I,II)], the rate increases, then decreases with increasing [Cl^-]; (c) at constant [Cl^-], the initial rate is approximately first order in [Rh_2(I,II)].

A reaction scheme can be proposed that is consistent with these observations in a qualitative manner. The higher order in [Rh_2(I,II)] is consistent with some form of disproportionation reaction. To account for the unusual effect of [Cl^-] on the rate, any proposed reaction scheme must allow for a reactive intermediate whose further reaction is inhibited by excess chloride. A reaction scheme that fits these criteria involves the rapid yet reversible formation of a monochloro-dirhodium(I,II) intermediate which then reacts with starting material:

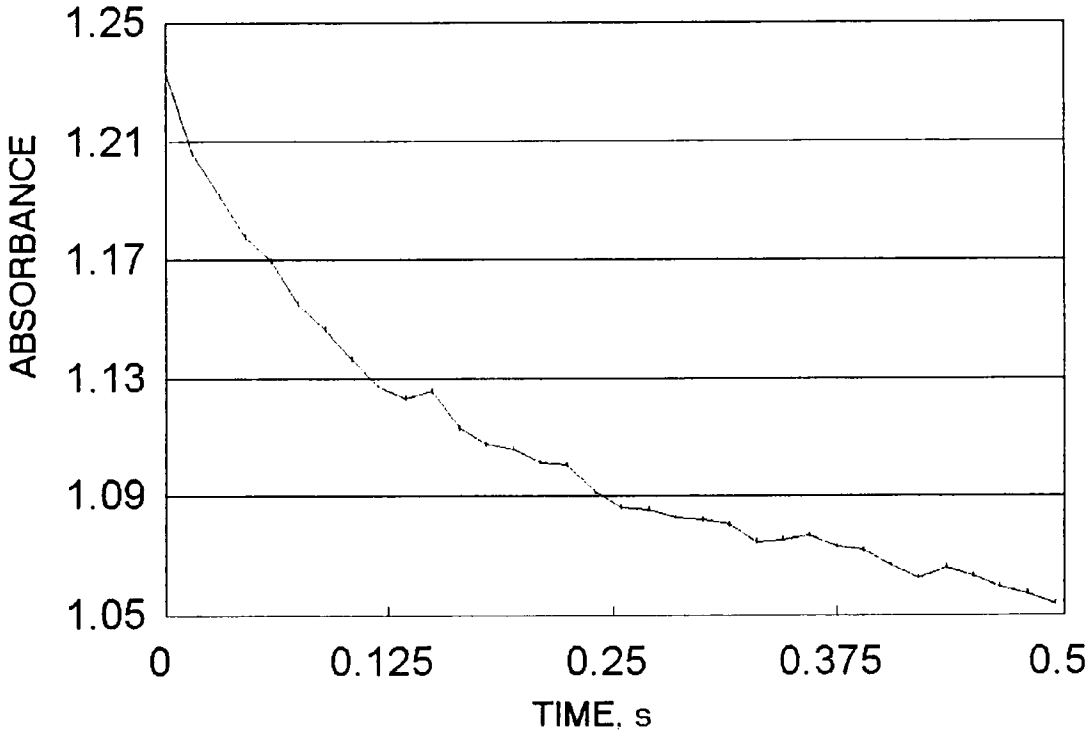

Figure 26. A plot of absorbance versus time for the first 0.5 s at 436 nm for the reaction of *48* (4.32 X 10^{-5} M) with Cl^- (1.14 X 10^{-3} M) (A_∞ = 0.99).

Table XXXII

Initial Concentrations and Average Initial Rates for the Kinetics Study Presented in Chapter 6.

$Rh_2(I,II)$ Species	$[Cl^-]$	$[Rh_2(I,II)]$	Initial Rate, M/s[a]
30	7.44E-03	1.30E-04	3.61E-05
30	7.44E-04	1.30E-04	2.78E-04
12	7.44E-05	1.30E-05	7.15E-06
12	7.44E-04	1.30E-05	1.03E-07
12	1.49E-03	1.30E-05	5.98E-07
12	7.44E-03	1.30E-05	5.07E-07
12	7.44E-04	2.60E-05	1.40E-05
12	1.49E-03	2.60E-05	1.30E-06
12	7.44E-03	2.60E-05	2.65E-06
12	7.44E-04	1.30E-04	5.11E-05
12	1.49E-03	1.30E-04	2.64E-05
12	7.44E-03	1.30E-04	4.03E-06
48	1.14E-03	4.32E-05	2.64E-04
48	1.14E-02	4.32E-05	6.05E-05
48	1.14E-04	8.65E-05	1.06E-04
48	1.14E-03	8.65E-05	7.31E-04
48	1.14E-02	8.65E-05	1.40E-04
48	1.14E-03	4.32E-04	5.66E-03
48	1.14E-02	4.32E-04	8.95E-04

[a] The initial rate of the disappearance of the $Rh_2(I,II)$ is reported as the product of the concentration of the dirhodium reactant and pseudo-first-order rate constant.

$$Rh_2(I,II) + Cl^- \rightleftharpoons Rh_2(I,II)\cdot Cl \quad (1)$$

$$Rh_2(I,II)\cdot Cl + Rh_2(I,II) \rightarrow Rh_2(II,II)\cdot Cl + Rh_2(I,I) \quad (2)$$

$$Rh_2(II,II)\cdot Cl + Cl^- \rightarrow Rh_2(II,II)Cl_2 \quad (3)$$

In a solution containing a large excess of chloride, the equilibrium in reaction (1) is shifted to the right and little of the starting material remains to react with the predominant intermediate in reaction (2). A reaction similar to (1) is postulated as the rate limiting step in the chloride-induced disproportionation of the $Rh_2(I,II)(dppm)_2(dimen)_2$ species.[81] Also, the observed rate decrease follows the trend of the oxidation potentials of the initial $Rh_2(I,II)$ complexes (going from the dppm complexes to the dpam complexes).

The redox reaction (2) is predicted based on the electrochemical behavior of dirhodium(I,I) species in the presence of chloride.[80] The oxidation potential of a chlorodirhodium(I,II) intermediate would be less than that of the dirhodium(I,II) starting material. In order to stabilize the Rh(II) centers, reaction (3) would be expected to be very fast relative to the other reactions.

In summary, the study of a complicated disproportionation reaction of the green dirhodium (I,II) bis(isocyanide) complex with chloride has been presented. Although the kinetics of the reaction cannot be fully explained through mathematical modeling, the initial rate is shown to be first order in the dirhodium(I,II) species and to depend on the chloride concentration in a peculiar but explicable fashion.

CONCLUSIONS

The results of a study of some dirhodium A-frame complexes have been presented. The relative effects of the modification of bridgehead, transoid-bridging, and terminal ligands on the chemical properties of the compounds have been discussed. The one-electron oxidation of dirhodium(I,I) complexes has also been investigated. The behavior of dpam-containing dirhodium-μ-pyrazolato complexes has been compared to that of the previously studied dapm and dppm analogs and found to adhere to trends established by those complexes. The unusual thermochromic property of the isocyanide-containing dirhodium(I,II) compounds has been examined. In order to further explore the nature of this thermochromic isomerism, btmp- and mtmp-containing dapm and dppm A-frame dirhodium species have been examined. It has been shown that when the electronegativity of the substituents on the pyrazole ring was increased, the transition temperature of the thermochromic isomerization decreased.

The behavior of the μ-pyrazolato-complexes led to a search for apex ligands with similar bonding abilities. Thus, an examination of dirhodium-μ-hydroxypyridinato A-frame complexes has been undertaken to evaluate the spectroscopic and structural effects of bifunctional asymmetric bridgehead

ligands. Neither dpam-containing, isocyanide-containing, nor oxidized dirhodium-μ-hydroxypyridinato analogs of dirhodium-μ-pyrazolato complexes could be isolated. The general spectroscopic properties of the isolated complexes have proved, in most cases, to be similar to those of the dirhodium-μ-pyrazolato A-frame complexes. Fluxional behavior of the apex hydroxypyridinate ligands has been identified and characterized using ^{31}P NMR. This fluxional behavior has been shown to vary depending on the bis-transoid bridges and on the 6-substitution of the hydroxypyridinate apex ligand. The crystal structure of two of these dirhodium-μ-hydroxypyridinato compounds have proven that hydroxypyridinate apex ligands bond in a bidentate fashion in the solid state. The crystal structure of an unusual trirhodium species has been determined, after a crystal was serendipitously grown.

A FAB and CID mass spectrometric study of a series of dirhodium-μ-pyrazolato A-frame complexes has been performed. In FAB both the primary atom beam and NBA have been shown to promote the oxidation and reduction of certain of the dirhodium species studied. While all FAB spectra are dominated by the singly-charged $Rh_2(I,I)$ molecular cation, interpretation of relevant structural information from the FAB spectra has proven to be complicated by the additional fragmentation patterns of the species formed by beam- and matrix-induced damage. The use of CID insures that detected daughter ions come from only one parent (barring isobaric interferences) and thus has allowed assignment of fragmentation reactions which reveal

information about relative bond strengths in these dirhodium-μ-pyrazolato complexes. CID has proven complementary to FAB for their characterization. The bond strengths and fragmentation patterns deduced from mass spectrometric studies of these dirhodium-μ-pyrazolato A-frame complexes can be understood by analogy to the reactivities of similar homobimetallic complexes.

Kinetics of the solution disproportionation of the dirhodium (I,II) bis(isocyanide) complexes with chloride were studied. The total reaction rate profiles were not amenable to manual or computerized curve fitting. A study of initial rates indicated the reaction starts as first order in dirhodium(I,II) species and depends on chloride in a variable but explicable fashion. To account for this unusual effect of [Cl^-] on the rate, the reaction scheme proposed allows for an intermediate whose forward reaction is inhibited by excess chloride. The proposed monochloro-dirhodium(I,II) intermediate would react with any unreacted starting material to disproportionate:

$$Rh_2(I,II) + Cl^- \rightleftharpoons Rh_2(I,II)\cdot Cl$$

$$Rh_2(I,II)\cdot Cl + Rh_2(I,II) \rightarrow Rh_2(II,II)\cdot Cl + Rh_2(I,I)$$

$$Rh_2(II,II)\cdot Cl + Cl^- \rightarrow Rh_2(II,II)Cl_2$$

One area of further study is suggested for future work. Proposed is an investigation into the effect of O_2 on the dirhodium(I,II) complexes discussed. This includes an examination into the influence of oxygen on the thermochromic behavior of the isocyanide-containing dirhodium(I,II) compounds presented in Chapter 3, in direct response to literature comparisons to the paramagnetic properties of $[Rh_2(\mu\text{-RNNNR})_2(CO)(P\phi_3)(bipy)](PF_6)$.[34]

LIST OF REFERENCES

1. (a) Howard, R.; Spring, T.; Bear, J. *Cancer Research*, **1976**, *36*, 4402. (b) Hughes, R.; Bear, J.; Kimball, A. *Proc. Am. Assoc. Cancer Res.* **1972**, *13*, 120.

2. (a) Kalck, Ph. in *Organometallics in Organic Synthesis*; de Meijere, A. and tom Dieck, H., Eds.; Springer-Verlag: Berlin, Germany, 1982; p 297. (b) Sanger, A. in *Homogeneous Catalysis with Metal Phosphine Complexes*, Pignolet, L. Ed.; Plenum, New York, 1983; p. 217. (c) Claver, C.; Masdue, A.; Ruiz, N.; Foces-Foces, C.; Cano, F.; Apreda, M.; Oro, L.; Garcia-Alejandre, J.; Torrens, H. *J. Organomet. Chem.* **1990**, *398*, 177. (d) Becalski, A.; Cullen, W.; Fryzuk, M.; James, B.; Kang, G.; Rettig, S. *Inorg. Chem.* **1991**, *30*, 5002.

3. Kubiak, C. P.; Eisenberg, R. *J. Am. Chem. Soc.* **1977**, *99*, 6129.

4. Tortorelli, L. J. Ph.D. Dissertation, The University of Tennessee, Knoxville, 1988.

5. DePriest, J. C. M.S. Thesis, The University of Tennessee, Knoxville, 1988.

6. Janke, C. J.; Tortorelli, L. J.; Burn, J. L. E.; Tucker, C. A.; Woods, C. *Inorg. Chem.* **1985**, *24*, 4597.

7. Balch, A. L.; Labadie, J. W.; Delker, G. *Inorg. Chem.* **1979**, *18*, 1224.

8. This study was performed with Reynolds, J. D. Ph.D. Dissertation, The University of Tennessee, Knoxville, 1990. Much of Chapter 5 is adapted from this source, although figures and some tables are presented intact.

9. (a) Puddephatt, R. J. *Chem. Soc. Rev.* **1983**, 99. (b) Chaudret, B.; Delavaux, B.; Poilblanc, R. *Coord. Chem Rev.* **1988**, 191.

10. Griffith, W. P. *The Chemistry of the Rarer Platinum Metals*; Wiley: London, 1967.

11. Chatt, J. in *Homogeneous Catalysis with Metal Phosphine Complexes*, Pignolet, L. Ed.; Plenum, New York, 1983; p. 1.

12. Partinton, J. R. *A History of Chemistry*; MacMillan: London, 1964.

13. Cotton, F. A.; Wilkinson, G. *Advanced Inorganic Chemistry*, Wiley: New York, 1980.

14. Young, J. F.; Osborn, J. A.; Jardine, F. H.; Wilkinson, G. *J. Chem. Soc., Chem. Comm.* **1965**, 131.

15. Cotton, F. A.; Walton, R. A. *Multiple Bonds Between Metal Atoms*, Wiley: New York, 1982.

16. Mague, J. T.; Mitchener, J. P. *Inorg. Chem.* **1969**, *8*, 119.

17. Mague, J. T. *Inorg. Chem.* **1969**, *8*, 1975.

18. Hieber, W.; Lagally, H. *Chem. Ber.* **1967**, *100*, 148.

19. Balch, A. L. *J. Am. Chem. Soc.* **1976**, *98*, 8049.

20. Lewis, N. S.; Mann, K. R.; Gordon, J. G.; Gray, H. B. *J. Am. Chem. Soc.* **1976**, *98*, 2354.

21. Lewis, N. S.; Mann, K. R. ; Gordon, J. G.; Gray, H. B. *J. Am. Chem. Soc.* **1976**, *98*, 7461.

22. Olmstead, M. M.; Balch, A. L. *J. Am. Chem. Soc.* **1976**, *98*, 2354.

23. Enlow, P. D.; Woods, C. *Organometallics* **1983**, *2*, 64.

24. Balch. A. L. In *Catalytic Aspects of Metal Phosphine Complexes*, Alyea, E. C.; Meek, D. W. Eds.; *Advances in Chemistry Series*, **1982**, *196*, 243.

25. Trofimenko, S. *Inorg. Chem.* **1971**, *10*, 1372.

26. Bayón, J. C.; Net, G.; Esteban, P.; Rasmussen, P. G.; Bergstrom, D. F. *Inorg. Chem.* **1991**, *30*, 4771.

27. Marshall, J. L.; Stobart, S. R.; Gray, H. B. *J. Amer. Chem. Soc.* **1984**, *106*, 3027.

28. Rodman, G. S.; Mann, K.R. *Inorg. Chem.* **1988**, *27*, 3338.

29. Boyd, D. C.; Szalapski, R.; Mann, K. R. *Organometallics* **1989**, *8*, 790.

30. Ciriano, M. A.; Villarroya, B. E.; Oro, L. A.; Apreda, M. A.; Foces-Foces, C.; Cano, F. H. *J. Organomet. Chem.* **1989**, *379*, 377.

31. Ciriano, M. A.; Villarroya, B. E.; Oro, L. A.; Apreda, M. A.; Foces-Foces, C.; Cano, F. H. *J. Chem. Soc., Dalton Trans.* **1987**, 981.

32. Sielisch, T; Cowie, M. *Organometallics* **1988**, *7*, 707.

33. Carriedo, C. *J. Organomet. Chem.* **1989**, *379*, 331.

34. (a) Connelly, N. G.; Crispin, J. F.; Freeman, M. J.; Orpen, A. G.; Stirling, J. *J. Chem. Soc., Chem. Commun.* **1984**, 1025. (b) Connelly, N. G.; Garcia, G.; Gilbert, M.; Stirling, J. *J. Chem. Soc., Chem. Commun.* **1987**, 246. (c) Brauns, T.; Carriedo, C.; Cockayne, J. S.; Connelly, N. G.; Herbosa, G. G.; Orpen, A. G. *J. Chem. Soc., Dalton Trans.* **1989**, 2049. (d) Connelly, N. G.; Loyns, A. C. *J. Organomet. Chem.* **1991**, *285*, 285.

35. Bear, J. L.; Yao, C.-L.; Capdevielle, F. J.; Kadish, K. M. *Inorg. Chem.* **1988**, *27*, 3782.

36. Claver, C.; Kalck, Ph.; Ridmy, M.; Thorez, A.; Oro, L. A.; Pinillos, M. T.; Apreda, M. C.; Cano, F. H.; Foces-Foces, C. *J. Chem. Soc., Dalton Trans.* **1988**, 1523.

37. Oro, L. A.; Carmona, D.; Reyes, J. *J. Organomet. Chem.* **1986**, *302*, 417.

38. Oro, L. A.; Carmona, D.; Pérez, P. L.; Esteban, M.; Tiripicchio A.; Tiripicchio-Camellini, M. *J. Chem. Soc., Dalton Trans.* **1985**, 973.

39. Che, C.; Lee, W.; Kwong, H.; Yam, V.; Cho, K. *J. Chem. Soc. Dalton Trans.* **1990**, 1717.

40. Che, M.; Lee, W. *J. Chem. Soc. Chem. Comm.* **1986**, 616.

41. (a) Mann, K. R.; Lewis, N. S.; Miskowski, V. M.; Erwin, D.K.; Hammond, G. S.; Gray, H. B. *J. Am. Chem. Soc.* **1977**, *99*, 5525. (b) Brown, G. M.; Brunschwig, B. G.; Creutz, C.; Endicott, J. F.; Sutin, N. *J. Am. Chem. Soc.* **1979**, 101, 1298.

42. Farr, D.; Olmstead, M. M.; Balch, A. L. *J. Am. Chem. Soc.* **1980**, *102*, 6654.

43. Rotondo, E.; Bruno, G.; Nicoló, F.; Schiavo, S. L.; Piraino, P. *Inorg. Chem.* **1991**, *30*, 1195.

44. Balch, A. L. *J. Am. Chem. Soc.* **1976**, *98*, 8049.

45. Balch, A. L.; Tulyathan, B. *Inorg. Chem.* **1977**, *16*, 2840.

46. (a) Hoffman, D. M.; Hoffman, R. *Inorg. Chem.* **1981**, *20*, 3543; (b) Kenney, M. I. S.; Kenney, J. W., Crosby G. A. *Inorg. Chem.* **1986**, *25*, 1506.

47. Carmona, D.; Oro, L. A.; Pérez, P.L.; Tiripicchio A.; Tiripicchio-Camellini, M. *J. Chem. Soc., Dalton Trans.* **1989**, 1427.

48. Woods, C.; Tortorelli, L. J., unpublished results.

49. Sharp, P. R.; Ge, Y. W. *J. Amer. Chem. Soc.* **1987**, *87*, 3796.

50. Deraniyagala, S. P.; Grundy, K. R. *Inorg. Chem.* **1985**, *24*, 50.

51. Deraniyagala, S. P.; Grundy, K. R. *Inorg. Chim. Acta* **1984**, *84*, 205.

52. Deraniyagala, S. P.; Grundy, K. R. *J. Chem. Soc., Dalton Trans.* **1985**, 1577.

53. (a) Berry, D. H.; Eisenberg, R. *Organometallics*, **1987**, *6*, 1796; (b) Cotton, F. A.; Dunbar, K. R.; Verbruggen, M. G. *J. Am. Chem. Soc.* **1987**, *109*, 5498-5506; (c) Cotton, F. A.; Eagle, C.T.; Price, A. C. *Inorg. Chem.* **1988**, *27*, 4362.

54. Balch, A. L.; Catalano, V. J.; Olmstead, M. M. *Inorg. Chem.* **1990**, *29*, 1638.

55. Woods, C.; Tortorelli, L. J.; Rillema, D. P.; Burn, J. L. E.; DePriest, J. C.; *Inorg. Chem.* **1989**, *28*, 1673.

56. Ladd, J. A.; Olmstead, M. M. Balch, A. L. *Inorg. Chem.* **1984**, *23*, 1638.

57. *Chem. Abstr.* **1975**, *82*, 112068c; [Upjohn Co. 1974].

58. Trofimenko, S. *J. Am. Chem. Soc.* **1967**, *89*, 3165.

59. Hope, H.; Moezzi, B. Department of Chemistry, University of California, Davis, California, software.

60. Sheldrick, G. M. *SHELXTL PLUS*, version 4.1, 1990, Siemens Analytical X-ray Instruments, Inc. Madison, Wisconsin.

61. Identification is based on infrared C≡N stretch as reported by Enlow and Woods in reference 23.

62. Mague, J. T.; Sanger, A. R. *Inorg. Chem.* **1979**, *18*, 2060.

63. Tocher, D. A.; Tocher, J. H. *Inorg. Chim. Acta* **1987**, *131*, 69.

64. Peterson, E. S.; Bancroft, D. P.; Min, D.; Cotton, F. A.; Abbott, E. H. *Inorg. Chem.* **1990**, *29*, 229.

65. Rodman, G. S.; Mann, K. R. *J. Organomet. Chem.* **1989**, *378*, 255.

66. Tortorelli, L. J.; Tinsley, P. W.; Woods, C.; Janke, C. *Polyhedron* **1988**, *7*, 315.

67. Guimerans, R.; Balch, A. L. *Inorg. Chim. Acta*, **1983**, *77*, L177.

68. Kang, S.; Albright, T.A.; Wright ,T. C.; Jones, R. A. *Organometallics* **1985**, *4*, 666, and references therein.

69. (a) Reynolds, J. D.; Cook, K. D.; Burn, J. L. E.; Woods, C. *J. Am. Soc. Mass Spectrom.* **1992**, *3*, 113; (b) Reynolds, J. D.; Burn, J. L. E.; Cook, K. D.; Woods, C. *Proc. 38th Ann. Conf. Amer. Soc. Mass Spectrom.*, Tucson, June 3-8, **1990**, 1431.

70. Kemp, T.R. *Mass Spectrometry* **1984**, *7*, 168.

71. Barber, M.; Bell, D.; Eckersley, M.; Morris, M.; Tetler, L. *Rapid Commun. Mass Spectrom.* **1988**, *2*, 18.

72. (a) Pelzer, G.; De Pauw, E.; Dung, D. V.; Marien, J. *J. Phys. Chem.* **1984**, *88*, 5065. (b) Miller, J. M.; Balasanmugam, K.; Nye, J.; Deacon, G. B.; Thomas, N. C. *Inorg. Chem.* **1987**, *26*, 560. (c) Gale, P. J.; Bentz, B. L.; Chait, B. T.; Field, F. H.; Cotter, R. J. *Anal. Chem.* **1986**, *58*, 1070. (d) Williams, D. H.; Findeis, A. F.; Naylor, S.; Gibson, B. W.

J. Amer. Chem. Soc. **1987**, *109*, 1980. (e) E. De Pauw, *Mass Spectrom. Rev.* **1986**, *5*, 191.

73. Neumann, G. M.; Derrick, P. J. *Org. Mass Spectrom.* **1984**, *19*, 165.

74. Callahan, J. H.; Hool, K.; Reynolds, J. D.; Cook, K. D. *Anal. Chem.* **1988**, *60*, 714.

75. Miller, J. M.; Balasanmugam, K.; Nye, J.; Deacon, G. B.; Thomas, N. C. *Inorg. Chem.* **1987**, *26*, 560.

76. (a) Gibson, N. A.; Weatherburn, D. C. *Anal. Chim. Acta* **1972**, *58*, 159. (b) Lias, S. G.; Bartmess, J. E.; Liebman, J. F.; Holmes, J. L.; Levin, R. D.; Mallard, W. G. *J. Phys. Chem. Ref. Data* **1988**, 17. (c) Bartmess, J. E. University of Tennessee, personal communication.

77. Liang, X.; Suwanrumpha, S.; Freas, R. B. *37th Ann. Conf. Mass Spectrom. Allied Topics*, Miami Beach, May 21-26, 1989, 173.

78. Dewar, M. J. S.; Dieter, K. M. *J. Am. Chem. Soc.* **1986**, *108*, 8075.

79. Hill, M. G.; Lamanna, W. M.; Mann, K. R. *Inorg. Chem.* **1991**, *30*, 4687.

80. Tortorelli, L. J.; Woods, C.; McPhail, A. T. *Inorg. Chem.* **1990**, *29*, 2726.

81. Hill, M. G.; Mann, K. R. *Inorg. Chem.* **1986**, *25*, 3331.

82. Hill, M. G.; Mann, K. R. *Inorg. Chem.* **1991**, *30*, 1429.

APPENDIX

Table XXXIII

Crystal data for *3* and *7*

formula	$C_{58}H_{50}NO_3F_6P_5Rh_2 \cdot ½(CH_3CH_2)_2O$	$C_{56}H_{44}F_6O_6P_5Rh_3$
fw	1320.7	1480.8
space group	$P2_1/c$	Cc
Z	4	4
a, Å	10.534(3)	19.582(5)
b, Å	27.073(9)	15.232(3)
c, Å	21.694(8)	20.607(4)
β, deg	103.39(3)	101.73(2)
v, $Å^3$	6018(3)	6018(2)
d(calcd), g/cm^3	1.452	1.611
radiation; λ, Å	Mo; 0.71073	Mo; 0.71073
temp, °C	25	-100
abs coeff, cm^{-1}	7.31	10.0
$R(R_w)$, %	4.87(6.73)	4.35(5.66)
GOF	1.21	0.98
Largest and Mean Δ/σ	0.724, 0.019	0.041, 0.002

Table XXXIV

Atomic coordinates (x 10^4) and equivalent isotropic thermal parameters ($Å^2$ X 10^3) for *32*

	x	y	z	U(eq)[1]
Rh(1)	3221(1)	6932(1)	8517(1)	26(1)
Rh(2)	3054(1)	6754(1)	7127(1)	30(1)
P(1)	3096(1)	7768(1)	8251(1)	33(1)
P(2)	3119(1)	6086(1)	8737(1)	27(1)
P(3)	3322(1)	5922(1)	7370(1)	30(1)
P(4)	2405(1)	7555(1)	6811(1)	33(1)
C(1)	1986(5)	7889(2)	7476(2)	36(2)
C(2)	2477(5)	5754(2)	7990(2)	30(2)
C(3)	524(5)	6808(2)	7665(3)	37(2)
C(4)	-860(6)	6835(3)	7483(3)	58(3)
C(5)	-1542(7)	6967(3)	7921(4)	68(3)
C(6)	-904(6)	7063(3)	8541(4)	60(3)
C(7)	420(6)	7046(2)	8702(3)	42(2)
C(8)	1116(6)	7149(2)	9374(3)	50(2)
N(1)	1134(4)	6924(2)	8278(2)	36(1)
C(11)	4987(6)	6969(2)	8784(3)	45(2)
O(1)	6092(4)	7000(2)	8951(3)	78(2)
O(2)	5532(5)	6802(2)	6730(3)	80(2)
C(22)	4572(6)	6787(2)	6885(3)	47(2)
O(3)	1190(4)	6676(2)	7268(2)	42(1)
C(111)	4585(6)	8109(2)	8223(3)	41(2)
C(112)	5552(6)	7890(3)	7985(3)	55(2)
C(113)	6632(7)	8157(3)	7929(4)	75(3)
C(114)	6777(8)	8639(4)	8099(4)	83(4)
C(115)	5821(9)	8862(3)	8335(4)	83(4)
C(116)	4702(7)	8605(2)	8390(3)	59(3)
C(121)	2402(6)	8133(2)	8800(3)	38(2)
C(122)	3127(7)	8174(2)	9422(3)	52(2)
C(123)	2646(8)	8438(3)	9866(3)	65(3)

Table XXXIV (continued)

	x	y	z	U(eq)[1]
C(124)	1445(9)	8657(3)	9693(4)	72(3)
C(125)	698(8)	8615(3)	9082(4)	69(3)
C(126)	1190(7)	8355(2)	8636(3)	53(2)
C(211)	4575(5)	5744(2)	9137(2)	29(2)
C(212)	5547(5)	5985(2)	9573(3)	38(2)
C(213)	6630(5)	5722(2)	9901(3)	43(2)
C(214)	6766(5)	5233(2)	9794(3)	41(2)
C(215)	5784(6)	4986(2)	9369(3)	44(2)
C(216)	4687(6)	5239(2)	9043(3)	38(2)
C(221)	2000(5)	5940(2)	9238(2)	29(2)
C(222)	790(5)	5716(2)	9021(3)	43(2)
C(223)	19(6)	5612(3)	9438(3)	58(3)
C(224)	402(6)	5728(3)	10065(3)	52(2)
C(225)	1583(6)	5951(2)	10288(3)	46(2)
C(226)	2386(6)	6052(2)	9878(3)	40(2)
C(311)	4914(5)	5638(2)	7618(2)	36(2)
C(312)	5065(6)	5131(2)	7557(3)	47(2)
C(313)	6272(8)	4910(3)	7755(3)	62(3)
C(314)	7365(7)	5203(3)	8020(3)	64(3)
C(315)	7222(6)	5707(3)	8094(4)	65(3)
C(316)	5999(6)	5924(2)	7882(3)	47(2)
C(321)	2558(6)	5554(2)	6686(2)	38(2)
C(322)	3212(8)	5524(3)	6198(3)	66(3)
C(323)	2689(10)	5236(3)	5675(3)	84(4)
C(324)	1596(10)	4975(4)	5626(4)	91(4)
C(325)	973(10)	4998(4)	6113(5)	102(4)
C(326)	1439(7)	5293(3)	6630(3)	70(3)
C(411)	3494(6)	7958(2)	6498(3)	42(2)
C(412)	3839(7)	8425(3)	6716(3)	57(3)
C(413)	4789(8)	8688(3)	6516(3)	74(3)
C(414)	5388(8)	8476(4)	6084(5)	83(4)
C(415)	5016(9)	8023(3)	5827(4)	83(4)
C(416)	4043(7)	7759(3)	6028(3)	60(3)
C(421)	882(5)	7563(2)	6207(3)	40(2)

Table XXXIV (continued)

	x	y	z	U(eq)[1]
C(422)	467(7)	7125(3)	5876(3)	57(2)
C(423)	-701(7)	7126(3)	5410(3)	71(3)
C(424)	-1426(7)	7551(4)	5281(4)	74(3)
C(425)	-1010(7)	7979(3)	5606(4)	76(3)
C(426)	148(7)	7988(3)	6070(3)	61(3)
P(5)	733(2)	748(1)	2987(1)	58(1)
F(1)	-780(11)	917(4)	2806(6)	65(3)
F(2)	2232(14)	612(5)	3082(7)	71(4)
F(3)	869(14)	1328(5)	2815(7)	65(3)
F(4)	628(14)	764(5)	2215(6)	71(4)
F(5)	446(11)	210(4)	3105(7)	63(3)
F(6)	976(15)	702(7)	3698(7)	94(4)
F(IA)	2117(10)	559(4)	2881(5)	82(3)
F(2A)	-631(9)	916(3)	3132(5)	83(3)
F(3A)	1329(16)	1301(6)	2996(9)	83(5)
F(4A)	155(18)	713(7)	2254(9)	101(6)
F(5A)	203(10)	166(3)	2796(6)	48(2)
F(6A)	1244(14)	951(7)	3709(7)	87(4)
F(3C)	746(31)	1116(15)	2482(18)	110(10)
F(4C)	-181(34)	409(16)	2489(18)	123(11)
F(5C)	711(27)	373(12)	3583(15)	93(8)
F(6C)	1492(25)	1196(11)	3400(16)	84(7)
C(100)	3597(21)	1221(8)	9800(12)	115(10)
C(200)	2943(20)	989(8)	9290(10)	95(9)
C(300)	2865(19)	-261(6)	8759(8)	77(7)
C(400)	2670(19)	268(7)	8739(8)	84(8)
0(100)	3117(12)	497(4)	9290(5)	77(5)

[1] Equivalent isotropic U defined as one third of the trace of the orthogonalized U_{ij} tensor.

Table XXXV

Bond length (Å) data for *32*·½$(CH_3CH_2)_2O$

Rh(1)-Rh(2)	3.019	(1)	Rh(1)-P(1)	2.332	(2)
Rh(1)-P(2)	2.347	(2)	Rh(1)-N(1)	2.139	(4)
Rh(1)-C(11)	1.818	(6)	Rh(2)-P(3)	2.315	(2)
Rh(2)-P(4)	2.328	(2)	Rh(2)-C(22)	1.797	(7)
Rh(2)-0(3)	2.067	(4)	P(1)-C(1)	1.842	(5)
P(1)-C(111)	1.833	(6)	P(1)-C(121)	1.825	(6)
P(2)-C(2)	1.840	(5)	P(2)-C(211)	1.829	(5)
P(2)-C(221)	1.822	(6)	P(3)-C(2)	1.833	(6)
P(3)-C(311)	1.810	(5)	P(3)-C(321)	1.814	(5)
P(4)-C(1)	1.841	(6)	P(4)-C(411)	1.825	(6)
P(4)-C(421)	1.821	(5)	C(3)-C(4)	1.421	(8)
C(3)-N(1)	1.373	(7)	C(3)-0(3)	1.282	(8)
C(4)-C(5)	1.366	(12)	C(5)-C(6)	1.381	(11)
C(6)-C(7)	1.357	(9)	C(7)-C(8)	1.499	(8)
C(7)-N(1)	1.357	(8)	C(11)-0(1)	1.139	(7)
0(2)-C(22)	1.138	(9)	C(111)-C(112)	1.380	(10)
C(111)-C(116)	1.389	(9)	C(112)-C(113)	1.377	(11)
C(113)-C(114)	1.353	(13)	C(114)-C(115)	1.371	(14)
C(115)-C(116)	1.397	(12)	C(121)-C(122)	1.393	(8)
C(121)-C(126)	1.381	(9)	C(122)-C(123)	1.387	(11)
C(123)-C(124)	1.368	(12)	C(124)-C(125)	1.379	(11)
C(125)-C(126)	1.391	(11)	C(211)-C(212)	1.386	(7)
C(211)-C(216)	1.392	(7)	C(212)-C(213)	1.393	(7)
C(213)-C(214)	1.358	(8)	C(214)-C(215)	1.387	(8)
C(215)-C(216)	1.387	(8)	C(221)-C(222)	1.391	(7)
C(221)-C(226)	1.386	(7)	C(222)-C(223)	1.377	(10)
C(223)-C(224)	1.362	(9)	C(224)-C(225)	1.367	(9)
C(225)-C(226)	1.389	(9)	C(311)-C(312)	1.394	(8)
C(311)-C(316)	1.389	(8)	C(312)-C(313)	1.380	(10)
C(313)-C(314)	1.408	(10)	C(314)-C(315)	1.386	(11)
C(315)-C(316)	1.393	(9)	C(321)-C(322)	1.392	(10)
C(321)-C(326)	1.356	(10)	C(322)-C(323)	1.382	(11)
C(323)-C(324)	1.335	(15)	C(324)-C(325)	1.369	(15)
C(325)-C(326)	1.371	(12)	C(411)-C(412)	1.368	(9)

Table XXXV (continued)

C(411)-C(416)	1.392	(10)	C(412)-C(413)	1.376	(12)
C(413)-C(414)	1.371	(13)	C(414)-C(415)	1.366	(13)
C(415)-C(416)	1.400	(13)	C(421)-C(422)	1.402	(9)
C(421)-C(426)	1.381	(9)	C(422)-C(423)	1.399	(9)
C(423)-C(424)	1.373	(12)	C(424)-C(425)	1.372	(12)
C(425)-C(426)	1.391	(10)	C(100)-C(200)	1.320	(29)
C(200)-0(100)	1.342	(23)	C(300)-C(400)	1.446	(24)
C(400)-0(100)	1.334	(19)	F(1)-P(5)	1.618	(11)
F(2)-P(5)	1.587	(15)	F(3)-P(5)	1.628	(14)
F(4)-P(5)	1.652	(14)	F(5)-P(5)	1.520	(12)
F(6)-P(5)	1.509	(16)	F(1A)-P(5)	1.610	(12)
F(2A)-P(5)	1.607	(10)	F(3A)-P(5)	1.622	(16)
F(4A)-P(5)	1.567	(18)	F(5A)-P(5)	1.690	(10)
F(6A)-P(5)	1.629	(15)	F(3B)-P(5)	1.483	(39)
F(4B)-P(5)	1.567	(37)	F(5B)-P(5)	1.649	(33)
F(6B)-P(5)	1.606	(28)			

Table XXXVI

Bond angle (°) data for *32*·½$(CH_3CH_2)_2O$

Rh(2)-Rh(1)-P(1)	85.4(1)	Rh(2)-Rh(1)-P(2)	93.0(1)
P(1)-Rh(1)-P(2)	174.1(1)	Rh(2)-Rh(1)-N(1)	86.4(1)
P(1)-Rh(1)-N(1)	87.4(1)	P(2)-Rh(1)-N(1)	86.9(1)
Rh(2)-Rh(1)-C(11)	98.4(2)	P(1)-Rh(1)-C(11)	91.2(2)
P(2)-Rh(1)-C(11)	94.6(2)	N(1)-Rh(1)-C(11)	174.9(2)
Rh(1)-Rh(2)-P(3)	87.2(1)	Rh(1)-Rh(2)-P(4)	95.2(1)
P(3)-Rh(2)-P(4)	170.0(1)	Rh(1)-Rh(2)-C(22)	115.7(2)
P(3)-Rh(2)-C(22)	92.5(2)	P(4)-Rh(2)-C(22)	95.1(2)
Rh(1)-Rh(2)-O(3)	72.9(1)	P(3)-Rh(2)-O(3)	86.4(1)
P(4)-Rh(2)-O(3)	85.1(1)	C(22)-Rh(2)-O(3)	171.2(2)
Rh(1)-P(1)-C(1)	112.8(2)	Rh(1)-P(1)-C(111)	119.8(2)
C(1)-P(1)-C(111)	104.3(3)	Rh(1)-P(1)-C(121)	111.8(2)
C(1)-P(1)-C(121)	103.5(2)	C(111)-P(1)-C(121)	102.9(3)
Rh(1)-P(2)-C(2)	108.8(2)	Rh(1)-P(2)-C(211)	121.1(2)
C(2)-P(2)-C(211)	105.5(2)	Rh(1)-P(2)-C(221)	113.5(2)
C(2)-P(2)-C(221)	105.3(2)	C(211)-P(2)-C(221)	101.2(2)
Rh(2)-P(3)-C(2)	110.8(2)	Rh(2)-P(3)-C(311)	122.5(2)
C(2)-P(3)-C(311)	104.5(2)	Rh(2)-P(3)-C(321)	109.9(2)
C(2)-P(3)-C(321)	105.3(2)	C(311)-P(3)-C(321)	102.4(3)
Rh(2)-P(4)-C(1)	109.5(2)	Rh(2)-P(4)-C(411)	120.0(2)
C(1)-P(4)-C(411)	106.4(3)	Rh(2)-P(4)-C(421)	111.8(2)
C(1)-P(4)-C(421)	103.1(3)	C(411)-P(4)-C(421)	104.5(3)
P(1)-C(1)-P(4)	114.3(3)	P(2)-C(2)-P(3)	112.5(3)
C(4)-C(3)-N(1)	118.5(6)	C(4)-C(3)-O(3)	120.9(5)
N(1)-C(3)-O(3)	120.6(5)	C(3)-C(4)-C(5)	119.4(6)
C(4)-C(5)-C(6)	120.7(6)	C(5)-C(6)-C(7)	119.0(7)
C(6)-C(7)-C(8)	119.2(6)	C(6)-C(7)-N(1)	122.0(6)
C(8)-C(7)-N(1)	118.8(5)	Rh(1)-N(1)-C(3)	117.5(4)
Rh(1)-N(1)-C(7)	122.2(3)	C(3)-N(1)-C(7)	120.2(4)
Rh(1)-C(11)-O(1)	178.9(6)	Rh(2)-C(22)-O(2)	179.3(6)
Rh(2)-O(3)-C(3)	139.3(3)	P(1)-C(111)-C(112)	120.5(5)
P(1)-C(111)-C(116)	120.3(5)	C(112)-C(111)-C(116)	119.0(6)
C(111)-C(112)-C(113)	120.3(7)	C(112)-C(113)-C(114)	121.7(8)

Table XXXVI (continued)

C(113)-C(114)-C(115)	118.7(8)	C(114)-C(115)-C(116)	121.3(8)
C(111)-C(116)-C(115)	119.0(7)	P(1)-C(121)-C(122)	117.5(5)
P(1)-C(121)-C(126)	123.6(4)	C(122)-C(121)-C(126)	118.8(6)
C(121)-C(122)-C(123)	120.5(6)	C(122)-C(123)-C(124)	119.7(6)
C(123)-C(124)-C(125)	120.9(8)	C(124)-C(125)-C(126)	119.3(7)
C(121)-C(126)-C(125)	120.8(6)	P(2)-C(211)-C(212)	119.5(4)
P(2)-C(211)-C(216)	121.2(4)	C(212)-C(211)-C(216)	119.2(4)
C(211)-C(212)-C(213)	119.8(5)	C(212)-C(213)-C(214)	121.2(5)
C(213)-C(214)-C(215)	119.4(5)	C(214)-C(215)-C(216)	120.4(5)
C(211)-C(216)-C(215)	119.9(5)	P(2)-C(221)-C(222)	124.2(4)
P(2)-C(221)-C(226)	118.0(4)	C(222)-C(221)-C(226)	117.8(5)
C(221)-C(222)-C(223)	120.1(5)	C(222)-C(223)-C(224)	121.6(6)
C(223)-C(224)-C(225)	119.4(6)	C(224)-C(225)-C(226)	120.0(5)
C(221)-C(226)-C(225)	121.1(5)	P(3)-C(311)-C(312)	120.6(4)
P(3)-C(311)-C(316)	120.3(4)	C(312)-C(311)-C(316)	119.1(5)
C(311)-C(312)-C(313)	121.0(6)	C(312)-C(313)-C(314)	119.4(7)
C(313)-C(314)-C(315)	120.1(6)	C(314)-C(315)-C(316)	119.6(6)
C(311)-C(316)-C(315)	120.8(6)	P(3)-C(321)-C(322)	116.7(5)
P(3)-C(321)-C(326)	124.8(5)	C(322)-C(321)-C(326)	118.4(6)
C(321)-C(322)-C(323)	118.9(8)	C(322)-C(323)-C(324)	122.5(9)
C(323)-C(324)-C(325)	118.2(8)	C(324)-C(325)-C(326)	120.9(9)
C(321)-C(326)-C(325)	121.0(8)	P(4)-C(411)-C(412)	124.3(5)
P(4)-C(411)-C(416)	116.3(5)	C(412)-C(411)-C(416)	119.3(6)
C(411)-C(412)-C(413)	121.5(7)	C(412)-C(413)-C(414)	118.9(8)
C(413)-C(414)-C(415)	121.3(9)	C(414)-C(415)-C(416)	119.6(9)
C(411)-C(416)-C(415)	119.2(7)	P(4)-C(421)-C(422)	118.5(4)
P(4)-C(421)-C(426)	121.4(5)	C(422)-C(421)-C(426)	120.1(5)
C(421)-C(422)-C(423)	119.1(7)	C(422)-C(423)-C(424)	120.2(7)
C(423)-C(424)-C(425)	120.4(7)	C(424)-C(425)-C(426)	120.6(7)
C(421)-C(426)-C(425)	119.6(7)	F(1)-P(5)-F(2)	172.8(7)
F(1)-P(5)-F(3)	78.8(6)	F(2)-P(5)-F(3)	96.6(7)
F(1)-P(5)-F(4)	85.2(7)	F(2)-P(5)-F(4)	88.3(8)
F(3)-P(5)-F(4)	74.4(7)	F(1)-P(5)-F(5)	95.0(6)
F(2)-P(5)-F(5)	89.3(7)	F(3)-P(5)-F(5)	173.5(7)
F(4)-P(5)-F(5)	103.1(8)	F(1)-P(5)-F(6)	101.2(8)
F(2)-P(5)-F(6)	85.4(8)	F(3)-P(5)-F(6)	108.1(9)
F(4)-P(5)-F(6)	173.4(9)	F(5)-P(5)-F(6)	75.1(9))

Table XXXVI (continued)

F(1A)-P(5)-F(2A)	176.4(5)	F(1A)-P(5)-F(3A)	86.3(8)
F(2A)-P(5)-F(3A)	95.6(7)	F(1A)-P(5)-F(4A)	89.3(8)
F(2A)-P(5)-F(4A)	93.5(8)	F(3A)-P(5)-F(4A)	97.3(10)
F(1A)-P(5)-F(5A)	85.8(5)	F(2A)-P(5)-F(5A)	92.9(5)
F(3A)-P(5)-F(5A)	165.6(9)	F(4A)-P(5)-F(5A)	70.6(8)
F(1A)-P(5)-F(6A)	97.9(7)	F(2A)-P(5)-F(6A)	80.0(7)
F(3A)-P(5)-F(6A)	68.7(9)	F(4A)-P(5)-F(6A)	163.6(10)
F(5A)-P(5)-F(6A)	124.5(8)	F(1A)-P(5)-F(3C)	86.9(14
F(2A)-P(5)-F(3C)	96.7(14)	F(1A)-P(5)-F(4C)	98.5(15)
F(2A)-P(5)-F(4C)	82.3(15)	F(3C)-P(5)-F(4C)	89.6(20)
F(1A)-P(5)-F(5C)	95.4(11)	F(2A)-P(5)-F(5C)	81.0(11)
F(3C)-P(5)-F(5C)	175.7(20)	F(4C)-P(5)-F(5C)	93.6(18)
F(1A)-P(5)-F(6C)	88.3(11)	F(2A)-P(5)-F(6C)	91.7(11)
F(3C)-P(5)-F(6C)	79.4(18)	F(4C)-P(5)-F(6C)	166.9(18)
F(5C)-P(5)-F(6C)	97.0(16)	C(100)-C(200)-O(100)	115.3(17)
C(300)-C(400)-O(100)	114.6(14)	C(200)-O(100)-C(400)	116.2(13)

Table XXXVII

Non-hydrogen Atomic coordinates (x 10^4) and equivalent isotropic thermal parameters ($Å^2$ X 10^3) for *39*

	x	y	z	U(eq)[1]
Rh(1)	0	8684(1)	0	29(1)
Rh(2)	-184(1)	7174(1)	-778(1)	22(1)
Rh(3)	1132(1)	7967(1)	-408(1)	23(1)
P(1)	9(2)	6276(3)	166(2)	26(1)
P(2)	-547(2)	8152(3)	-1657(2)	24(1)
P(3)	1361(2)	7250(3)	618(2)	24(1)
P(4)	918(2)	8899(3)	-1340(2)	26(1)
C(3)	773(9)	6894(11)	-1014(9)	34(6)
C(4)	936(8)	9200(10)	180(6)	23(5)
C(5)	-900(10)	8087(10)	-199(8)	34(6)
C(6)	-804(9)	6316(10)	-1209(8)	33(6)
C(7)	2110(9)	8064(10)	-330(7)	34(6)
C(8)	-301(10)	9589(14)	480(10)	55(8)
0(3)	1013(6)	6377(7)	-1315(5)	34(4)
0(4)	1332(6)	9748(7)	405(6)	40(4)
0(5)	-1483(6)	7990(8)	-217(6)	45(5)
0(6)	-1173(7)	5801(8)	-1494(6)	53(5)
0(7)	2688(6)	8113(9)	-262(6)	56(5)
0(8)	-481(9)	10159(10)	770(10)	96(8)
C(1)	-12(8)	9122(10)	-1595(7)	26(5)
C(2)	565(8)	6830(9)	863(7)	27(5)
C(11)	409(8)	5202(10)	110(8)	34(6)
C(12)	449(9)	4810(11)	-490(10)	47(7)
C(13)	767(12)	4005(13)	-510(10)	64(9)
C(14)	1023(10)	3551(10)	65(10)	51(7)
C(15)	972(11)	3935(11)	668(10)	54(8)
C(16)	667(9)	4724(11)	701(8)	39(6)
C(21)	-755(8)	5993(9)	494(8)	29(5)
C(22)	-1021(9)	6593(10)	883(8)	35(6)

Table XXXVII (continued)

	x	y	z	U(eq)[1]
C(23)	-1611(10)	6381(12)	1146(10)	55(8)
C(24)	-1942(9)	5592(12)	983(8)	46(7)
C(25)	-1701(11)	5009(13)	600(10)	59(8)
C(26)	-1104(10)	5213(12)	347(10)	51(7)
C(31)	1955(8)	6317(10)	712(7)	29(5)
C(32)	2180(8)	5929(12)	187(8)	34(6)
C(33)	2607(10)	5196(12)	272(10)	49(7)
C(34)	2801(10)	4830(14)	916(11)	58(8)
C(35)	2579(9)	5204(12)	1427(9)	44(6)
C(36)	2160(7)	5915(10)	1323(8)	31(6)
C(41)	1748(8)	7959(9)	1303(7)	29(5)
C(42)	2467(8)	8153(10)	1387(8)	31(5)
C(43)	2766(8)	8727(10)	1874(8)	35(6)
C(44)	2364(8)	9096(12)	2297(8)	43(6)
C(45)	1687(10)	8916(12)	2230(9)	44(7)
C(46)	1359(9)	8334(10)	1718(8)	36(6)
C(51)	-574(8)	7737(10)	-2502(7)	28(5)
C(52)	-904(7)	8267(10)	-3051(8)	27(5)
C(53)	-929(9)	7975(11)	-3677(8)	37(6)
C(54)	-621(11)	7216(14)	-3801(9)	55(7)
C(55)	-303(11)	6684(12)	-3273(9)	49(7)
C(56)	-287(9)	6948(11)	-2617(8)	37(6)
C(61)	-1415(9)	8582(10)	-1697(8)	30(6)
C(62)	-1536(9)	9466(12)	-1553(8)	41(6)
C(63)	-2233(9)	9724(11)	-1609(9)	45(7)
C(64)	-2783(10)	9148(14)	-1754(10)	54(8)
C(65)	-2661(9)	8286(13)	-1917(8)	45(7)
C(66)	-1989(8)	8009(10)	-1880(8)	32(5)
C(71)	1209(8)	8541(9)	-2081(8)	31(5)
C(72)	943(8)	8935(12)	-2708(8)	40(6)
C(73)	1177(10)	8692(12)	-3244(8)	44(6)
C(74)	1692(10)	8082(13)	-3222(9)	52(7)
C(75)	1985(11)	7689(16)	-2603(10)	65(9)
C(76)	1713(10)	7914(12)	-2058(9)	48(7)

Table XXXVII (continued)

	x	y	z	U(eq)[1]
C(81)	1303(8)	9976(11)	-1148(9)	39(6)
C(82)	2025(9)	10089(11)	-1037(10)	49(7)
C(83)	2327(11)	10864(14)	-877(9)	59(8)
C(84)	1935(10)	11600(15)	-807(10)	57(8)
C(85)	1234(11)	11515(13)	-927(10)	58(8)
C(86)	916(9)	10730(10)	-1109(9)	40(6)
P(5)	9322(3)	1424(4)	7301(3)	60(2)
F(1)	9296(12)	1542(10)	6543(7)	134(9)
F(2)	9371(9)	1289(10)	8067(7)	102(7)
F(3)	8569(10)	1668(16)	7168(10)	163(11)
F(4)	9105(9)	429(9)	7161(7)	100(7)
F(5)	10096(8)	1019(14)	7401(10)	134(9)
F(6)	9493(19)	2380(10)	7412(10)	227(19)
O(1W)	4175(18)	3318(23)	4498(14)	50
O(2W)	3767(11)	1311(16)	3811(11)	50
O(3W)	5510(10)	1262(13)	2510(10)	50
O(4W)	5019(12)	575(14)	2565(11)	50
O(5W)	3146(18)	3161(23)	3873(17)	50
O(6W)	3734(24)	3291(25)	4343(20)	50
O(7W)	4271(18)	2766(27)	4468(16)	50
O(8W)	3645(20)	2728(25)	3960(19)	50
O(9W)	3850(21)	1989(29)	3840(20)	50
O(10W)	5453(22)	475(26)	2411(19)	50

[1] Equivalent isotropic U defined as one third of the trace of the orthogonalized U_{ij} tensor.

Table XXXVIII

Bond length (Å) data for *39*·xH_2O

Rh(1)-Rh(2)	2.785	(2)	Rh(1)-Rh(3)	2.752	(2)
Rh(1)-C(4)	1.96	(2)	Rh(1)-C(5)	1.95	(2)
Rh(1)-C(8)	1.86	(2)	Rh(2)-Rh(3)	2.807	(2)
Rh(2)-P(1)	2.345	(4)	Rh(2)-P(2)	2.341	(4)
Rh(2)-C(3)	2.07	(2)	Rh(2)-C(5)	2.45	(2)
Rh(2)-C(6)	1.88	(2)	Rh(3)-P(3)	2.340	(4)
Rh(3)-P(4)	2.357	(4)	Rh(3)-C(3)	2.09	(2)
Rh(3)-C(4)	2.31	(2)	Rh(3)-C(7)	1.90	(2)
P(1)-C(2)	1.82	(1)	P(1)-C(11)	1.83	(2)
P(1)-C(21)	1.82	(2)	P(2)-C(1)	1.80	(2)
P(2)-C(51)	1.84	(2)	P(2)-C(61)	1.81	(2)
P(3)-C(2)	1.85	(2)	P(3)-C(31)	1.82	(2)
P(3)-C(41)	1.82	(1)	P(4)-C(1)	1.82	(2)
P(4)-C(71)	1.82	(2)	P(4)-C(81)	1.82	(2)
C(3)-0(3)	1.16	(2)	C(4)-0(4)	1.17	(2)
C(5)-0(5)	1.14	(2)	C(6)-0(6)	1.14	(2)
C(7)-0(7)	1.11	(2)	C(8)-0(8)	1.15	(3)
C(11)-C(12)	1.39	(3)	C(11)-C(16)	1.42	(2)
C(12)-C(13)	1.38	(3)	C(13)-C(14)	1.38	(3)
C(14)-C(15)	1.40	(3)	C(15)-C(16)	1.35	(2)
C(21)-C(22)	1.39	(2)	C(21)-C(26)	1.37	(2)
C(22)-C(23)	1.41	(3)	C(23)-C(24)	1.38	(3)
C(24)-C(25)	1.34	(3)	C(25)-C(26)	1.41	(3)
C(31)-C(32)	1.38	(2)	C(31)-C(36)	1.38	(2)
C(32)-C(33)	1.39	(3)	C(33)-C(34)	1.42	(3)
C(34)-C(35)	1.34	(3)	C(35)-C(36)	1.35	(2)
C(41)-C(42)	1.41	(2)	C(41)-C(46)	1.38	(2)
C(42)-C(43)	1.37	(2)	C(43)-C(44)	1.41	(3)
C(44)-C(45)	1.33	(3)	C(45)-C(46)	1.43	(2)
C(51)-C(52)	1.43	(2)	C(51)-C(56)	1.37	(2)
C(52)-C(53)	1.36	(2)	C(53)-C(54)	1.35	(3)
C(54)-C(55)	1.40	(3)	C(55)-C(56)	1.41	(2)
C(61)-C(62)	1.41	(2)	C(61)-C(66)	1.41	(2)

Table XXXVIII (continued)

C(62)-C(63)	1.40	(3)	C(63)-C(64)	1.37	(3)
C(64)-C(65)	1.39	(3)	C(65)-C(66)	1.37	(2)
C(71)-C(72)	1.42	(2)	C(71)-C(76)	1.37	(2)
C(72)-C(73)	1.33	(3)	C(73)-C(74)	1.36	(3)
C(74)-C(75)	1.42	(3)	C(75)-C(76)	1.38	(3)
C(81)-C(82)	1.40	(2)	C(81)-C(86)	1.39	(2)
C(82)-C(83)	1.33	(3)	C(83)-C(84)	1.38	(3)
C(84)-C(85)	1.35	(3)	C(85)-c(86)	1.37	(3)
P(5)-F(1)	1.56	(2)	P(5)-F(2)	1.57	(2)
P(5)-F(3)	1.49	(2)	P(5)-F(4)	1.58	(2)
P(5)-F(5)	1.61	(2)	P(5)-F(6)	1.50	(2)

Table XXXIX

Bond angle (°) data for *39*·xH_2O

Rh(2)-Rh(1)-Rh(3)	60.9(1)	Rh(2)-Rh(1)-C(4)	116.5(4)
Rh(3)-Rh(1)-C(4)	55.7(4)	Rh(2)-Rh(1)-C(5)	59.2(5)
Rh(3)-Rh(1)-C(5)	120.0(5)	C(4)-Rh(1)-C(5)	175.6(7)
Rh(2)-Rh(1)-C(8)	154.2(6)	Rh(3)-Rh(1)-C(8)	144.9(6)
C(4)-Rh(1)-C(8)	89.3(7)	C(5)-Rh(1)-C(8)	95.0(8)
Rh(1)-Rh(2)-Rh(3)	58.9(1)	Rh(1)-Rh(2)-P(1)	91.4(1)
Rh(3)-Rh(2)-P(1)	92.4(1)	Rh(1)-Rh(2)-P(2)	84.5(1)
Rh(3)-Rh(2)-P(2)	93.1(1)	P(1)-Rh(2)-P(2)	170.1(2)
Rh(1)-Rh(2)-C(3)	106.7(4)	Rh(3)-Rh(2)-C(3)	47.8(4)
P(1)-Rh(2)-C(3)	94.2(5)	P(2)-Rh(2)-C(3)	95.5(5)
Rh(1)-Rh(2)-C(5)	43.2(4)	Rh(3)-Rh(2)-C(5)	102.0(4)
P(1)-Rh(2)-C(5)	86.4(4)	P(2)-Rh(2)-C(5)	84.4(4)
C(3)-Rh(2)-C(5)	149.9(6)	Rh(1)-Rh(2)-C(6)	147.3(5)
Rh(3)-Rh(2)-C(6)	153.8(5)	P(1)-Rh(2)-C(6)	88.0(5)
P(2)-Rh(2)-C(6)	90.7(5)	C(3)-Rh(2)-C(6)	105.9(7)
C(5)-Rh(2)-C(6)	104.2(7)	Rh(1)-Rh(3)-Rh(2)	60.1(1)
Rh(1)-Rh(3)-P(3)	85.9(1)	Rh(2)-Rh(3)-P(3)	92.4(1)
Rh(1)-Rh(3)-P(4)	89.4(1)	Rh(2)-Rh(3)-P(4)	92.1(1)
P(3)-Rh(3)-P(4)	170.8(2)	Rh(1)-Rh(3)-C(3)	107.4(5)
Rh(2)-Rh(3)-C(3)	47.3(5)	P(3)-Rh(3)-C(3)	98.9(5)
P(4)-Rh(3)-C(3)	90.1(5)	Rh(1)-Rh(3)-C(4)	44.5(4)
Rh(2)-Rh(3)-C(4)	104.5(4)	P(3)-Rh(3)-C(4)	85.9(4)
P(4)-Rh(3)-C(4)	85.2(4)	C(3)-Rh(3)-C(4)	151.4(6)
Rh(1)-Rh(3)-C(7)	143.8(5)	Rh(2)-Rh(3)-C(7)	155.8(5)
P(3)-Rh(3)-C(7)	87.4(5)	P(4)-Rh(3)-C(7)	91.8(5)
C(3)-Rh(3)-C(7)	108.8(7)	C(4)-Rh(3)-C(7)	99.6(6)
Rh(2)-P(1)-C(2)	110.7(5)	Rh(2)-P(1)-C(11)	118.0(6)
C(2)-P(1)-C(11)	105.6(7)	Rh(2)-P(1)-C(21)	116.2(5)
C(2)-P(1)-C(21)	102.8(7)	C(11)-P(1)-C(21)	101.9(7)
Rh(2)-P(2)-C(1)	112.7(5)	Rh(2)-P(2)-C(51)	117.3(5)
C(1)-P(2)-C(51)	104.6(7)	Rh(2)-P(2)-C(61)	113.6(6)
C(1)-P(2)-C(61)	103.5(7)	C(51)-P(2)-C(61)	103.6(7)
Rh(3)-P(3)-C(2)	113.0(5)	Rh(3)-P(3)-C(31)	117.4(5)

Table XXXIX (continued)

C(2)-P(3)-C(31)	104.9(7)	Rh(3)-P(3)-C(41)	113.4(5)
C(2)-P(3)-C(41)	103.6(7)	C(31)-P(3)-C(41)	103.0(7)
Rh(3)-P(4)-C(1)	110.5(5)	Rh(3)-P(4)-C(71)	118.0(5)
C(1)-P(4)-C(71)	106.2(7)	Rh(3)-P(4)-C(81)	111.7(6)
C(1)-P(4)-C(81)	104.0(7)	C(71)-P(4)-C(81)	105.5(8)
Rh(2)-C(3)-Rh(3)	84.8(7)	Rh(2)-C(3)-O(3)	138.4(13)
Rh(3)-C(3)-O(3)	136.7(13)	Rh(1)-C(4)-Rh(3)	79.9(5)
Rh(1)-C(4)-O(4)	151.8(13)	Rh(3)-C(4)-O(4)	128.4(12)
Rh(1)-C(5)-Rh(2)	77.6(6)	Rh(1)-C(5)-O(5)	156.9(14)
Rh(2)-C(5)-O(5)	125.2(12)	Rh(2)-C(6)-O(6)	177.2(17)
Rh(3)-C(7)-O(7)	177.6(14)	Rh(1)-C(8)-O(8)	178.7(19)
P(2)-C(1)-P(4)	113.6(8)	P(1)-C(2)-P(3)	110.3(8)
P(1)-C(11)-C(12)	122.9(12)	P(1)-C(11)-C(16)	119.1(12)
C(12)-C(11)-C(16)	117.9(15)	C(11)-C(12)-C(13)	121.0(17)
C(12)-C(13)-C(14)	120.6(19)	C(13)-C(14)-C(15)	118.4(16)
C(14)-C(15)-C(16)	122.1(17)	C(11)-C(16)-C(15)	119.8(16)
P(1)-C(21)-C(22)	119.6(11)	P(1)-C(21)-C(26)	122.3(14)
C(22)-C(21)-C(26)	118.1(16)	C(21)-C(22)-C(23)	120.3(15)
C(22)-C(23)-C(24)	119.3(18)	C(23)-C(24)-C(25)	121.3(19)
C(24)-C(25)-C(26)	119.4(18)	C(21)-C(26)-C(25)	121.5(18)
P(3)-C(31)-C(32)	123.3(11)	P(3)-C(31)-C(36)	120.2(12)
C(32)-C(31)-C(36)	116.3(14)	C(31)-C(32)-C(33)	121.7(15)
C(32)-C(33)-C(34)	118.5(18)	C(33)-C(34)-C(35)	119.8(18)
C(34)-C(35)-C(36)	119.9(18)	C(31)-C(36)-C(35)	123.6(17)
P(3)-C(41)-C(42)	117.8(12)	P(3)-C(41)-C(46)	122.2(12)
C(42)-C(41)-C(46)	120.0(14)	C(41)-C(42)-C(43)	119.3(15)
C(42)-C(43)-C(44)	120.0(14)	C(43)-C(44)-C(45)	121.7(16)
C(44)-C(45)-C(46)	119.5(18)	C(41)-C(46)-C(45)	119.5(16)
P(2)-C(51)-C(52)	118.3(11)	P(2)-C(51)-C(56)	122.0(11)
C(52)-C(51)-C(56)	119.6(14)	C(51)-C(52)-C(53)	119.3(14)
C(52)-C(53)-C(54)	121.9(15)	C(53)-C(54)-C(55)	119.6(17)
C(54)-C(55)-C(56)	120.2(17)	C(51)-C(56)-C(55)	119.2(15)
P(2)-C(61)-C(62)	122.3(13)	P(2)-C(61)-C(66)	118.5(12)
C(62)-C(61)-C(66)	119.1(15)	C(61)-C(62)-C(63)	117.0(16)
C(62)-C(63)-C(64)	123.0(17)	C(63)-C(64)-C(65)	119.5(18)
C(64)-C(65)-C(66)	119.2(16)	C(61)-C(66)-C(65)	121.9(15)
P(4)-c(71)-C(72)	121.1(12)	P(4)-C(71)-C(76)	121.9(13)

Table XXXIX (continued)

C(72)-C(71)-C(76)	117.0(16)	C(71)-C(72)-C(73)	120.7(16)
C(72)-C(73)-C(74)	122.6(16)	C(73)-C(74)-C(75)	118.5(19)
C(74)-C(75)-C(76)	118.4(20)	C(71)-C(76)-C(75)	122.7(17)
P(4)-C(81)-C(82)	120.6(13)	P(4)-C(81)-C(86)	123.6(12)
C(82)-C(81)-C(86)	115.8(15)	C(81)-C(82)-C(83)	122.2(18)
C(82)-C(83)-C(84)	121.2(20)	C(83)-C(84)-C(85)	118.0(20)
C(84)-C(85)-C(86)	121.6(19)	C(81)-C(86)-C(85)	121.1(16)
F(1)-P(5)-F(2)	178.1(11)	F(1)-P(5)-F(3)	87.6(12)
F(2)-P(5)-F(3)	94.3(11)	F(1)-P(5)-F(4)	88.6(8)
F(2)-P(5)-F(4)	91.0(8)	F(3)-P(5)-F(4)	89.2(12)
F(1)-P(5)-F(5)	90.5(11)	F(2)-P(5)-F(5)	87.6(10)
F(3)-P(5)-F(5)	171.4(13)	F(4)-P(5)-F(5)	82.4(10)
F(1)-P(5)-F(6)	90.1(10)	F(2)-P(5)-F(6)	90.5(10)
F(3)-P(5)-F(6)	88.2(17)	F(4)-P(5)-F(6)	177.1(14)
F(5)-P(5)-F(6)	100.2(16)		

VITA

James "Jack" Lane Edwin Burn, Jr. was born in Knoxville, Tennessee on July 18, 1962. The first of two children to Marthanne Smith Burn and James Lane Edwin Burn, he was the sixth generation of the Burn family to be raised in or near Niota, formerly Mouse Creek, McMinn County, Tennessee. He graduated high school at T. M. I. Academy, Sweetwater, Tennessee in May of 1979. He received a Bachelor of Science in Chemistry from The University of the South in May of 1985. On May 28, 1988, he was married to Kathleen Jean Malm in the Niota First Baptist Church. Two daughters, Katherine Mahala (born June 25, 1989) and Olivia LaRose (born December 14, 1991) have been born into their family. He is currently employed by Bechtel Environmental, Inc. as a scientist and supervisor of the Close Support Laboratory for the Oak Ridge National Laboratory Remedial Investigation/Feasibility Study. Jack received his Doctor of Philosophy in Chemistry from The University of Tennessee in May of 1993.